STRUCTURAL INSIGHTS INTO THE ROLE OF ASSEMBLY FACTORS IN THE

ASSEMBLY, FUNCTION AND FLAVINYLATION OF COMPLEX II

By

Chrystal Ama Rhea Starbird

Dissertation

Submitted to the Faculty of the

Graduate School of Vanderbilt University

in partial fulfillment of the requirements

for the degree of

DOCTOR OF PHILOSOPHY

in

Chemical and Physical Biology

August 11, 2017

Nashville, Tennessee

Approved:

Charles Sanders, Ph. D

Brian Bachmann, Ph. D.

Martin Egli, Ph. D.

Tina Iverson, Ph. D.

I dedicate this work to my children; Brian, Aaliyah and Liam. May you follow the path to your dreams and stay on course despite any bumps in the road or even if a giant sinkhole opens up and requires you to dig deeper in order to complete your journey.

ACKNOWLEDGEMENTS

No journey in my life, including the one that led to writing my dissertation, has been completed entirely alone. I have been lucky to have great advisors, supporters and cheerleaders, some of whom I acknowledge here.

First, I would like to thank several of my past mentors, without whose support I would have been unlikely to have the level of success I have achieved thus far. Even at the best of times, working to achieve goals that sometimes seem out of reach can seem nearly impossible, and inspiration and support is important. When your life is complicated by challenges that society and yourself consider difficult to overcome, that support becomes invaluable. I have been lucky to have several past advisors that continuously encouraged me to never give up. Specifically, I would like to thank Dr. Brian Strahl, in whose lab I encountered my first truly challenging scientific project and who taught me that the curious mind never stops seeking ways to find the answers. I would also like to thank Dr. Joshua "Awesome" Hall, who worked with me in the PREP program to open up new possibilities for graduate training and to set me up for great success. Lastly, I would like to thank Dr. Robert Bourret, who has gone far beyond the duties of a typical scientific mentor and advisor. He has been my advocate and a consistent voice of support and the belief in my potential.

I would also like to thank the members of my committee: Dr. Tina Iverson (my mentor), Dr. Charles Sanders (my chair), Dr. Martin Egli, Dr. Borden Lacy and Dr. Brian Bachmann. Thank you all for your guidance and advice during the evolution of my thesis research. In particular, I would like to thank Dr. Charles Sanders for serving as my committee chair and for sharing his wisdom to help me navigate many aspects of my graduate career. I would also like to thank my advisor of nearly six years, Dr. Tina Iverson. She has helped me to

develop into a much stronger scientist and she has put me on the path to learning to better balance life with work. She has also taught me that in the lab and in your career, the key to finding the solution to any problems that may arise is often to be willing to change your approach as often as is needed. She has taught me the importance of both understanding the theory and the practice, of developing concrete plans to improve your skills and the discipline to carry them out.

In addition to the support of Dr. Iverson, I could not have completed this work without the assistance and advice of many members of the Iverson Lab. During my time at Vanderbilt, I have had the pleasure of working with many members of the lab and there are a few members in particular that I would like to acknowledge here. Prashant Singh worked with me very closely for my first few months in the lab. He taught me the protocols for purification of QFR and essentially everything that led me up to the point at which my project started, allowing me to have a strong foundation to begin my thesis work. He also developed the protocols for purification of the QFR:FliG complex and working together, we obtained the first LCP crystals of the complex. Dr. Kathyrn McCulloch helped me to learn many of the computational programs and imaging software with which I was less familiar. As a wonderful friend and advisor, we spent many hours discussing our work and working together to figure out problems in the lab, such as with the one AKTA that liked to break down. I would also like to thank Izumi Yamakawa, who has been an unbelievable help in many aspects of my work, from staying a few extra hours to help me finish an experiment when I had to go home to helping me navigate new experiments, including circular dichroism, dynamic light scattering and negative stain electron microscopy. It is only necessary to mention you are having trouble understanding how to do

something, and Izumi works her 'magic' to find more resources for information. She has been invaluable to the Iverson lab and to me personally, and I know she has a very bright future ahead.

Outside of the Iverson Lab, I have had the great pleasure of working closely with many collaborators at other institutions. One very strong and fruitful collaboration that I was able to participate in was between our lab and the Cecchini lab at UCSF. Almost every aspect of my work was possible, in part, by this collaboration. Dr. Gary Cecchini and Elena Maklashina. They provided plasmids and strains and experimental guidance. We discussed hypothesis and used those discussions to guide experiments carried out in both labs to complement one another. They helped me in writing, most notably in the review article I submitted as well as a recently submitted manuscript on covalent flavinylation. I have learned a great amount during my graduate career from their approach to scientific questions and thank them for their professional support and guidance.

Outside of those with whom I worked directly on scientific projects, several members of the Vanderbilt community have been instrumental to my success as a graduate student. I thank Dr. Bruce Damon, my graduate program director, for his support and commitment to my success and Patty Mueller for going above and beyond her duties as a Program Manager in assisting me. I thank Dean Roger Chalkley for his continued support, for his wit and for keeping such an open door policy. I thank Dr. Linda Sealy for her strong leadership of the IMSD program and for her unwavering support of the success of all of her students, myself included. I thank Dr. John York, for encouraging conversations about the future of science and for his belief that I have a place in that future. And last, but certainly not least, I want to thank Dr. Walter Chazin. Dr. Chazin is a major part of the reason why I came to Vanderbilt. He has been my advocate and an invaluable advisor.

Lastly, I am incredibly blessed to have the family that I do. Without their love and support, none of this would have been possible. Without the support of my in-laws, Delia and Daniel, it may not have even been possible for me to apply to all of the graduate programs that I dreamed of and to ultimately choose Vanderbilt. Whether by babysitting or sharing advice, many family members made it possible for me to consider graduate school. For six years I kept pictures of my ever-growing children at my bench for motivation and to remind me that on difficult days, I do this for them and to teach them the wonder and joy that is scientific discovery. On days off from school, Brian, Aaliyah and Liam came into the lab to pipette 'buffers' and to ask a million questions that reminded me that being able to practice science is exciting and an amazing privilege. And to my husband and my best friend, Doug, I offer more thanks and gratitude than I can ever hope to express. Graduate school is fun, but it can be hard. Graduate school with three children was at times nearly impossible, but you never let me fail. We have survived this together. Now we will continue to thrive together.

TABLE OF CONTENTS

Chapter

LIST OF TABLES

Table   Page

LIST OF FIGURES

LIST OF ABBREVIATIONS

FAD..Flavin adenine dinucleotide

QFR...quinol:fumarate reductase

SQR.. succinate:quinone oxidoreductase

LCP ....lipidic cubic phase

NMR .... nuclear magnetic resonance

IPTG...Isopropyl β-D-1-thiogalactopyranoside

HIC... Hydrophobic interaction chromatography

BpF...*para*-benzoyl-L-phenylalanine

MST ....microscale thermophoresis

CHAPTER 1

INTRODUCTION

Work included in this chapter was published in as part of a review in eLS online library in

September of 2015 entitled "Flavoenzymes: Covalent versus Noncovalent" and authored by

Chrystal Starbird, Elena Maklashina, Gary Cecchini and Tina Iverson (1).

The work described in this thesis outlines progress towards understanding the

mechanisms of assembly and covalent flavinylation in the Complex II family of enzymes and the

role of assembly factors in assembly and function. Complex II has been extensively studied for

its roles in both energy metabolism and cell survival and it was the first enzyme identified over

sixty years ago as having a covalent flavin cofactor. Although well studied, recently discovered

assembly factors that have roles in assembly and covalent flavinylation of the complex and that

point to a newly proposed role of Complex II in chemotaxis signaling have highlighted that there

is still much to learn about this important respiratory complex. In the work described here,

structural and biochemical techniques were used to explore the contribution of these newly

identified assembly factors to our understanding of assembly, function and covalent flavinylation

in Complex II.

Enzymes with flavin cofactors: covalent versus non-covalent

Enzyme-associated flavin cofactors include flavin mononucleotide (FMN) and flavin

adenine dinucleotide (FAD), which are the most prevalent biologically useful derivatives of

riboflavin (vitamin B_2). The conjugated ring system of the oxidized isoalloxazine group of flavins (**Figure 1.1**) absorbs light at 450 nm to give a bright yellow appearance and fluoresces under UV light. The readily observed yellow colour of flavoenzymes meant they were among the earliest enzymes to be isolated. Indeed, the historically-named "old yellow enzyme" was purified as early as the 1930s (2).

Flavoenzymes catalyse either oxidoreduction or promote group transfer reactions using the conjugated isoalloxazine ring system to promote the chemistry (3). As oxidoreductases, the capacity of the isoalloxazine ring system to cycle between one- and two-electron reduction allows flavoenzymes to catalyse either one- or two-electron redox reactions. Flavoenzyme-catalyzed group transfer reactions take advantage of reactive positions on the isoalloxazine ring system to activate molecular oxygen or other species. Group transfer reactions include but are not limited to oxygenation, nitrosylation, halogenation and hydroxylation.

This wide range of supported chemistry allows flavoenzymes to participate in many important physiological processes. Flavoenzyme redox activity is intimately linked with the energy harvesting processes of biology, including metabolic processes ranging from the many types of anaerobic respiration (for examples, see: (4-6) to photosynthesis (7) to oxidative phosphorylation (8). When acting in group transfer reactions, flavoenzyme chemistry contributes to diverse biological processes including doxorubicin induced chromatin remodelling (9) DNA lesion repair caused by UV radiation damage (10), and secondary metabolite production (11). Many of these activities have industrial and therapeutic applications (for example, (12)).
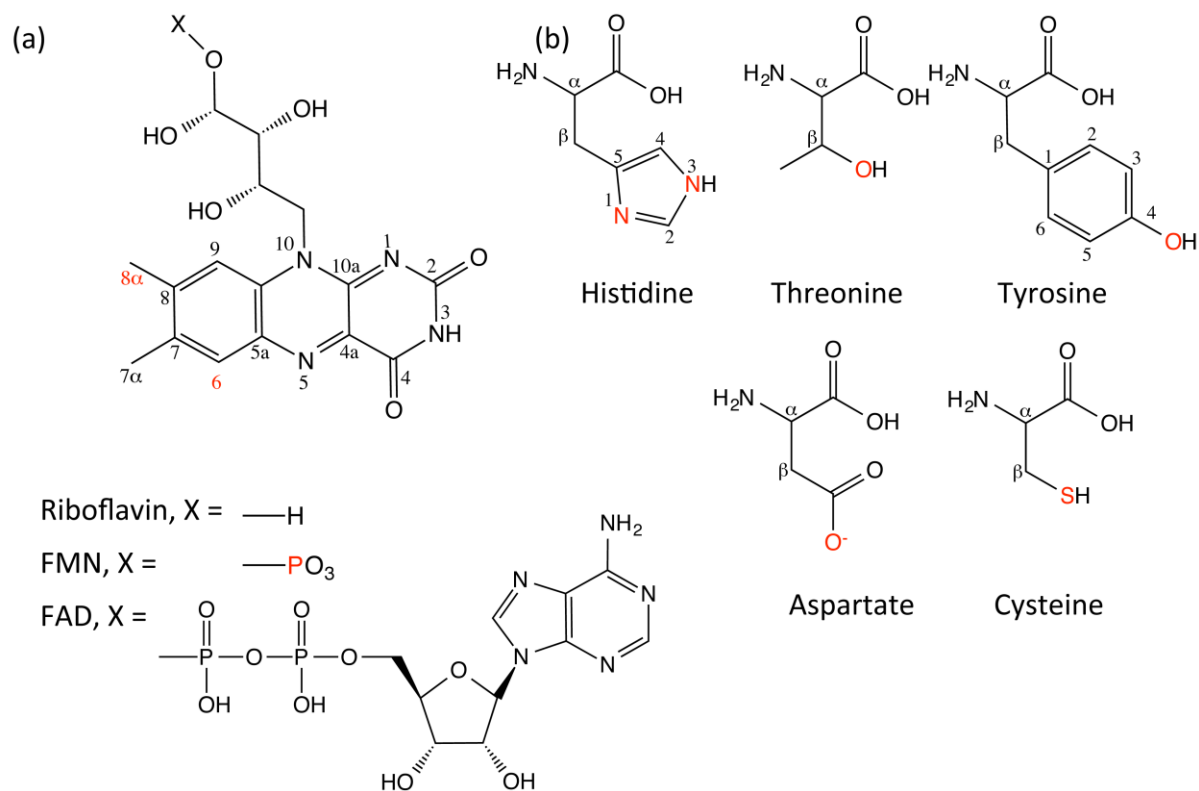
Figure 1.1: Chemical structure of riboflavin with FAD and FMN groups: A. Chemical structure of riboflavin with the isoalloxazine labeled in a manner consistent with this text. The flavin mononucleotide and flavin adenine dinucleotide additions to the ribityl side chain are shown. B. Chemical structures of the amino acids known to form a covalent bond with flavin. The associated ring structures are numbered. For all structures, potential sites of covalent linkage are in colored red. Figure originally published in eLS review (1).

The vast majority of flavin cofactors are tightly, but non-covalently associated with their cognate enzymes. These non-covalent flavoenzymes retain the cofactor by virtue of a high-affinity binding pocket that usually fully shields the ribityl side chain from solvent. However, as early as the 1950s, it was discovered that flavin cofactors can also be covalently attached to enzymes (13), and it is estimated that ~10% of biological flavin is covalently associated with a protein.

The first identified covalently-attached flavin cofactor was FAD attached to succinate dehydrogenase (13), an integral-membrane enzyme that functions in both the citric acid cycle

3

and oxidative phosphorylation. Spectroscopic studies on succinate dehydrogenase revealed the covalent linkage as an 8α-N(3)-histidyl linkage (14). This nomenclature defines the position of the covalent bond on each respective molecule, with 8α referring to the specific atom of the isoalloxazine ring and N(3) similarly referring to a specific atom on the enzyme-associated histidine (see numbering in Figure 1.1). The 8α-N(3)-histidyl linkage is the most commonly observed covalent linkage in all flavoenzymes characterized to date. However, there is significant diversity in known flavin-peptide linkages. For example, there are characterized linkages between either FAD or FMN and a cysteine, threonine, aspartate, or tyrosine residue from the protein. These linkages can be to the histidine side chain at position N1 or N3 of the imidazole group, and they can be to different positions on the flavin (to either 8α or 6 on the isoalloxazine, or to the phosphoester of the ribityl side chain). There are even characterized bicovalent bonds with a flavin tethered between two residues. Many of these covalent linkages have been characterized using a combination of spectroscopic methods and atomic resolution structures.

The importance of covalent flavinylation: examples from the literature

An intriguing observation on covalent flavin attachment is the lack of conservation in closely related enzymes. One striking example of this is found in the amine oxidase family of flavoenzymes, which includes mitochondrial monoamine oxidases A and B. Monoamine oxidases oxidise neurotransmitters, and modulation of their activity by pharmaceuticals is therefore used in the treatment of a range of psychiatric disorders. Human monoamine oxidase has two isoforms, and both contain covalent flavin (15,16). In contrast, other members of the amine oxidase family instead contain non-covalent flavin. This has been unambiguously demonstrated in crystal structures, which show an 8α-6-S-Cysteinyl linkage in monoamine

oxidases (17) and non-covalent linkage in the related cyclohexylamine oxidase (34% identical, 50% similar) (18), putrescine oxidase (33% identical, 50% similar) (19), and lysine specific demethylase (23% identical, 41% similar) (20-22).

Why has a subset of enzymes evolved to have a covalent bond to the FMN or FAD cofactor when related enzymes lack this bond? Multiple hypotheses have been proposed to address this question. The most common explanations for the introduction of covalent flavinylation in enzymes are the alteration of flavin midpoint potential and the retention of the flavin cofactor.

Covalent flavinylation and the increase of flavin midpoint potential

The consensus in the field is that the most important role of covalent flavin attachment is to raise the midpoint potential of the flavin cofactor, which increases the thermodynamic driving force available to the chemical reactions catalysed by these enzymes. This increase in midpoint potential is universal in all covalent flavins studied to date.

Studies on the bacterial bioenergetic protein quinol:fumarate reductase (QFR) first suggested that covalent ligation of the flavin could influence the chemical reaction supported by the enzyme (23). Quinol:fumarate reductase is a sequence, structural, and functional homolog of the succinate dehydrogenase enzyme in which covalent FAD was first identified. Indeed, quinol:fumarate reductase and succinate dehydrogenase both catalyse bidirectional interconversion of the dicarboxylates fumarate and succinate. In seminal studies, a creative strategy generated variants of quinol:fumarate reductase lacking the histidine side chain necessary for covalent linkage. These variants still retained tightly associated non-covalent flavin; however, in the absence of the covalent linkage quinol:fumarate reductase lacked detectable succinate oxidation activity, but retained fumarate reduction activity, albeit at a

reduced level (23). Succinate oxidation requires a greater thermodynamic driving force than fumarate reduction, and covalently attached FAD in quinol:fumarate reductase has a redox potential ($E_m \approx$ -55 mV) much higher than free FAD (-219 mV), suggesting that the covalent link alters the midpoint potential of the FAD. Consistent with this is the existence of homologous fumarate reductase enzymes in *Shewanella* that lack the histidine ligand for covalent attachment and instead bind FAD non-covalently. The *Shewanella* enzymes have a pH-dependent midpoint potential of -100 mV to -200 mV, catalyse unidirectional fumarate reduction, and have undetectable succinate oxidation activity (24).

The vast majority of later studies investigating the role of covalent flavinylation in other proteins adopted the strategy that mutagenized the protein linkages and measured the impact of this mutation on the non-covalent variant. Loss of the covalent linkage universally decreased the flavin midpoint potential. A survey of such studies suggests that on average, a single covalent linkage between enzyme and flavin increases the reduction potential of the flavin by ~80 mV. This was shown clearly by studies of vanillyl-alcohol oxidase, a fungal enzyme with multiple phenolic compound targets. Like quinol:fumarate reductase and succinate dehydrogenase, vanillyl-alcohol oxidase contains an 8α-*N*(3)-histidyl linkage and this is associated with an unusually high midpoint potential of +55 mV. Following alanine substitution of the histidine involved in the 8α-*N*(3)-histidyl linkage, the enzyme was associated with tightly-bound non-covalent FAD with a midpoint potential of -65 mV (25). Structural analysis indicated both that the active site geometry had not changed and that the enzyme-substrate complex was unchanged, strongly suggesting that the changes in FAD potential were due only to loss of the covalent bond. Careful kinetic measurements demonstrated that the mechanism of the enzyme was unchanged in the absence of the covalent link to FAD. However, the decrease in thermodynamic driving force

of the non-covalent FAD slowed the electron transfer between substrate and flavin, resulting in a ~10-fold decrease in substrate turnover (25).

The first example of a bicovalent flavin linkage was discovered 60 years after the discovery of covalent flavin in succinate dehydrogenase when an 8α-*N*(1)-histidyl/6-*S*-Cysteinyl linkage was identified. This bicovalent linkage tethers FAD to glucooligosaccharide oxidase, an enzyme that oxidises sugars in the fungal pathogen *Acremonium strictum* (26). Site specific mutagenesis demonstrated that each linkage is responsible for increasing the redox potential of the FAD by ~60 mV, and that each linkage has an independent effect on the FAD potential (27). This is consistent with the observation that enzymes harbouring bicovalent flavin generally exhibit a significantly higher redox potential than enzymes with a monocovalent flavin linkage.

Often, the best support for a hypothesis comes from the ability to recreate a predicted effect *de novo*. In the case of covalent flavins, several recent studies have done just that. One such study is based upon the flavoenzyme 6-hydroxy-D-nicotine oxidase, a homolog of vanillyl-alcohol oxidase that is involved in nicotine degradation and contains a monocovalent FAD linkage. Use of mutagenesis to add a second covalent linkage converted 6-hydroxy-D-nicotine oxidase to a bicovalent enzyme, and the FAD potential in the engineered, bicovalent enzyme increased by 50 mV as compared to the wild-type enzyme (28).

Covalent flavinylation and retention of the flavin cofactor

Most flavin binding pockets are deep and contain extensive contacts to the cofactor, resulting in a high affinity interaction with the enzyme. Despite this, the flavin may still disassociate from the enzyme. Dissociation is especially likely if the active site is particularly large or exposed, or if the enzyme functions within a microenvironment of the cell that is flavin

poor and/or requires a longer association with the cofactor. In these cases, a covalently bound flavin ensures cofactor retention during catalysis.

Support for the covalent linkage playing a role in flavin retention comes from several indirect observations, the first of which is in laboratory purification of non-covalent flavoenzymes. A flavin-free purification could mimic a cellular microenvironment where little flavin is available. Loss of a non-covalent flavin from a flavoenzyme during purification is surprisingly common, as demonstrated in flavin-free crystal structures of normally non-covalent flavoenzymes such as the nitrosynthases (29,30). A particularly compelling example is that of *Rhodococcus erythropolis* putrescine oxidase, which is normally associated with non-covalent flavin. Following heterologous expression and laboratory purification, ~50% of the FAD binding sites of putrescine oxidase misincorporate ADP, which shares chemical features with the FAD cofactor (31). In contrast, monoamine oxidase, a mammalian homolog of putrescine oxidase, contains covalent FAD. Monoamine oxidases have an important role in inactivation of monoamine neurotransmitters and require tight regulation, which may make retention of the cofactor critical (15,16).

Another example is quinol:fumarate reductase, which normally contains covalent flavin. Quinol:fumarate reductase has a complex role in respiration that is intimately related to the covalent FAD. Quinol:fumarate reductase normally catalyses the terminal step in anaerobic respiration with fumarate in both facultative anaerobes such as *E. coli* (which can switch between anaerobic and aerobic respiration) and obligate anaerobes such as *Wolinella succinogenes* (which can only perform anaerobic respiration) (6). During anaerobic respiration, quinol:fumarate reductase reduces fumarate to succinate, which does not require an increased midpoint potential of the FAD. In facultative anaerobes, quinol:fumarate reductase likely

8

switches the direction of its reaction when the organism switches from anaerobic to aerobic respiration, such that instead of reducing fumarate to succinate, it oxidises succinate. Here, a covalent FAD is key since the succinate oxidation reaction requires an increased driving force.

Obligate anaerobes never switch to aerobic respiration. While some obligate anaerobes contain quinol:fumarate reductase homologs lacking the covalent linkage, some of the quinol:fumarate reductases from obligate anaerobes have covalently linked FAD despite it being unnecessary to catalyse the fumarate reduction reaction. This may speak to a second role for the bond *in vivo*. Quinol:fumarate reductase has been shown to undergo a conformational change during catalysis that transiently exposes the FAD to solvent (32) and could result in loss of non-covalent FAD. Indeed, non-covalent FAD in quinol:fumarate reductase variants is labile. As discussed above, while site-specific variants associated with non-covalent FAD did retain the ability to reduce fumarate, the efficiency was reduced to 17-30% of wild-type enzyme (23). The FAD in these variant enzymes could be removed by dialysis against KBr, resulting in complete loss of activity. Activity could be restored when excess free FAD was added to the variant enzymes. Interestingly, L-aspartate oxidase, a homolog of quinol:fumarate reductase that naturally contains non-covalent FAD, can lose the cofactor upon purification, as demonstrated by the crystal structure (33).

Cofactor retention may have other effects on covalent flavoenzymes. For example, cofactor binding and protein stability are intimately linked, with loss of cofactor binding reducing protein stability. Similarly, the loss of the cofactor may promote misfolding. Since removal of the covalent bond from flavin increases the likelihood that the cofactor will disassociate, studies to distinguish the direct contribution of the covalent bond to protein stability and folding as compared to a contribution in retaining the cofactor are a challenge.

9

Mechanism of covalent flavin attachment in Complex II and related enzymes

Until very recently, the dogma in the field has been that the formation of the covalent bond between an enzyme and flavin is a fully autocatalytic process. However, recent work identified the first assembly factor important for covalent flavinylation through the formation of the 8α-N(3)-histidyl linkage to FAD in eukaryotic succinate dehydrogenase (34). Current research in the field both focuses on identifying what other systems require assembly factors to form a covalent bond to flavin, and seeks to determine how assembly factors promote covalent flavinylation.

The autocatalytic hypothesis of covalent flavinylation

One example of the many studies suggesting autocatalytic covalent flavinylation used 6-hydroxy-D-nicotine oxidase as a model system. Conveniently for studies of flavinylation, overexpression of 6-hydroxy-D-nicotine oxidase results in a significant amount of flavin deficient enzyme (35). The amount of apoenzyme can be increased further with modification of experimental conditions. Incubation of the 6-hydroxy-D-nicotine oxidase apoenzyme with [^{14}C] labelled FAD and glycerol-3-phosphate as an electron acceptor suggested autocatalytic covalent flavinylation occurred *in vitro* (36), but these studies were performed in cell lysate, which could also suggest that another factor was required for covalent flavinylation. Similar methods were used to probe the mechanism of covalent flavinylation in other flavoenzymes that do not efficiently incorporate flavin during heterologous expression (for example, dimethylglycine dehydrogenase (37).

A complementary, novel approach for studying the covalent linkage used enzymes expressed in a strain of bacteria that is riboflavin auxotrophic and therefore cannot produce FAD or FMN (38). This system produces FAD or FMN deficient enzyme, and allows studies on the

10

mechanism of covalent flavinylation to be performed on a broader range of covalent flavoenzymes. For monomeric sarcosine oxidase, an enzyme that demethylates sarcosine, *in vitro* reconstitution of covalently attached FAD cofactor with apoenzyme could be measured by following FAD reduction and peroxide production during the formation of the covalent bond (39). Similar studies have been performed on vanillyl-alcohol oxidase (40).

Identified assembly factors in covalent flavinylation

For many years, it was not considered necessary to have additional assembly factors for *in vivo* covalent flavinylation. In 2009, however, a combination of yeast genetics and DNA sequencing of patients with succinate dehydrogenase deficiency identified a small protein required for covalent flavinylation of human succinate dehydrogenase (34). This ~10 kD protein, termed SdhAF2 in humans, Sdh5 in yeast (34), and SdhE in bacteria (41), has sequence homologs in all kingdoms of life, but previously had no known function.

In bacteria, the SdhE assembly factor contributes to covalent flavin attachment in bacterial succinate dehydrogenase and its homologue quinol:fumarate reductase (41,42). Curiously it does not appear as essential in bacteria as it is in higher organisms, although it appears to be important, especially under aerobic conditions. Targeted deletion of the *sdhE* gene results in reduction, but not abrogation, of covalent flavinylation in *E. coli* (43), while the thermophiles *Thermus thermophilus* and *Sulfolobus tokodaii* lack a homolog of SdhE and appear to have fully flavinylated succinate dehydrogenase in the absence of this assembly factor (44).

The involvement of SdhAF2/Sdh5/SdhE in covalent flavinylation has raised questions on how an accessory protein might contribute to covalent flavinylation. Three predominant theories suggest that: (1) SdhAF2/Sdh5/SdhE is an FAD transferase, with a role in direct transfer to and placement of FAD into the enzyme; (2) SdhAF2/Sdh5/SdhE is a chaperone-like protein,

important for the proper folding of the succinate dehydrogenase flavoprotein; and (3)

SdhAF2/Sdh5/SdhE transiently stabilizes a high-energy conformation of a fully folded succinate

dehydrogenase flavoprotein that optimally aligns amino acids of either succinate dehydrogenase

or SdhE around the 8α position of the isoalloxazine ring into an active site that catalyses FAD

attachment.

Chemical mechanism of covalent flavinylation

Regardless of whether covalent flavinylation is autocatalytic or assisted by an ancillary

protein, the most plausible mechanism for covalent flavinylation at the 8α carbon requires attack

of the quinone methide form of the isoalloxazine ring by nucleophilic amino acid side chains

(**Figure 1.2**) (45). Termed the quinone methide mechanism, this prediction is consistent with a

large body of work that tested the influence of amino-acid substitutions and flavin analogues

with modified chemical properties on the formation of the covalent flavin adduct.
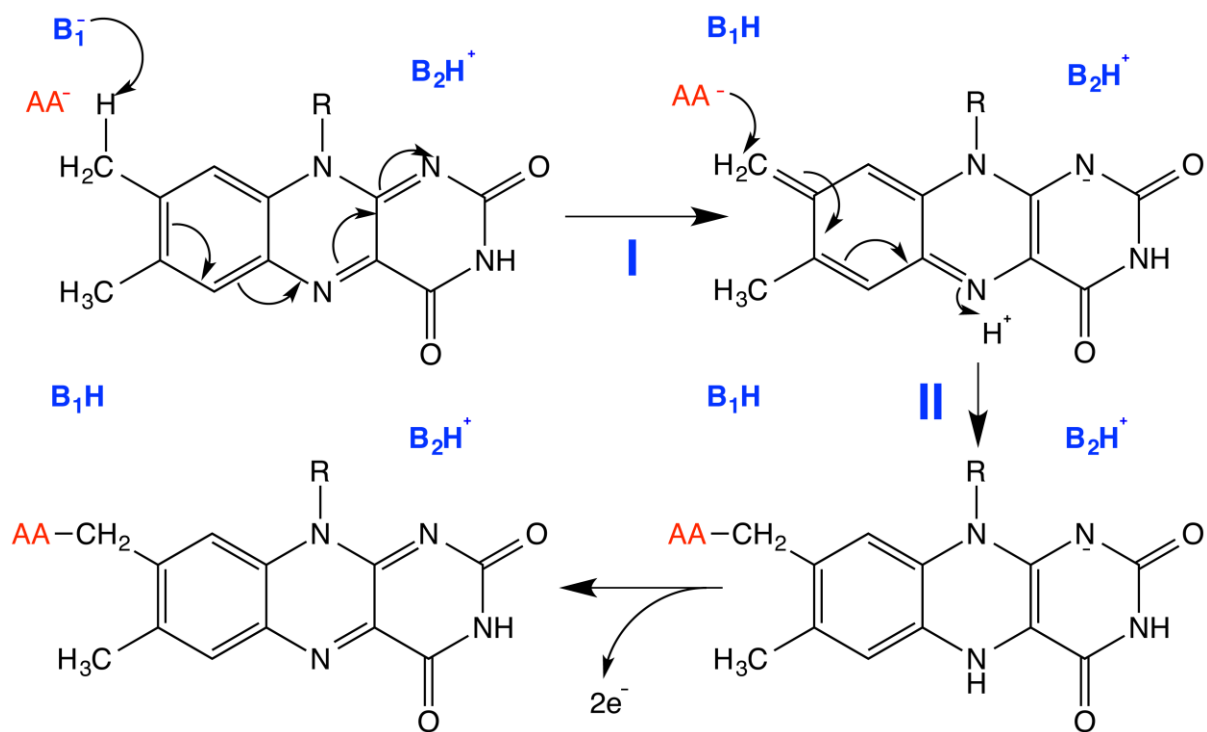
Figure 1.2: Quinone methide mechanism for attachment at the 8α carbon of the flavin. Blue "B"s represent catalytic bases, which are likely amino acid side chains. The red "AA" indicates the amino acid that is covalently attached. Figure originally published in eLS review (1).

Complex II homologs: A powerful model system

As discussed above, Complex II or succinate dehydrogenase is a mitochondrial respiratory

enzyme complex that functions in both the electron transport chain and the Citric Acid Cycle

with structural and functional homologs in all kingdoms of life (8,46) (**Figure 1.3**). Complex II

couples the oxidation of succinate to fumarate with reduction of ubiquinone to ubiquinol, but it is

capable of the bi-directional catalysis of either fumarate or succinate. In bacteria, two homologs

of Complex II exist: QFR and SQR. Both are capable of bidirectional interconversion of

succinate and fumarate, but are divided into two classes: (i) succinate: ubiquinone

oxidoreductases preferentially oxidize succinate and reduce quinone in aerobic respiration, (ii)

13

and quinol:fumarate reductases preferentially reduce fumarate and oxidize quinol to participate

in anaerobic respiration with fumarate as the terminal electron acceptor.
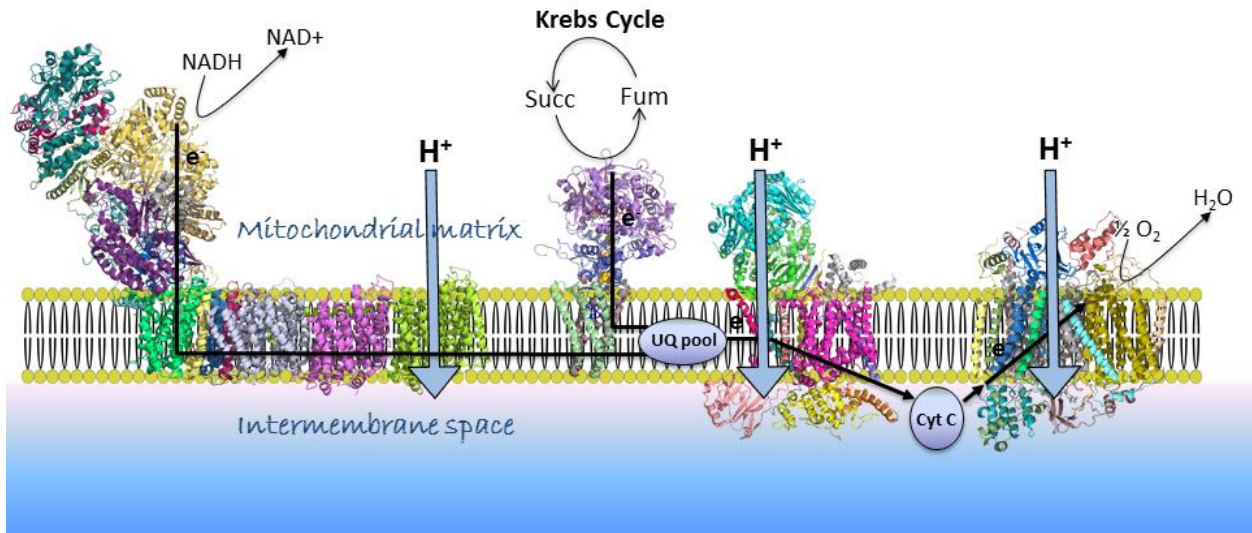
Figure 1.3: Overview of aerobic respiration. The transport of electrons (black arrows) and the
development of a proton gradient across the inner mitochondrial membrane (blue arrows) is shown as
facilitated by the four complexes involved in the electron transport chain (shown in numerical order as
complex 1-4 from left to right). Important outputs of the cycle, including interconversion of succinate to
fumarate in the Krebs cycle by Complex II is also shown.

The *E. coli* homologs QFR and SQR have a high degree of structural and functional

homology to the mammalian complexes, as does SQR, and has been used extensively as a model

system to investigate assembly, function and covalent flavinylation of Complex II. Indeed, the

first structures of a member of the Complex II superfamily were of bacterial homologs (47,48)

and provided the first view of this shared global architecture. Complex II superfamily members

are heterotetramers with two soluble domains and two membrane spanning domains. The soluble

portion is comprised of the flavoprotein subunit (termed FrdA in QFR), which contains a

covalently attached flavin and the dicarboxylate binding site and the iron-sulfur subunit (termed

FrdB in QFR), which contains three iron-sulfur clusters that facilitate electron transfer to the quinone-binding site formed at the interface of the two membrane spanning subunits (termed FrdC and FrdD in QFR). In SQRs, there is also a heme molecule enclosed by the membrane subunits (**Figure 1.4**).
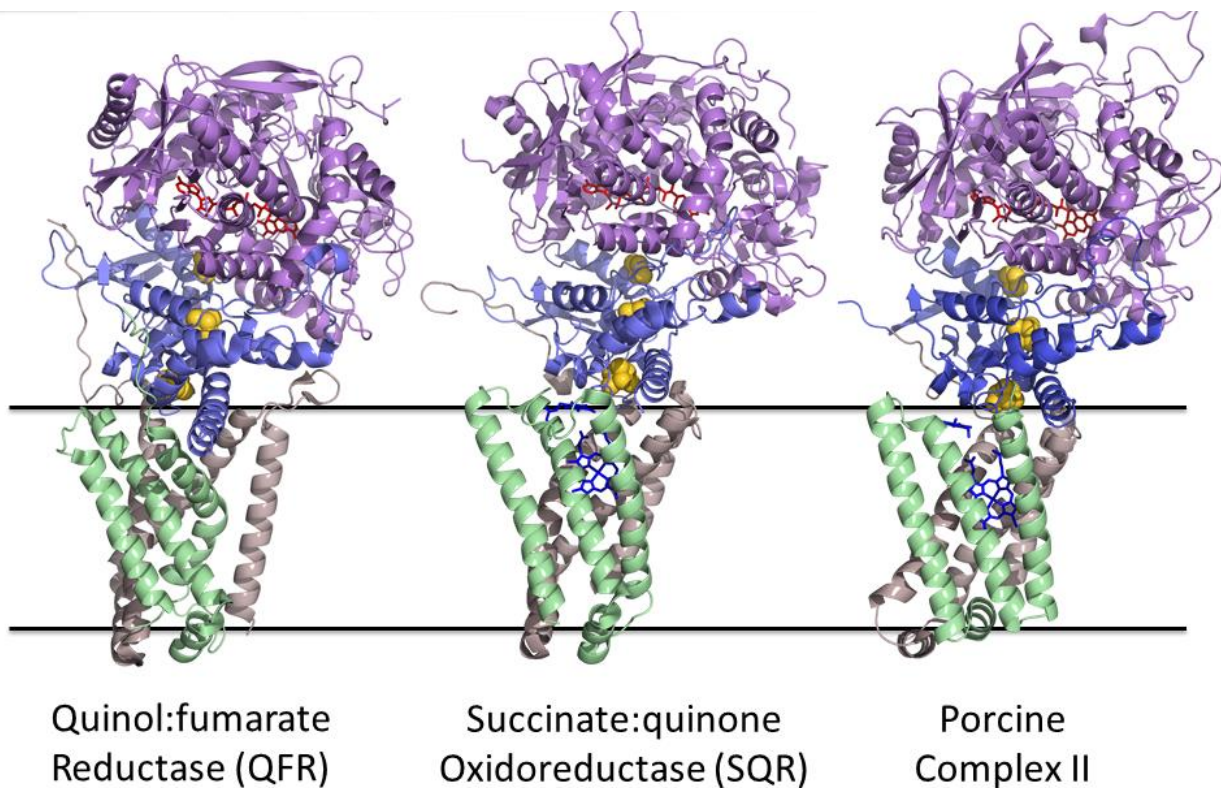
Figure 1.4: Comparison of representative Complex II superfamily structures. The structures of the E.coli bacterial homologs QFR (PDB 3P4P) and SQR (PDB 1NEK) are compared to a mammalian complex structure (PDB 3AEE)). The flavoprotein domain (purple) is shown with bound FAD (red sticks). The iron-sulfur subunit is shown in blue with 3 iron-sulfur clusters as yellow spheres. The membrane spanning subunits of the SQR and Complex II are shown with bound quinone and heme (blue sticks).

Structural approaches to membrane protein crystallography and complex structures

Membrane proteins are historically difficult to crystallize and currently represent less than 2% of the structures in the Protein Data Bank (49). Due to the physical and chemical

properties of membrane proteins, including the need for stabilization in a membrane like environment, obtaining the large quantity of pure, well-folded protein required for more traditional crystallization methods can be challenging. However, membrane proteins play important roles in cell vitality and many therapeutics target proteins on the cell surface, with over 50% of drugs targeting one of four classes of membrane proteins (50). As such, improvement of current methods for membrane protein crystallization or the development of alternative methods is important.

Traditionally, membrane proteins have been crystallized after stabilization in detergent micelles followed by a search for the appropriate crystallization conditions that result in crystals that are homogenous in composition and regular in structure. Screening for detergents that support a solubilized membrane protein in a stable, native state is required and complicated by the purity of the detergent itself in solution. A number of techniques have been proposed to identify the optimal detergents and to increase membrane protein stability, including the rapid screening of detergents (51) and improving stability with by adding additional lipids (52), searching for mutants with increased stability and even the design of nanobodies for stabilization (53).

Newer methods in protein crystallography have provided alternatives to the more traditional approach. Among these, lipidic cubic phase crystallization has proven a powerful method for the crystallization of challenging membrane proteins. In this method, membrane proteins are crystallized in a three-dimensional lipid matrix which mimics the hydrophobic lipid bilayer of the native membrane environment and provides adequate diffusion space to support nucleation and the growth of crystals (54). This method has been used to obtain high resolution structures of several high impact membrane protein targets, including the β(2) adrenergic

receptor (55) and a human glucose transporter at 1.5Å resolution (56), and has significantly impacted the number of membrane protein structures in the PDB, with over 350 records currently noted in the PDB.

Summary

The study of flavoproteins has extended over 100 years, yet major discoveries continue to be made. The increasing availability of biochemical and structural information has increased our understanding of flavoenzyme chemistry and the specific advantages conferred by tethering an FAD or FMN molecule to the enzyme via covalent linkage. The recent identification of assembly factors with differing roles in the process of covalent flavinylation highlights that there are still unexplored areas of chemical biology within a seemingly mature field. The quinone methide mechanism, for example, was developed prior to knowledge of these assembly factors. While the mechanism appears plausible even with assembly factors, it may not prove be applicable in cases where an assembly factor is required. Investigation of these assembly factors has the potential to reveal new insights into the mechanism of covalent bond formation in Complex II superfamily members, which will expand our understanding of flavin reactivity in biology.

CHAPTER 2

THE *ESCHERICHIA COLI* FLAVINYLATION ASSEMBLY FACTOR ACTS DIRECTLY IN
ASSEMBLY OF THE MATURE FLAVOPROTEIN RATHER THAN AS A SIMPLE FAD
TRANSPORTER

Work included in this chapter was published in as part of a review in eLS online library in
September of 2015 entitled "Flavoenzymes: Covalent versus Noncovalent" and authored by
Chrystal Starbird, Elena Maklashina, Gary Cecchini and Tina Iverson.

Introduction

The *Escherichia coli* assembly factor, SdhE, is conserved through all kingdoms of life
and is important for covalent incorporation of the FAD cofactor into QFR and SQR. It has been
proposed that SdhE may act as an FAD transporter or as an assembly factor for FrdA that either
stabilizes a conformation of the succinate dehydrogenase flavoprotein conducive to the
formation of a covalent linkage or directly contributes a catalytic residue that activates FAD for
the linkage. Structural and functional studies have provided the insights into the role of SdhE in
covalent flavinylation, but have not yet resolved the mechanism of SdhE action. The structure of
E. coli SdhE was the first homolog of this large superfamily to be determined (**Figure 2.1**) (57),
albeit before the true function of this protein was known. Known as YgfY at the time, the
structure revealed a five-helix bundle with no apparent FAD binding site. However, work done
in Serratia supported the model that SdhE binds FAD directly, even covalently (41), and acts as
an FAD transporter.

Nuclear magnetic resonance (NMR) work with the yeast counterpart Sdh5 (58) identified a highly conserved surface of residues (**Figure 2.1A, B**) proposed to function as the site of protein-protein interaction. Scanning mutagenesis of SdhE confirmed that residues within the conserved surface are important for the function as a flavinylation-promoting factor. Specifically, scanning mutagenesis identified both an RGxxE motif and an N-terminal arginine residue within this conserved surface as important for the protein's function (59). Furthermore, mutation of this N-terminal arginine (Arg8 in *E. coli* SdhE) to an aspartate seemed to result in a more stable complex with flavoprotein.
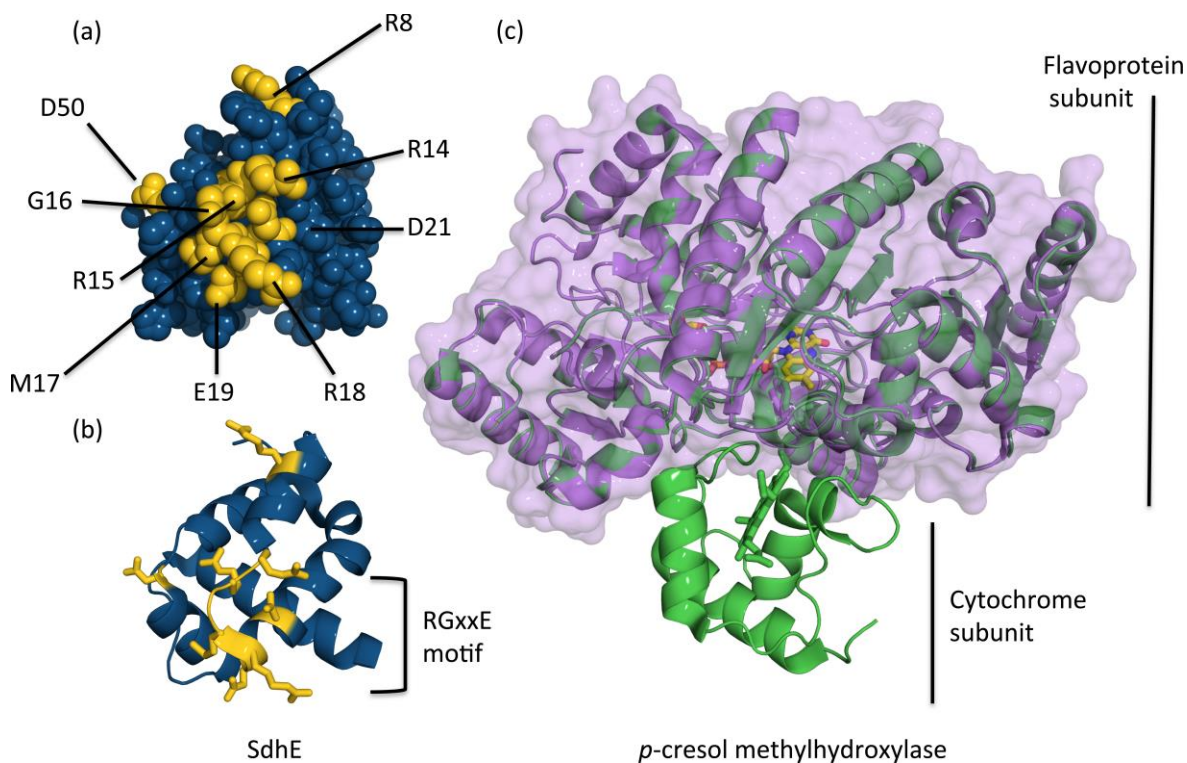
Figure 2.1: A. Space filling model of SdhE (PDB 1X6J, blue (57)) with the most highly conserved residues shown in gold. B. Ribbons model of SdhE shown in the same orientation as panel, with the RGxxE motif highlighted (A). C. Alignment of the structures of *p*-cresol methylhydroxylase (60) with (PDB 1WVE, green) and without the cyctochrome subunit (PDB 1WVF, purple) identifies slight conformational changes in the flavoprotein upon cytochrome association. Figure originally published in eLS review (1).

In parallel, work on succinate dehydrogenase and quinol:fumarate reductase investigated how the SdhE assembly factor might interact with each of those flavoproteins. Circular dichroism suggested that the flavoprotein subunit of succinate dehydrogenase is fully folded prior to interaction with the assembly factor and contains non-covalently bound FAD (59). These findings were supportive of an alternative role for SdhE, where it acts as an assembly factor rather than an FAD transporter. This proposed mode of action for SdhE has parallels to that proposed for *p*-cresol methylhydroxylase, a multisubunit enzyme that contains both a flavoprotein subunit with an 8α-O-tyrosyl linkage to the FAD and a heme-containing cytochrome subunit. Interestingly, interaction between the flavoprotein subunit and the cytochrome subunit is required for covalent flavin incorporation (61). A comparison of the structures of *p*-cresol methylhydroxylase with and without the cytochrome subunit revealed small but significant conformational changes to the enzyme in the area surrounding the FAD binding site associated with cytochrome interaction (**Figure 2.1C**) (60). These structures suggested that the cytochrome subunit orients key FAD binding residues for catalysis of the covalent bond. It is worth noting that although an ancillary polypeptide chain is required for catalysis, covalent flavinylation is still considered an autocatalytic reaction since the cytochrome subunit is a part of a stable complex.

Materials and Methods

Cloning and expression of SdhE and SdhE R8D mutant

Wild-type and variant SdhE were expressed from the T5 promoter of a plasmid engineered after cloning into the pQE-80L and pQE-30 (Qiagen) vectors. To generate the plasmids, the *E. coli ygfYX* operon was synthesized with a 5' *BamHI* site and a 3' *SalI* site for

20

insertion into the Qiagen vectors (43). In *E. coli*, YgfX (or SdhE) is part of an operon also containing a putative membrane protein YgfX. In order to prevent expression of *ygfX*, a stop codon was introduced after SdhE. The resulting plasmid encodes an IPTG inducible *SdhE* gene with an N-terminal His$_6$ tag that contains a Factor Xa cleavage site in the pQE-30 derived construct. The SdhE-R8D variant was generated by QuikChange site directed mutagenesis (Agilent Technologies). The resultant plasmids were transformed into either *E. coli* strain DW35, where both the *frd* and *sdh* operons are disrupted via the insertion of a kanamycin gene (62) or BSV11, a riboflavin auxotrophic strain (38).

For growth in DW35, LB supplemented with ampicillin (150 µg/ml) (2 ml in a 14 ml round bottom Falcon tube) was inoculated with a single colony. The cells were grown overnight at 37 °C with 220 rpm shaking. The overnight culture was used to inoculate 1 L of LB supplemented with ampicillin (150 µg/ml) and cells were grown at 37 °C with shaking until an OD$_{600}$ of approximately 1.0 was achieved. Expression was induced with the addition of 1 mM IPTG and growth resumed at 37 °C for 4 hours. Cells were harvested by centrifugation at $9200 \times g$ and stored at -80 °C. For growth in BSV11, all conditions were the same except as noted. The initial culture was supplemented with kanamycin (50 µg/ml), ampicillin (150 µg/ml) and riboflavin (100 µg/ml). The overnight culture was then used to inoculate 1 L of LB also supplemented with kanamycin (50 µg/ml), ampicillin (150 µg/ml) and riboflavin (100 µg/ml). Once an OD$_{600}$ of ~0.6 was achieved, cells were washed by three cycles of gentle centrifugation followed by resuspension in riboflavin-free LB. After the last wash, expression was induced with the addition of 1 mM IPTG and grown overnight at 18 °C. Cells were harvested by centrifugation at $9200 \times g$ and stored -80 °C.

Cloning and expression of flavoprotein

Flavoprotein (FrdA) was expressed using a three different strains from *E. coli*. For wild-type holoenzyme, FrdA was obtained from the ASKA Library of clones (63). Individual genes from this library are cloned from *E. coli* K12 W3110 into the high copy number plasmid pCA24N. This plasmid has a modified pMB1 replication origin (same as pQE30 from Qiagen) and chloramphenicol resistance. The cloned ORF is under control of the IPTG-inducible T5-lac promoter. The resulting plasmid encodes *FrdA* gene with an N-terminal His_6 tag. The plasmid from this clone was also transformed into a ΔSdhE strain obtained from the Keio deletion collection (64), where the *SdhE* gene is disrupted by the insertion of a kanamycin resistance cassette. Lastly, the FrdA-containing pCA24N plasmid was transformed into BSV11, the riboflavin auxotrophic strain described above, both separately and co-transformed with the plasmid encoding SdhE.

For growth in AG1, LB supplemented with chloramphenicol (34 µg/ml) was inoculated with a single colony. The cells were grown overnight at 37 °C with 220 rpm shaking. The overnight culture was used to inoculate 1 L of LB supplemented with chloramphenicol (34 µg/ml) and cells were grown at 37 °C with shaking until an OD_{600} between 0.4 and 0.6 was achieved. Expression was induced with the addition of 1 mM IPTG and growth resumed at 37 °C for 3-4 hours. Cells were harvested by centrifugation at $9200 \times g$. For growth in ΔSdhE, cells from a single colony were used to inoculate LB supplemented with chloramphenicol (34 µg/ml) and kanamycin (50 µg/ml). The cells were grown overnight at 37 °C with 220 rpm shaking. The overnight culture was used to inoculate 1 L of LB with antibiotics and cells were grown at 37 °C with shaking until an OD_{600} between 0.4 and 0.6 was achieved. Expression was induced with the addition of 1 mM IPTG followed by overnight growth at 18 °C. Cells were harvested by

centrifugation at 9200 × *g*. FrdA was expressed in BSV11 under the same conditions as indicated above for SdhE grown in the same strain.

Purification of isolated SdhE and flavoprotein

Following cell disruption by sonication in 25 mM Tris pH 7.4 with complete protease inhibitor tablets (Roche), wild-type SdhE, SdhE-R8D and FrdA were purified first by nickel affinity chromatography. Lysate was cleared by centrifugation at 34,000 x *g* and applied to a nickel column in buffer containing 25 mM Tris pH 7.4 and 100 mM sodium chloride (NaCl), and eluted with a linear imidazole gradient from 25 mM to 300 mM. The imidazole concentration was reduced via three rounds of 1:10 dilution and reconcentration using a 3 kD and 30 kD molecular weight cut-off filter (Amicon) for SdhE and FrdA, respectively. For SdhE expressed from pQE-30, the His$_6$ tag was cleaved overnight with the addition of 1 unit/μl of Factor Xa Protease (NEB) followed by a repeat nickel purification in which the flow through was collected. For SdhE and SdhE-R8D, nickel purified protein was then concentrated as above and injected onto a Superdex75 column. This gel filtration step was used to exchange into various buffers including only Tris pH 7.0-8.0, MES pH 6.0-6.5, HEPES pH 7.5-8.0, and potassium phosphate buffer pH 8.0. For SdhE grown in DW35, the average protein yield of ~40-60 mg per Liter of culture was much higher than resulted from growth in BSV11, which yielded ~5-15 mg per Liter of culture (for SdhE-R8D and wild-type SdhE, respectively). A similar pattern was observed for FrdA, where the yield was lowest in the BSV11 strain, followed by ΔSdhE. The highest yield was obtained when expressed in the AG1 strain (~40 mg/L). Protein concentration was determined using the Bradford assay.

Purification of co-expressed SdhE and FrdA

Lysate from FrdA and SdhE co-expressed in BSV11 was cleared by centrifugation at 34,000 x *g* and applied to a nickel column in buffer containing 50 mM Tris pH 7.4, 100 mM sodium chloride (NaCl) and 5% glycerol, and eluted with a linear imidazole gradient from 25 mM to 500 mM. The imidazole concentration was reduced via dilution and reconcentrated using a 30 kD molecular weight cut-off filter (Amicon) in buffer containing no salt. The protein was concentrated and further purified by gel filtration.

Crystallization of SdhE and SdhE-R8D

Wild-type SdhE was initially crystallized using previously published conditions using protein with and without cleaved polyhistidine tag (57). The resultant crystals were grown using hanging-drop vapor diffusion method in drops set up with 1 µl of protein solution (15-20 mg/ml in 25 mM Tris pH 7.4) and 1 µl of the reservoir solution at 20° C. Crystals used for diffraction grew over the reservoir solution containing 0.9-1.3 M sodium malonate solution buffered with 0.1 M Tris HCl (pH 7.5-8.0). Additional crystals of SdhE grew in 0.8-1.2 M sodium citrate tribasic buffered with 100 mM imidazole pH 8.0. Broad crystallization screens of SdhE with and without FAD were set up using a Mosquito nanoliter drop setter in a high-throughput crystallization core as part of the Vanderbilt Center for Structural Biology. As a result of these screens, additional crystals of SdhE were optimized in 0.8-1.2 M sodium citrate tribasic buffered with 100 mM imidazole pH 8.0. Crystals were cryo-protected with a solution that was 80% reservoir solution and 20% of a 1:1 mix of glycerol and ethylene glycol, and flash freezing with liquid nitrogen. Crystals were screened for X-ray diffraction at a temperature of 100 K using a wavelength of ~1 Å and a MarMosaic225 CCD detector at the Advanced Photon Source (Argonne, IL) LS-CAT beamlines 21-ID-G and 21-ID-D.

Gel filtration studies with and without FAD

FrdA protein isolated from strains lacking endogenous *frdA*, flavin or SdhE were combined with SdhE grown in DW35 (cleaved or uncleaved), SdhE grown in BSV11 and the SdhE-R8D variant and run over a Superdex75 gel filtration column. The samples were incubated using various iterations with respect to concentration and incubation time prior to gel filtration. In some of the samples, 1 to 50 µm FAD or 2-10 mM dicarboxylate were added. SdhE proteins were also incubated with FAD in isolation followed by gel filtration.

Mass spectrometry

Purified samples of wild-type SdhE and FrdA were independently separated by SDS-PAGE. Bands that were clearly visible after the final purification step were excised and subjected to in-gel trypsin digestion. For FrdA, this included the ~67 kDa band corresponding intact FrdA and a band of unknown origin at ~45 kDa. For SdhE, an ~10 kDa band was isolated corresponding to SdhE and an ~22 kDa band of unknown origin. The resulting peptides were analyzed by a LC-MS/MS analysis. MS/MS spectra were searched via SEQUEST again an *E. coli* database. Identifications were filtered and collated at the protein level using Scaffold (Proteome software). Mass Spectrometry was undertaken at the Vanderbilt Mass Spectrometry Research Center.

<div align="center">

Results and Discussion

</div>

Analysis of SdhE expression and purification

SdhE expressed from the Qiagen vectors was purified using two chromatography steps: nickel affinity and gel filtration. Following a single pass of size exclusion, the protein was sufficiently pure for crystallization (**Figure 2.2A**). However, if the protein was overloaded on the

gel, bands at ~22 kDa and ~67 kDa were observed (**Figure 2.2B**). Mass spectrometry of the

excised bands confirmed the presence of SdhE in the predominant band, with 96% coverage. The

~22 kDa band was identified as primarily belonging to catabolite gene activator, a mostly

uncharacterized gene identified by sequence homology to transcription factors. The ~67 kDa

band was identified as having peptides from both *E. coli* FrdA (QFR) and SdhA (SQR). It was

also observed in fractions corresponding to a relatively small peak that eluted following the void

volume and appeared to be slightly overexpressed in cultures expressing SdhE (as compared to

the corresponding band in E. coli cultures not used for SdhE or flavoprotein expression) (**Figure

2.2A, lane 1**). While the presence of flavoprotein in gel filtration fractions cannot reliably

confirm an interaction with SdhE, it is supportive of that possibility.
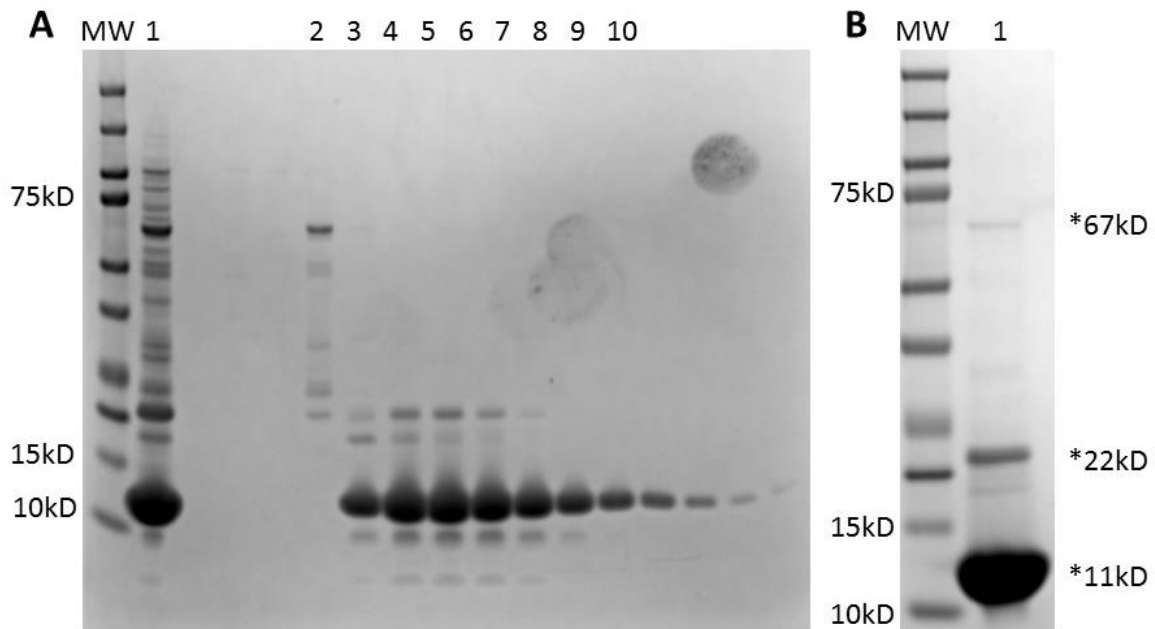
Figure 2.2: A. Cleared lysate (lane 1) and gel filtration fractions were loaded onto a NuPAGE 4-12% Bis-Tris protein gel. Lane "MW" is a molecular weight marker (Precision Plus Standard). Lane 2 is from a peak that eluted after the aggregate peak and the peak corresponding to SdhE begins in lane 3. B. Pooled fractions from size exclusion run on a NuPAGE 4-12% Bis-Tris protein gel. The starred bands are those that were excised for mass spectrometry analysis.

Crystallization of SdhE

As a crystal structure of E. coli SdhE was already published by a structural genomics group at 1.2 Å resolution (57), our goal was to determine the SdhE structure as a complex with either FAD or flavoprotein. As SdhE was believed to bind FAD tightly, possibly even covalently, a structure with bound ligand seemed a reasonable place to start. Sparse matrix screening of previously published conditions resulted in crystals with a hexagonal morphology that appeared form from multiple plates (**Figure 2.3A**). Attempts to further optimize the quality of these crystals included altering the temperature for crystal growth (4 °C-25 °C), the pH and salt concentration in the reservoir solution, the drop ratio and size and seeding, and were unsuccessful.
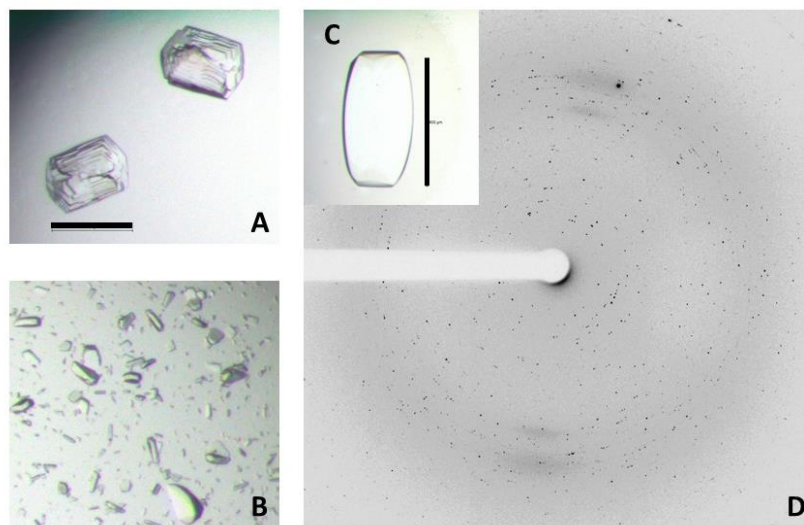
Figure 2.3: A. Crystals of SdhE grown after optimization of previously published conditions (57). The black line represents a marker for 150 µm. B. Representative image of crystals grown in broad crystallization screens. C. Example of crystal grown as a result of optimization of positive crystal hits from broad crystallization screening. The black line represents a marker for 400 µm. D. Example of diffraction obtained from screening of initial SdhE crystals (seen in panel A). Resolution limit is ~ 1.3 Å.

Similar screening was also done using SdhE with a cleaved polyhistidine tag and did not result in better quality crystals. These crystals were screened for x-ray diffraction and diffractions spots were observed to 1.3 Angstroms, although the diffraction was of poor quality (**Figure 2.3B**). Broad crystallization screening resulted in several new conditions for crystal growth that were further optimized to yield improved crystals in sparse matrix screening (**Figure 2.3C**).

Once optimized conditions for SdhE crystal growth were determined, efforts were made to soak these crystals with FAD at various time points and with various concentrations. At no time was successful crystal soaking observed as determined visually (FAD is yellow) and tested with diffraction. Efforts to co-crystallize SdhE with FAD were also unsuccessful. Co-crystallization was attempted using crystallization conditions previously established for SdhE either through published conditions or broad screening and by setting up new broad screens with SdhE and FAD incubated at various ratios. Small, needle like crystals were observed as a result of these screens and these conditions were scaled up for optimization. However, diffraction patters obtained during screening were consistent with these being crystals of FAD alone.

Gel filtration studies with isolated SdhE and FAD

As the current literature suggested FAD bound very tightly and possibly covalently to the small, alpha helical protein, SdhE, difficulty obtaining co-crystals was not anticipated. However, crystallization can be challenging and there are numerous possible explanations for why this might occur. For example, it is possible that the conformation of SdhE in the crystal lattice precluded FAD binding and that conditions suitable for crystallization of an SdhE;FAD complex were not tested for either in the broad screens or using previous crystallization conditions. However, it would be reasonable to expect that a tight interaction would be maintained through

28

size exclusion. Using an AKTA purification system capable of monitoring up to three simultaneous wavelengths, we monitored SdhE fractions for the presence of flavin. FAD exhibits absorbance at 375 nm and 450 nm.

Absorbance at 375 nm or 450 nm was not observed in the gel filtration peaks corresponding to SdhE in any of the samples purified normally (**Figure 2.4A**). As a result, SdhE samples were incubated with FAD at concentrations from 5 µm to 1mm and at time periods from 30 minutes to overnight. This approach was considered reasonable, as the published protocol required an overnight incubation of purified SdhE (0.85 mg/ml) with FAD at a concentration of 200 µm followed by dialysis to remove excess FAD (41). Absorbance at wavelengths corresponding to FAD was not observed in any of the samples of SdhE pre-incubated with FAD (**Figure 2.4B**).
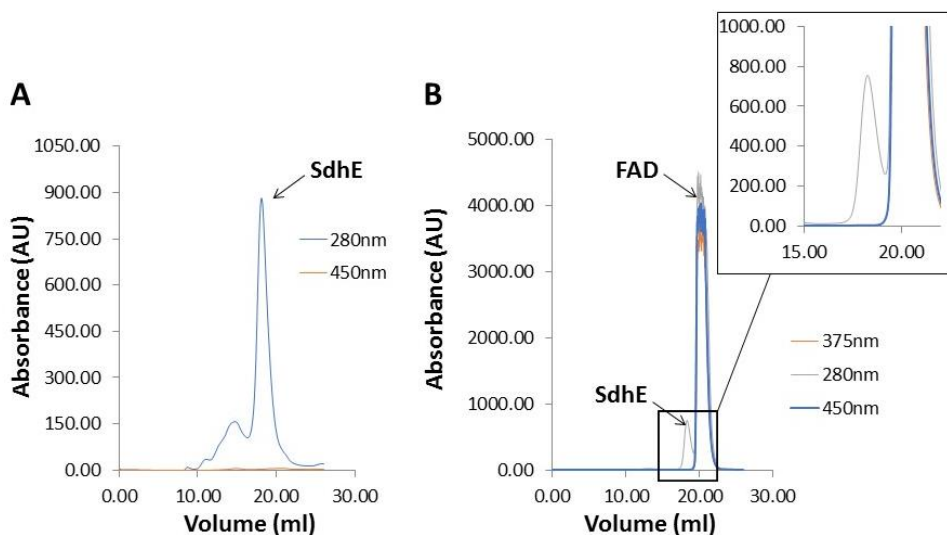
Figure 2.4: A. Representative elution profile for gel filtration of isolated SdhE. The first major peak was identified as primarily corresponding to flavoprotein (as seen in Figure 2.2). The SdhE peak is identified with an arrow. B. Representative elution profile for gel filtration of purified SdhE incubated with FAD. Zoomed window shows a close up of the SdhE peak to demonstrate that no overlapping absorbance is seen at the wavelengths corresponding to FAD (375 nm or 450 nm).

While size exclusion cannot be substituted for more direct studies of binding, the lack of absorbance corresponding to FAD within the SdhE peaks and the inability to obtain ligand bound crystals, either by soaking or through additional screens, suggested that FAD might not bind tightly or covalently to SdhE. Furthermore, UV fluorescence was not observed in any of our SDS-PAGE gels corresponding with the SdhE band. As FAD exhibits UV fluorescence and covalently bound flavin survives the denaturing conditions of SDS-PAGE, gel bands with covalently bound flavin, such as the flavoprotein subunit of fumarate reductase, can be observed with UV light illumination (43). These studies were also repeated using SdhE-R8D under similar conditions and no differences were observed from experiments using wild-type SdhE and FAD.

Gel filtration studies of SdhE with FrdA

While an interaction between FAD and SdhE could not be affirmatively ruled out, given the inability to co-elute or co-crystallize FAD and SdhE, it seemed likely that SdhE may not be a simple FAD transporter. To investigate the possibility that an interaction with FAD might require the flavoprotein, similar studies were carried out using SdhE and FrdA (from QFR) with and without FAD. These studies also preceded efforts to identify and co-crystallize the relevant SdhE:FrdA complex. In structural studies aimed at co-crystallizing two proteins, one of the early stages is often to identify conditions under which the complex might be more stable. Under the appropriate conditions, even transient complexes can often be observed on gel filtration, as a shift in the peak associated with the size of the complex.

Until this point, flavoprotein had not been isolated from the complex for any known studies in the literature. As such, it was important to identify conditions for expression and purification of stable flavoprotein. Flavoprotein expressed in the AG1 strain was covalently flavinylated and appeared to be the most stable based on gel analysis. In contrast, FrdA

expressed in a strain lacking SdhE and in BSV11, which lacked FAD, was prone to proteolysis, as demonstrated by the appearance of multiple bands on an SDS-PAGE gel of the purified protein. Purified flavoprotein from these strains also initially has two peaks on gel filtration, both of which appeared to contain flavoprotein. Mass spectrometry identified all of the purified bands as corresponding to flavoprotein and gel analysis was used to identify the first peak in size exclusion as corresponding to fractions that were mainly full-length FrdA. It was determined that overnight expression at lower temperatures reduced the amount of apparent proteolysis. Additional steps in flavoprotein purification were also determined to help reduce the level of proteolysis. Sonication time was reduced and the samples were kept cold with stirring on ice. The entire purification needed to be completed in a single day with the samples on ice. As such, gel filtration immediately followed nickel chromatography with protease inhibitor added at each step.

Purified flavoprotein and SdhE were combined for size exclusion, to determine conditions under which a complex might be observed. SdhE was combined with FrdA in three forms; with covalent flavin (from AG1 strain), with tightly but non-covalently bound flavin (from ΔSdhE strain), and without flavin (from BSV11 strain). As very little was known about the interaction between SdhE and flavoprotein, the proteins were incubated at various concentrations (up to a 10 fold excess) and time points (0 minutes to overnight) before injection onto the gel filtration column. No conditions were found under which evidence for complex formation could be seen in the gel filtration elution profile. In all cases, two clearly resolved peaks were observed corresponding to the expected elution time for each of the individual proteins (**Figure 2.5A**). FAD and dicarboxylate (fumarate and succinate) were also added in various iterations to determine if the presence of ligand might influence complex formation. However, no gel

31

filtration shifts were observed in the presence of ligand (**Figure 2.5B**). Lastly, these experiments

were repeated using SdhE-R8D, a variant expected to form a more stable complex with

flavoprotein, with the same results (**Figure 2.5C**). Fractions from these samples were also

analyzed by SDS-PAGE to look for evidence of co-purification, but no overlap was observed.
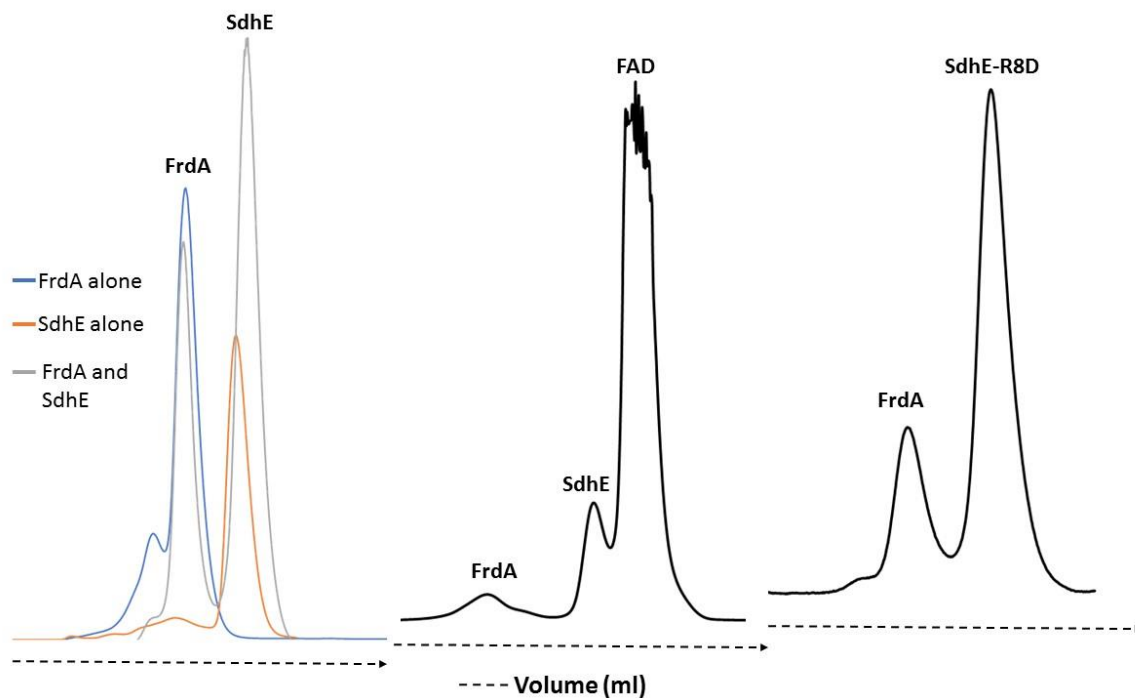
Figure 2.5: A. Representative elution profiles for gel filtration of isolated SdhE (red), isolated FrdA (blue) and combined SdhE and FrdA (gray). The elution profiles are aligned starting at the injection point. B. C. Representative chromatogram for FrdA combined with an SdhE variant, SdhE-R8D.

Gel filtration studies using SdhE and FrdA co-expressed in BSV11 had slightly different

results. Flavoprotein expressed from this strain does not have flavin and may produce a more

stable complex with SdhE, as covalent attachment of flavin is expected to coincide with the

release of SdhE. The elution profile for SdhE and FrdA had a third peak in-between the peaks

corresponding with FrdA and SdhE. This peak was consistent (in all BSV11 runs) and not

observed in any of the previous gel filtration studies with SdhE and FrdA. A complex between

SdhE and FrdA is ~80 kD and should elute from the gel filtration column before FrdA, making

this an unexpected observation. Surprisingly, fractions from this peak showed the presence of

both FrdA and SdhE (**Figure 2.6**). This contrasted previous gel filtration studies with FrdA and

SdhE, where SDS-PAGE gels showed no overlap between the two proteins and supported two

independent peaks. Although the appearance of a third peak for FrDA and SdhE expressed in

BSV11 and the overlapping fractions might be suggestive of a more stable interaction, based on

the expected size of the complex (~80 kDa), this seemed unlikely. However, these fractions were

collected and used in crystallization studies.
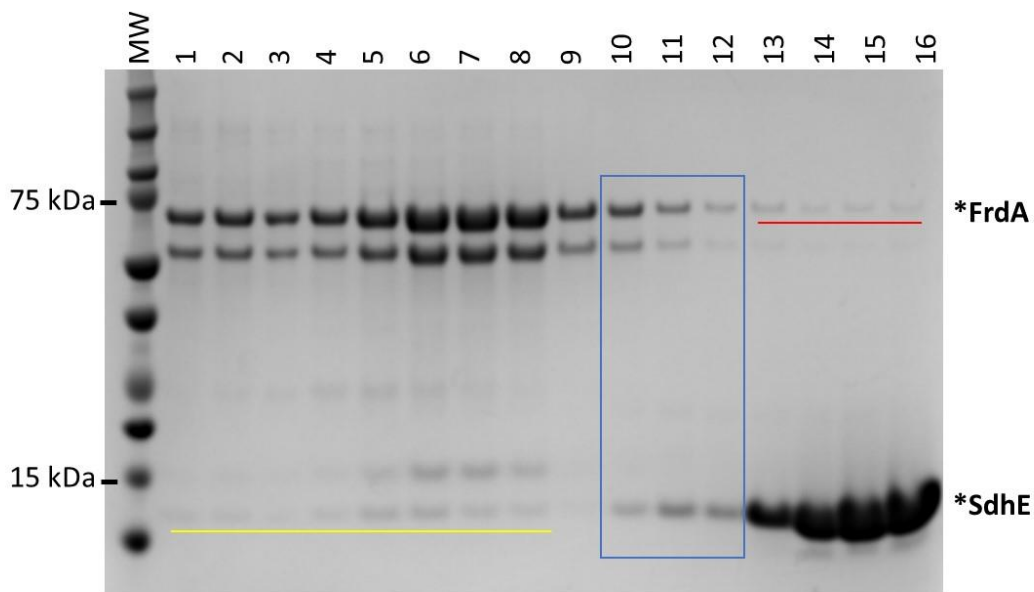
Figure 2.6: A. Representative SDS-PAGE gel of fractions eluted from gel filtration for SdhE and FrdA co-expressed in BSV11. The blue box highlights fractions corresponding to a relatively small third peak observed in the chromatograms from these samples. In past gels, SdhE was not observed in any of the fractions associated with the flavoprotein, even when a large quantity was loaded onto the gel, but was observed in these samples (underlined in yellow). FrdA, underlined in red, has been observed to overlap with SdhE in gel filtration profiles for samples expressed in different *E. coli* strains and combined.

Crystallization of SdhE and FrdA

Although complex formation was not observed under the conditions for size exclusion, we attempted to co-crystallize SdhE and FrdA. In addition to the BSV11 fractions outlined above, co-crystallization was also attempted combining FrdA expressed from ΔSdhE with SdhE. The proteins were concentrated (3-9 mg/ml isolated from BSV11 and 5-25 mg/ml in other samples) and standard broad crystallization screens from Hampton and Rigaku set up using a Mosquito robot using 3-well Griener plates. Using a Rock Imager, wells containing crystallization drops were visually screened for crystals using natural and UV light. Under the conditions tested, no crystals were observed that contained the FrdA and SdhE complex. Crystal growth was observed, but contained either salt or SdhE alone.

Summary

The results presented here provide early evidence that SdhE does not act as a simple FAD transporter and that SdhE likely has an alternative role in the mechanism of covalent flavin attachment. Indeed, these results agreed with findings that were published after this work in which NMR titration studies showed no evidence of FAD binding to SdhE (58). This made a role as a flavoprotein assembly factor more likely, but our studies were unable to demonstrate a direct interaction between SdhE and FrdA using purified protein. Work done in the yeast counterparts also failed to demonstrate an interaction between recombinant flavoprotein and SdhE (unpublished observation), despite *in vivo* work that suggested a direct interaction. These results argued that either the interaction was not direct or more likely that we had not yet found conditions that permitted an interaction between these two proteins.

CHAPTER 3

FLAVINYLATION ASSEMBLY FACTORS PROMOTE CONFORMATIONAL CHANGES
THAT SUPPORT AUTOCATALYTIC COVALENT FLAVIN ATTACHMENT IN
COMPLEX II HOMOLOGS

Work included in this chapter was published in *The Journal of Biological Chemistry* in 2016
entitled "Binding of the Covalent Flavin Assembly Factor to the Flavoprotein Subunit of
Complex II" and authored by Elena Maklashina, Sany Rajagukguk, Chrystal Starbird, Hayes
McDonald, Anna Koganitsky, Michael Eisenbach, Tina Iverson and Gary Cecchini.

Introduction

Escherichia coli harbors two highly conserved homologs of the mitochondrial respiratory
Complex II, both capable of the bidirectional interconversion of succinate and fumarate (65).
Normally, under aerobic conditions SQR is synthesized to participate in its electron transport
chain while QFR is primarily synthesized under anaerobic conditions. Both QFR and SQR
contain a covalently bound FAD that is required for succinate oxidation and without which
fumarate reduction activity is reduced (23). For many years incorporation of this essential flavin
cofactor was considered to be autocatalytic (36,37,40), but the identification of an assembly
factor, termed SdhE in bacteria, that was important for covalent attachment raised the possibility
that this was not entirely an autocatalytic process (34). Early work suggested that SdhE was not a
simple FAD transporter and was likely to function as an assembly factor (58), either through
direct participation in the chemistry associated with covalent flavin linkage or by facilitating the

proper folding in FrdA to support autocatalysis. However, it was unclear as to how SdhE might facilitate formation of the covalent bond and how it might interact with flavoprotein.

Although Complex II enzymes have been well studied, very little was known about assembly of the mature complex. This further complicated efforts to understand the role of SdhE in covalent flavinylation, as it was unclear at which stage in assembly SdhE interacted with the flavoprotein. Immunoprecipitation studies in the yeast and bacterial counterparts indicated that the assembly factor binds directly to the flavoprotein subunit of Complex II enzymes (34,41,42). In our studies, however, we were unable to establish evidence for a direct interaction between recombinant assembly factor and flavoprotein from *E. coli*. Working with our collaborators in Gary Cecchini's laboratory, we developed a method to stabilize the interaction between SdhE and FrdA in E. coli using *in vitro* photoaffinity crosslinking methods. This allowed us to investigate the molecular mechanism of assembly of the covalent linkage and the role of SdhE in this mechanism. In addition, this stable, covalently-crosslinked complex was an excellent candidate for co-crystallization of the SdhE:FrdA complex, with the potential to provide more insight into the role of SdhE in covlalent flavinylation.

Materials and Methods

Expression and purification of isolated FrdA subunits

Isolated FrdA was expressed in *E. coli* strain RP-2 (*ΔfrdABCD, ΔsdhCDAB*) a plasmid that inserted an additional stop codon after the *frdA* gene in the pH3 plasmid (43). Expression is induced under micro-aerophilic conditions, which is achieved in Terrific Broth (TB) medium by increasing the culture volume in the flasks (1.6 L in a 2 L growth flask), and reducing the shaking to 160 rpm. Cells were harvested by centrifugation at 9200 x *g* and stored at -80°C. The

cells were then resuspended in 20 mM potassium phosphate pH 7.4 with complete protease

inhibitors (Roche). Cells were lysed by three cycles of vortexing (3 min) with protein extraction

beads (diameter < 1 mm) followed by a freeze-thaw at -20 °C. Lysate was cleared by

centrifugation at 34,000 x g and the supernatant was stored at -20° C. For photocrosslinking

experiments, no additional purification was performed.

Expression and purification of SdhE containing the artificial amino acid pBpF

The *sdhE* gene with an amber codon substituting R8 was cotransformed with the

pEVOL-pBpF to express pBpF-containing SdhE into a triple deletion strain RP-3

(*ΔsdhΔfrdΔsdhE*) (43). The pEVOL-pBpF (catalog no. 31190) and pEVOL-pAzF (catalog no.

31186) vectors were obtained from Addgene (Cambridge, MA). Site-directed variants were

obtained from the Cecchini laboratory at UCSF and constructed using the QuikChange II XL

site-directed mutagenesis kit (Agilent). SdhE-R8BpF was grown in LB medium containing 0.5

mM para-benzoyl-1-phenylalanine (BpF). After 1 hr, the temperature was adjusted to 30 °C.

SdhE-R8BpF was induced by the addition of 0.1 mM isopropyl β-D-1-thiogalactopyranoside

(IPTG) and the tRNA synthase/tRNA for pBpF was induced with 0.2 mM arabinose. Cells were

harvested by centrifugation and lysed by sonication. The lysate was cleared of cellular debris by

centrifugation for 45 min at 34,000 × g. SdhE-R8pBpF was purified by nickel affinity

chromatography.

Far-UV CD spectroscopy

Wild-type SdhE and two SdhE amber variants (R8BpF and M17BpF) were purified by

the addition of a gel filtration step (Superdex 200 Increase column) following the nickel

purification described earlier. Spectra were collected on a Jasco J-810 CD spectropolarimeter

using the Spectra analysis program. Spectra were collected at 20 °C using a 0.1 cm path length

quartz cuvette. Measurements were taken from 190 to 260 nm in 1 nm intervals. Secondary structure was analyzed using the DichroWeb analysis server (66). Data are the average of two runs and have been corrected for the subtraction of the buffer spectra.

Crosslinking of FrdA subunits to pBpF-incorporated SdhE

Purified His$_6$-SdhE-R8BpF was mixed with *E. coli* strain RP-2 lysate containing overexpressed and untagged FrdA in a Corning 6-well plate on ice. Crosslinking was induced by illumination with 365 nm light (Black-Ray 100 Watt UV lamp). The SdhE-FrdA crosslinked complex was purified by Ni^{2+} affinity chromatography and analyzed by SDS-PAGE, where a characteristic shift in molecular weight was observed. The presence of SdhE in the shifted band was verified by Western analysis with a primary antibody against the His$_6$-tag; the presence of FrdA in the shifted band was confirmed by monitoring UV fluorescence. Protein concentration was determined using the Bradford assay

Analysis of cross-linked products by mass spectrometry

Purified samples of crosslinked SdhE variants and FrdA were separated by SDS-PAGE and the ~80 kDa band corresponding to SdhE-R8BpF-FrdA was excised and subjected to in gel trypsin digestion, whereas complexes arising from the SdhE-M17BpF-FrdA were subjected to in-gel chymotrypsin digestion. The resulting peptides were analyzed by a LC-MS/MS analysis, as described (43). MS/MS spectra were searched via SEQUEST again an *E. coli* database. Identifications were filtered using Scaffold (Proteome Software) and confirmed the presence of SdhE:FrdA complex within the excised bands. The StavroX program was used to identify cross-linked peptides. Extracted ion chromatograms and modeling of predicted isotopic proportions were performed using Skyline. Mass Spectrometry was undertaken at the Vanderbilt Mass Spectrometry Research Center.

Molecular docking analysis

Docking was performed in two stages. Initial docking between the *E. coli* FrdA subunit

of QFR (PDB code 1KF6) (67) and SdhE (PDB code 1X6I) (57) with both the distal N and C

termini removed was performed using ZDOCK (68). Initial docking calculations constrained

SdhER8, SdhE-M17, FrdA-M176, and FrdA-E460 as part of the binding surfaces. The top 10

poses were manually curated; the pose that most closely satisfied the cross-linking distances was

selected for use as a starting point for high resolution docking in Rosetta v2015.19 (69).

Docking in Rosetta included distance restraints derived from the cross-linking data (with

a minimum distance of 9 Å and a maximum distance of 13 Å) between the β-carbons of relevant

SdhE-FrdA β-carbons. For the distance between SdhE-R8 and FrdA-M176, this was a single

constraint. Because the precise site of cross-linking to the FrdA-456-GLAMEEG- 462 peptide

could not be unambiguously determined, a series of calculations used each amino acid

(excluding the glycines) to estimate the likelihood that the cross-link could be formed at that

position. Docking was performed with and without the capping domain of FrdA. The final

calculations were performed with the restraint between FrdA-E460 and SdhE-R17, which

resulted in 168 poses that satisfied these restraints, all of which effectively formed a single

cluster.

Crystallization of the crosslinked SdhE:FrdA complex

For crystallization, the crosslinked SdhE:FrdA complex was purified by nickel affinity

chromatography followed by gel filtration using a Superdex 200 Increase 10/300 column

immediately following crosslinking by UV exposure. Fractions associated with the crosslinked

complex were isolated and further purified using an octyl sepharose Fast Flow column

(hydrophobic interaction column (HIC)) in buffer containing 25 mM Tris-HCl pH 7.4, 2 M

ammonium sulfate and a linear salt reduction gradient from 2M to 50 mM ammonium sulfate.
This was followed by an additional gel filtration step to remove aggregate and to exchange into
buffer container 25 mM Tris pH 7.4, 50 mM HEPES pH 8.0, 50 mM MES pH 6.5, 50 mM
potassium phosphate pH 8.0 or 50 mM ammonium sulfate buffered with 25 mM Tris pH 7.4.
Elution was monitored by following A_{280}. The protein was concentrated from 2-40 mg/ml and
broad crystallization screens were set up using a Mosquito nanoliter drop setter in a high-
throughput crystallization core as part of the Vanderbilt Center for Structural Biology. Standard
crystallization screens from Hampton (Index HT, Crystal Screen HT, PEG/Ion HT) and Rigaku
(Wizard Screens I-IV) were used to set up sitting drops in 3-drop 96-well Greiner CrystalQuick
trays.

Results and Discussion

Crosslinking of SdhE-BpF variants to Flavoprotein

Early attempts to isolate SdhE:FrdA complex using fully recombinant proteins failed,
likely due to the transient nature of the complex. As such, a method was devised for producing a
more stable, covalently-linked complex using photoaffinity crosslinking (70) for investigation of
the specific interaction site. Artificial amino acids were substituted at various sites within SdhE.
These sites were chosen to span the surface of SdhE and to include residues identified
experimentally to be important for an interaction with flavoprotein, such as those belonging to
the RGxxE motif in a conserved surface patch of SdhE (59).

SdhE amber variants were purified by nickel affinity chromatography in ambient light,
which was not sufficient to produce crosslinking under normal conditions. As an AKTA
purification system was used, UV monitoring at 280 nm was disrupted prior to elution from the

column. Fractions containing SdhE-xBpF were identified by SDS-PAGE. Following a reduction

of imidazole, fractions containing SdhE-xBpF were concentrated and mixed with lysate

containing overexpressed and untagged FrdA. Crosslinking did not occur when SdhE and FrdA

were combined in the absence of lysate, suggesting that is an unknown factor required to

promote their interaction. Samples were stirred on ice over the course of a 3-hour illumination

with UV light and analyzed by SDS-PAGE. Successful crosslinking can be verified by the

appearance of an ~80 kDa band associated with covalently linked complex between FrdA (~67

kDa) and SdhE (~10 kDa).

Of the amber SdhE variants tested, only SdhE-R8BpF showed the appearance of an ~80

kDa consistent with crosslinking to FrdA (**Figure 3.1A**). Positive FAD-UV fluorescence

suggested the presence of FrdA within the suspected crosslink band (**Figure 3.1B**) and

immunoblot analysis confirmed the presence of SdhE (**Figure 3.1C**). Interestingly, substitution

of this arginine with aspartate was identified in the yeast homolog as promoting a more stable

complex with flavoprotein (58). Mass spectrometry of the excised ~80 kDa band confirmed the

presence of both FrdA and SdhE-R8BpF and identified the specific site of crosslinking in FrdA

as corresponding to Met176 (43). In addition, mass spectrometry identified the prominent ~22

kDa band observed on the anti-His$_6$ blot following UV exposure (**Figure 3.1C**) as catabolite

gene activator, a transcription factor seen in our earlier expression studies with wild-type SdhE.

This finding alone does not support a role for the transcription factor in promoting the SdhE:

FrdA complex, but is an interesting finding considering that the interaction between SdhE and

FrdA has unknown elements.

An initial model was designed by manually orienting structural models of SdhE (PDB

1X6J) and FrdA (PDB 1L0V) such that Arg8 of SdhE and Met176 of FrdA were in close

proximity. Modeling highlighted several locations where SdhE and FrdA come close enough to

crosslink, but where the wild-type residues may not support the chemistry associated with

covalent crosslinking. As such, the model was used to predict locations on FrdA where the

introduction of methionine residues might induce crosslinking. Using this method, it was

determined that one of the SdhE amber variants, SdhE-R17BpF, crosslinked to several of the

methionine mutants, including FrdA K130M, FrdA G206M and FrdA-S239M. Crosslinking to

multiple methionine variants made it difficult to identify the specific site of cross-linking, but

mass spectrometry reduced the likely candidates to residues within the 456-GLAMEEG-462

peptide of FrdA.
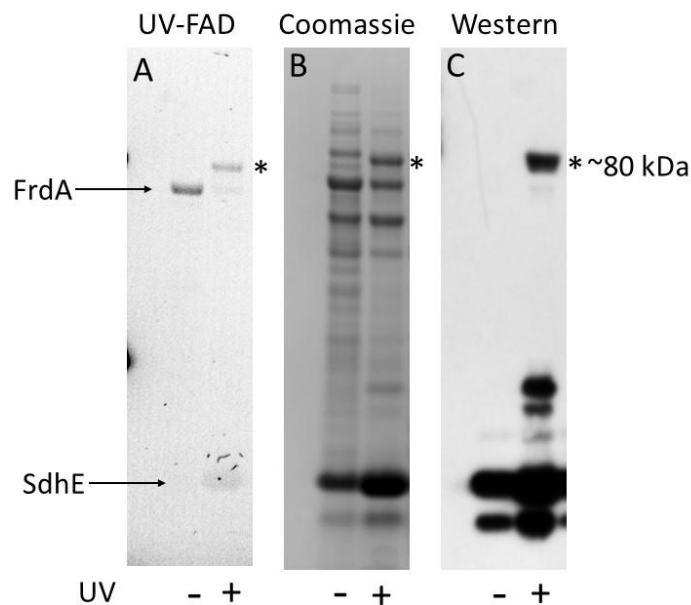
Figure 3.1: A. UV-FAD fluorescence of photoaffinity crosslinking of His-tagged SdhE-R8BpF to FrdA. FrdA containing cell lysate and nickel purified SdhE-R8BpF were incubated and exposed to UV light for ~3 hours. FrdA contains covalently bound flavin, which can be illuminated with UV light. Crosslinked samples are shown before and after exposure to UV light and the ~80 kDa band is highlighted with an asterisk. B. Coomassie Blue-stained SDS-PAGE of the same samples. C. Western blotting with anti-His antibodies of the same samples as in A and B.

To investigate whether the SdhE-BpF variants that proved positive for crosslinking to FrdA were correctly folded, these variants were purified and analyzed by far CD spectroscopy. The SdhE amber variants were purified using Ni-NTA agarose followed by gel filtration in 25 mM potassium phosphate pH 7.4. The proteins were concentrated using Amicon ultracentrifugal filters (3-kDa cutoff) and the concentration carefully measured and normalized using a standard Bradford assay. Far-UV CD spectra were collected for wild-type and variant SdhE, as well as for buffer alone. It can be seen that the SdhE-R8BpF and SdhE-M17BpF variant proteins showed a spectra similar to wild-type SdhE (**Figure 3.2**). This is consistent with a largely α-helical protein as it has been determined by the x-ray and NMR structures of SdhE and yeast Sdh5, respectively (57,58).
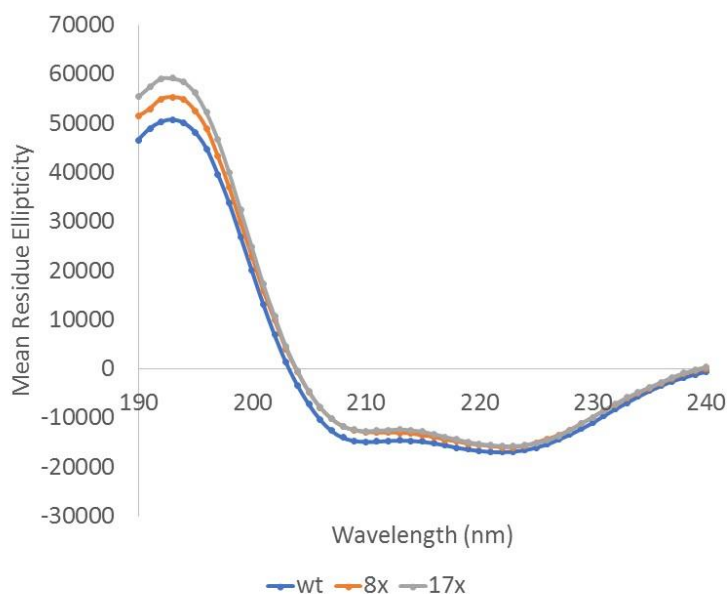
Figure 3.2: Far-UV CD spectra of purified wild-type SdhE (blue), SdhE-R8BpF (orange) and SdhE-R17BpF (gray). Data represent the average of two runs and are corrected for the subtraction of buffer spectra.

Computational modeling of the crosslinked complex

Photoaffinity crosslinking identified two distant sites of interaction between SdhE and

FrdA, namely between Arg8 in SdhE and Met176 in FrdA, and Arg17 and a 456-GLAMEEG-

462 peptide in FrdA. These sites were used as constraints in two-step modeling using ZDOCK

followed by Rosetta ligand. In ZDOCK, the two crosslinked sites were used as anchor points for

modeling using previously published structure of SdhE (PDB 1X6J) and the flavoprotein subunit

of QFR (PDB 1L0V). A crystal structure of liver oncoprotein gankyrin and the C-terminal

domain of the S6 proteasomal protein crosslinked with pBpF was used to define reasonable bond

distances as from 9 to 13 Angstroms between β-carbons (71). Using these guidelines, one model

from the ZDOCK output was selected for further refinement by Rosetta Ligand.

Initial results from modeling in Rosetta at lower resolution suggested that placement of

SdhE might be difficult without removal or re-orientation of the capping domain. In ~11, 000

docking calculations of 2 systems using the 2 constraints (initially set between 8 and 15

Angstroms for bonding distance), simulations with the capping domain in place yielded ~3000

structures, many of which had clashes upon inspection while simulations with the capping

domain removed yielded ~5000 structures. In addition, careful inspection of the ZDOCK models

indicated that the position of the capping domain of the FrdA flavoprotein in the structure might

prevent satisfaction of the distance restraints. As a result, the capping domain was removed in

subsequent docking calculations.

Higher resolution docking was completed using the distance between SdhE-R8BpF and

FrdA-M176 as a single constraint. As the site of SdhE-M17BpF crosslinking could not be

unambiguously determined using mass spectrometry, a series of calculations were completed

using each of the residues of the FrdA-456-GLAMEEG-262 peptide as a constraint, with the

exception of the glycine residues. Using this method, the greatest number of low energy poses (168 total) occurred when a constraint between SdhE-M17 and FrdA-E460 was used, suggesting that this may be the most likely site of attachment. These models generated by Rosetta were of striking similarity and effectively formed a single cluster (**Figure 3.3A**). The effectively single solution may arise from having two widely spaced constraints to define the binding location and lends confidence to the identification of both the interacting surfaces and the orientation of the two proteins in the complex. It is notable that in all of the docked poses, the conserved surface patch of SdhE (RGxxE motif) was oriented in a manner suggesting an interaction with FrdA consistent with previously reported mutagenesis. The docking poses also suggest that SdhE interacts with the same surface of the flavoprotein subunit as does the N-terminal domain of the iron-sulfur protein subunit in intact complex II (**Figure 3.3B**).
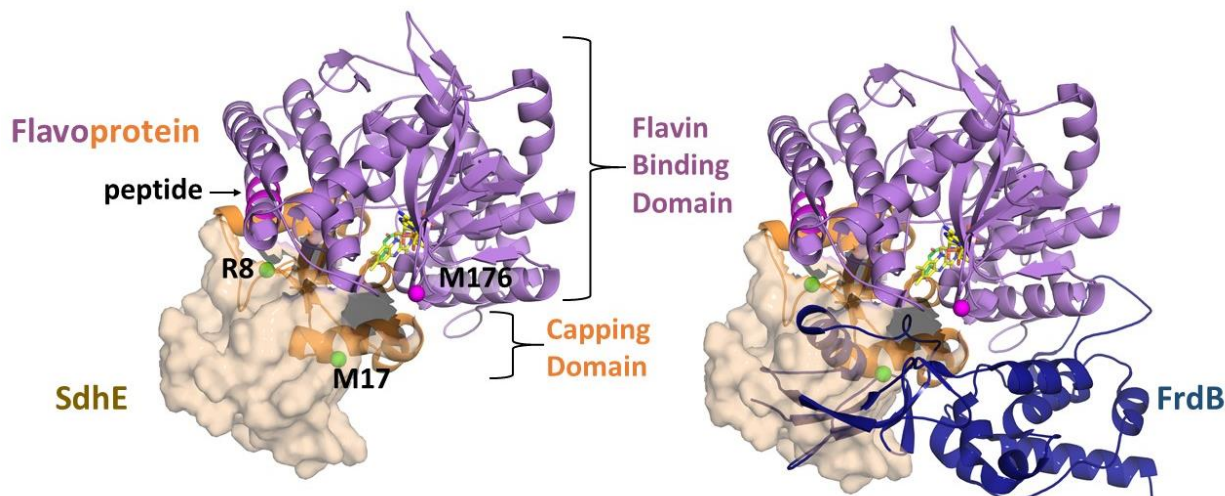
Figure 3.3: A. Representative model of the SdhE:FrdA complex. In the Rosetta generated model, SdhE (copper surface) and FrdA (purple) are constrained by interactions between residues of FrdA (pink) and SdhE (green spheres). Placement of the capping domain is modeled back into the image using FrdA (PDB 1L0V) as a guide and overlap with the predicted SdhE binding site is visualized. Placement of the FAD cofactor is modeled as yellow sticks. B. The same model showing an overlap between the iron-sulfur subunit (blue) and SdhE.

Model for assembly of mature Complex II

The placement of SdhE in models generated by Rosetta appears to overlap with placement of the flavin binding domain in the currently available structures as well as the iron-sulfur subunit and is far removed from the site of covalent flavin attachment (H44S in QFR, 9 Å closest model distance). These findings were combined with previous experimental evidence to generate a model for SdhE interaction with the flavoprotein, whereby it interacts with flavoprotein prior to assembly into the mature complex and does not directly participate in the chemistry associated with covalent flavin attachment (**Figure 3.4**).

Flavoprotein has two domains with conformational flexibility between them. In structures of closely related homologs, a wide array of orientations is observed with respect to these two domains with a few distinct states identified as "open" (33,72), "closed" (48,73) or "intermediate"(47,74,75). Modeling of the flavoprotein/SdhE interaction, based on the two restraints, positions SdhE at the junction of these two domains at a site where the N-terminal domain of the iron-sulfur protein subunit resides in the fully assembled complex II structure (**Figure 3.3B**). In this position, SdhE would make most of its contacts with a helical region of the flavin domain of the flavoprotein. The least number of clashes are observed when the capping domain is in the closed conformation with both FAD and dicarboxylate present. The "open" state of the capping domain is anticipated when flavin is not bound (76). presence of dicarboxylate substrates has been shown to stimulate covalent flavinylation (77). Considering this, we propose a model whereby SdhE acts as a wedge between the two domains and promotes a conformation that is closed with respect to the dicarboxylate binding site. This would stabilize bound dicarboxylate to stimulate covalent flavinylation and may orient residues in FrdA that are key for self-catalysis of covalent linkage. This interaction would precede assembly into the mature

complex, as the iron-sulfur subunit would be unable to bind with SdhE present, providing new

insight into assembly of the mature complex.
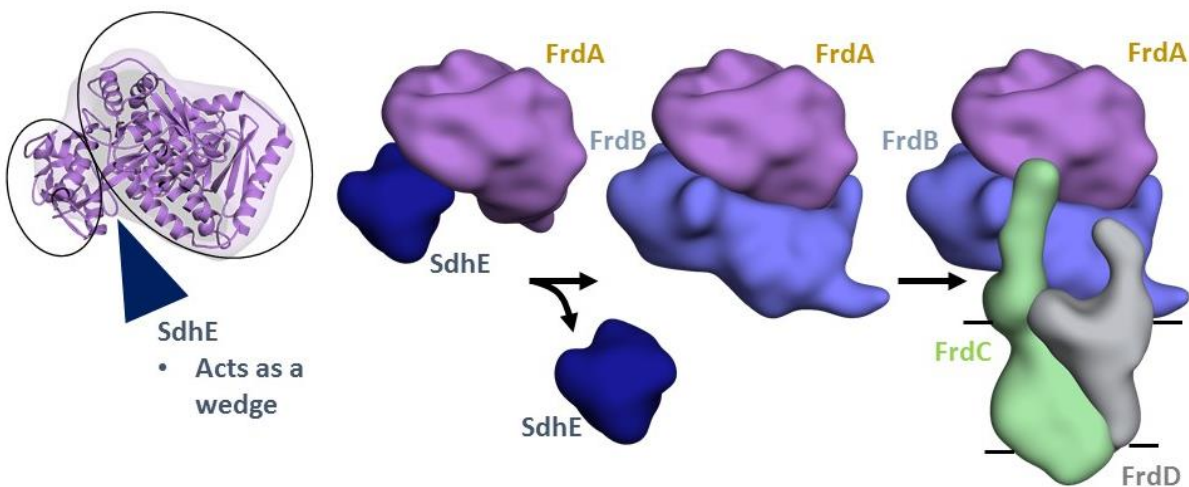
Figure 3.4: Scheme for SdhE function in covalent FAD incorporation and Complex II assembly. SdhE acts as a wedge between the capping and flavin binding domains of the flavoprotein (purple, PDB 1L0V) to promote closure over dicarboxylate and orientation of the two domains to support self-catalyzed covalent flavin linkage. Following SdhE removal, the mature complex is assembled.

Crystallization of the crosslinked SdhE-R8BpF:FrdA complex

Although models of the SdhE:FrdA complex generated in this study allow us to propose a

potential model for the interaction between SdhE and FrdA, a co-structure would provide

additional insight into the specifics of that interaction. In addition, photoaffinity crosslinking of

SdhE-R8BpF and FrdA provided a stable complex for attempts as co-crystallization. As such,

efforts were made to co-crystallize SdhE and FrdA by scaling up the expression and purification

of covalently crosslinked complex.

Initial purification of the crosslinked SdhE-R8BpF:FrdA complex revealed difficulty in

removing FrdA that was not crosslinked and that had the potential to complicate crystallization

efforts. Crystallization typically requires highly concentrated protein that is homogenous with

respect to composition and conformation of high purity. Proteins that are heterogenous are less likely to nucleate and result in a uniform crystal lattice, although exceptions occur. In the case of the crosslinked complex, the potential for difficulties in crystallization was great, as the much larger size of FrdA compared to SdhE made it possible that a crystal lattice might form that was partially composed of FrdA crosslinked to SdhE and isolated FrdA. Efforts were made to remove unlinked FrdA using numerous methods, including isolation in different buffers with increased salt content, alteration of UV exposure time, slower elution times and alternative methods of chromatography. FrdA has a hydrophobic surface patch at the proposed site of interaction with SdhE and this was exploited with the use of Hydrophobic interaction column (HIC) chromatography. HIC chromatography provided the greatest separation of the complex and unlinked FrdA, but no method completely removed the contaminating FrdA.

Protocols for purification using HIC columns were designed using a HiTrap HIC Selection Kit (GE Healthcare) that allowed for relatively rapid screening containing the following media: phenyl sepharose high performance, butyl sepharose high performance, phenyl sepharose 6 fast flow, butyl-S sepharose fast flow and octyl sepharose fast flow. The crosslinked complex was screen for use of these media using buffers containing ammonium sulfate and sodium chloride as a salt for creating of an elution gradient. Unbound FrdA was reduced to the highest degree in preparations using ammonium salt run through either butyl or octyl sepharose columns (**Figure 3.5**). Using both methods, three peaks resulted from elution of the crosslinked complex using a linear gradient from 2M to 50 mM ammonium sulfate. In butyl sepharose, the first peak corresponded to complex of the highest purity and in octyl sepharose the purest complex eluted as the third peak. Both methods, however, resulted in a great loss of protein and

48

decreased the yield of crosslinked complex by approximately 65%. Octyl sepharose yielded the

most consistent results and was used in future experiments.
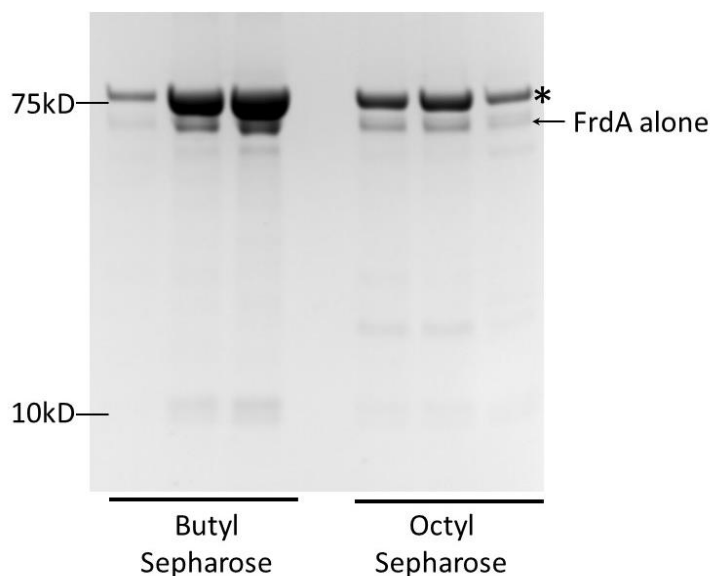
Figure 3.5: Purification trials SdhE-R8BpF:FrdA using hydrophobic interaction chromatography. Pooled fractions from three peaks resulting from butyl sepharose and octyl sepharose purification are shown. The band corresponding with the ~80 kDa complex is highlighted using an asterisk and sits above isolated FrdA that proved difficult to separate from the complex.

HIC chromatography was followed by an additional gel filtration step to remove

aggregate and exchange into a buffer suitable for crystallization. This final purification starting

with the initial purification of SdhE for crosslinking using Ni-NTA agarose was completed in 2

days with the samples kept on ice or at 4 °C at all times, as this reduced the amount of

aggregation. Crosslinked protein could be easily concentrated up to 50 mg/ml and a

concentration range from 2-40 mg/ml was employed in crystallization trials. Broad

crystallization screens were set up using a Mosquito nanoliter drop setter at 1:1 ratios of 200 nl

protein to reservoir solution. Standard crystallization screens from Hampton (Index HT, Crystal

49

Screen HT, PEG/Ion HT) and Rigaku (Wizard Screens I-IV) were used for rapid screening of crystallization conditions in sitting drop vapor diffusion. 3-drop 96-well Greiner CrystalQuick trays were used to test different concentrations within the same buffer. Numerous buffers were tested, including 25 mM Tris pH 7.4, 50 mM HEPES pH 8.0, 50 mM MES pH 6.5, 50 mM potassium phosphate pH 8.0 or 50 mM ammonium sulfate buffered with 25 mM Tris pH 7.4.

Of the hundreds of conditions screened, crystals were observed to grow in ~22 conditions, primarily with protein buffered in 25 mM Tris pH 7.4 with and without ammonium sulfate (**Figure 3.6A**). Crosslinked crystals were readily identified by their yellow color and positive UV illumination. The majority of crystals grew in drops with protein concentrations greater than 20 mg/ml and in conditions containing salt (potassium, sodium and calcium chloride) and a lowered pH (4.5-6.5). Many of the crystals appeared to form as clusters of plates and likely formed from multiple nucleation points. Despite this, several crystals were collected from the mico-screening drops, cryo-protected in reservoir solution containing 20% glycerol and screened for diffraction at various time points. Low resolution diffraction was observed in a few of the crystals isolated from confirming that they were protein crystals but failing to result in useable data.

These initial conditions were expanded in sparse matrix screening for 15 of the 22 positive crystal hits found in broad screening conditions. In the majority of expansion screens, no crystal growth was observed or microcrystals grew and additional expansion of the crystallization conditions, altering the drop ratio and protein concentration did not improve crystal quality. However, crystals of unusual morphology resulted (**Figure 3.6C**) from an expansion of conditions from the PEG/Ion HT screen (0.2 M ammonium chloride and 20% PEG 3350). These crystals were cryo-protected with a solution that was 80% reservoir solution and

20% of a 1:1 mix of glycerol and ethylene glycol prior to flash cooling with liquid nitrogen. X-ray diffraction data were collected at the Advanced Photon Source (APS) beamline 21-ID-G at -173 °C using a wavelength of 0.9798 Å and a MarMosaic225 CCD detector. A complete dataset was collected with diffraction to 4.8 Å, but the data were twinned and a structure could not be determined (**Figure 3.6B**). Further optimization of the crystal growth conditions through additive screening, for example, might yield a usable dataset for the determination of the SdhE-R8BpF:FrdA structure.
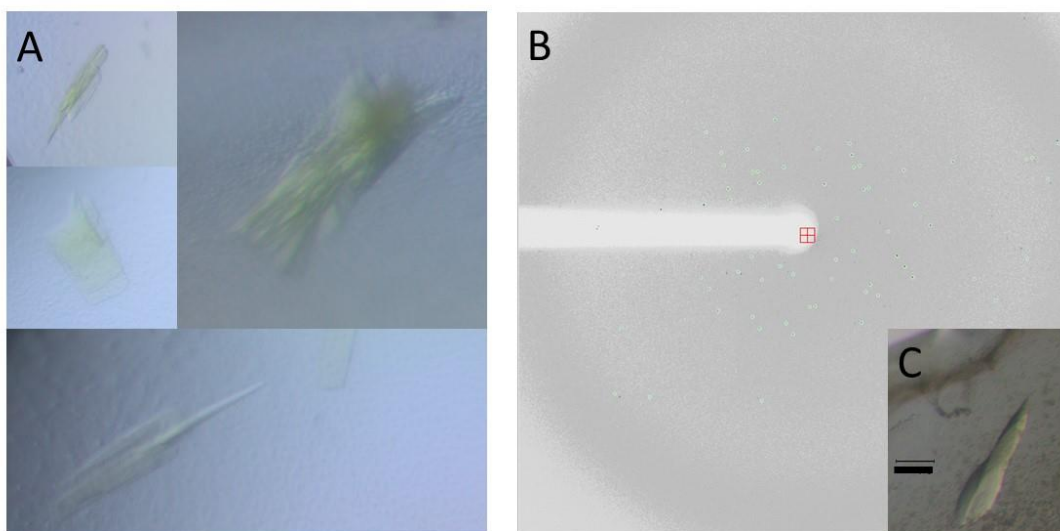
Figure 3.6: A. Examples of crystals that grew as a result of broad crystallization screening of the SdhE-R8BpF:FrdA complex. B. Representative diffraction image from crystals of the crosslinked complex. The diffraction limit is 4.8 Angstroms. C. Crystal grown in 0.2 M ammonium chloride and 18% PEG 3350. The black bar indicates a size of 150 microns.

Summary

Our results support a model for SdhE that is consistent with the previously proposed auto-catalytic mechanism of covalent FAD attachment (45). In this model, SdhE acts an assembly factor to promote the auto-catalytic attachment of FAD to the flavoprotein by

promoting an orientation of the flavoprotein domains that stabilizes bound dicarboxylate and

potentially aligns flavoprotein residues involved in the chemistry of covalent attachment.

Additionally, the identification of a binding site that overlaps with that of the iron-sulfur subunit

of Complex II provides new insight into complex assembly and suggests that the flavoprotein

exists independent of the complex prior to covalent flavin incorporation. Although the model

developed using photoaffinity crosslinking of SdhE to FrdA suggests a proposed binding site that

is consistent with earlier experimental data, a high resolution co-structure of SdhE and FrdA

would provide specific information about their interaction and additional information about the

role of SdhE in facilitating the covalent bond.

CHAPTER 4

STRUCTURAL AND BIOCHEMICAL ANALYSES REVEAL INSIGHTS INTO COVALENT

FLAVINYLATION OF THE ESCHERICHIA COLI COMPLEX II HOMOLOG

QUINOL:FUMARATE REDUCTASE

Work included in this chapter was published or accepted as the following:

Maklashina, E., Rajagukguk, S., Starbird, C. A., McDonald, W. H., Koganitsky, A., Eisenbach, M., Iverson, T. M., and Cecchini, G. (2016) Binding of the Covalent Flavin Assembly Factor to the Flavoprotein Subunit of Complex II. *The Journal of Biological Chemistry* 291, 2904-2916

Starbird, C. A., Maklashina, E., Sharma, P., Qualls-Histed, S., Cecchini, G., and Iverson, T. M. (2017) Structural and biochemical analyses reveal insights into covalent flavinylation of the *Escherichia coli* Complex II homolog quinol:fumarate reductase. Accepted by *The Journal of Biological Chemistry*

Introduction

Although structural and biochemical studies have provided insights into how SdhE might

function, the mechanism for how SdhE/Sdh5/SdhAF2 promotes covalent flavinylation is not

clear. We previously proposed a hypothesis where closure of the flavoprotein capping domain

over bound dicarboxylate at the active site promotes alignment of the FrdA/SdhA active site side

chains near the bound flavin (43). This scenario could allow the FrdA/SdhA protein to adopt a

conformation that stabilizes the quinone-methide tautomer at the C(8)α position on the

isoalloxazine ring of the flavin. Tight closure of the flavoprotein capping domain would be

followed by nucleophilic attack by the nearby histidyl residue to form the covalent bond at the

C(8) position. An alternative proposal could be that residues of SdhE/Sdh5/SdhAF2 directly

participate in the chemistry of covalent bond formation. This alternative is not favored because

of recent evidence that the SdhAF2 assembly factor enhances covalent flavinylation, but is not essential (44,78). For both scenarios, the observation that SdhE and FrdB bind to the same surface of FrdA indicates that the flavoprotein-assembly factor complex must disassociate prior to assembly of FrdA/SdhA into the intact QFR/SQR heterotetramer.

In this study, we demonstrate that in *E. coli* QFR and SQR, the influence of deleting SdhE on covalent flavinylation depends upon the redox environment of the cell. To investigate SdhE-independent mechanisms of covalent flavinylation, we next identified variants of the QFR FrdA subunit with levels of covalent flavinylation below those observed in the Δ*sdhE* strains. We selected the FrdA^{E245Q} variant for in-depth study; this side chain has previously been suggested as a part of the proton delivery pathway during fumarate reduction (32,79) but has not been identified as participating in covalent flavinylation. We identify that the QFR-FrdA^{E245Q} variant retains a structure similar to the wild-type enzyme, but exhibits impaired dicarboxylate binding and catalytic activity. Because covalent flavinylation is normally anticipated to occur in the isolated FrdA subunit prior to assembly into the QFR (FrdABCD) complex, we additionally investigated the effects of this variant in the context of isolated FrdA subunit. We found similar stability of wild-type FrdA and FrdA^{E245} variants, but impaired interactions with the SdhE assembly factor. SAXS data indicate that this residue is unlikely to interact directly with SdhE. Because no single auxiliary factor is essential for the formation of the covalent flavin linkage, the most likely conclusion from these data is that covalent flavinylation is autocatalytic. One interpretation of much of the data is that factors stimulating covalent flavinylation would pre-organize the active-site, suggesting that the autocatalytically-formed quinone-methide tautomer originally proposed by Walsh remains the most likely pathway to covalent flavinylation (45).

Materials and Methods

Expression and purification of the QFR complex (FrdABCD)

Wild-type and variant QFR (FrdABCD) were expressed as described (43) from plasmid pH3, which encodes the $frdA^+B^+C^+D^+$ operon under the control of the fumarate reductase (FRD) promoter. QFR was expressed in *E. coli* strain DW35, where both the *frd* and *sdh* operons are disrupted via the insertion of a kanamycin gene. Expression is induced under micro-aerophilic conditions, which is achieved in Terrific Broth (TB) medium by increasing the culture volume in the flasks (1.6 L in a 2 L growth flask), and reducing the shaking to 160 rpm. Cells were harvested by centrifugation at $9200 \times$ g and disrupted by sonication. Membranes were isolated by ultracentrifugation. QFR comprises ~50% of the total membrane protein when expressed using this protocol, and covalent flavinylation was assessed on this membrane-embedded QFR without further purification.

For crystallization, the QFR-FrdA^{E245Q} variant was purified as described (80). Membranes were resuspended in 25 mM Tris pH 7.4, 0.1 mM EDTA containing complete protease inhibitor tablets (Roche) and solubilized in 2% thesit detergent ($C_{12}E_9$, Anatrace). The insoluble fraction was removed by centrifugation at $34000 \times$ g, and the supernatant containing membranes was filtered and applied to a Q-Sepharose column. The protein was eluted with a linear NaCl gradient from 50 mM to 1 M. The NaCl concentration was reduced via three rounds of 1:10 dilution and reconcentration using a 30 kD molecular weight cut-off filter (Amicon). QFR was then further purified using a Poros 50HQ column, eluting with a linear NaCl gradient from 50 mM to 1 M. The protein was then concentrated as above and injected onto a Superdex 200 Increase 10/300 column. Protein concentration was determined using the Bradford assay.

Expression and purification of isolated FrdA subunits

Isolated wild-type and variant FrdA subunits were expressed in *E. coli* strain RP-2

(*ΔfrdABCD, ΔsdhCDAB*) a plasmid that inserted an additional stop codon after the *frdA* gene in

the pH3 plasmid, as described (43). Cells were grown as described above for the intact complex.

Cells were harvested by centrifugation and stored at -80º C. The cells were then resuspended in

20 mM potassium phosphate pH 7.4 with complete protease inhibitors (Roche). Cells were lysed

by three cycles of vortexing (3 min) with protein extraction beads (diameter < 1 mm) followed

by a freeze-thaw at -20 °C. Lysate was cleared by centrifugation at 34,000 x g and the

supernatant was stored at -20º C. For photocrosslinking experiments, no additional purification

was performed. For circular dichroism (CD) spectroscopy experiments, isolated FrdA subunits

were purified using an anion-exchange Poros 50HQ column in buffer containing 25 mM Tris-

HCl pH 7.4 and a linear NaCl gradient from 50 mM to 1 M NaCl. This was followed by gel

filtration in the same buffer on a Superdex 200 Increase 10/300 column. Elution was monitored

by following A_{280}. Following this procedure, the FrdA subunits were estimated to be 95% pure

based on SDS-PAGE.

Expression and purification of SdhE containing the artificial amino acid pBpF

The *sdhE* gene with an amber codon substituting R8 was cotransformed with the

pEVOL-pBpF to express pBpF-containing SdhE, as described (43). SdhE-R8BpF was grown in

LB medium containing 0.5 mM pBpF. After 1 hr, the temperature was adjusted to 30 °C. SdhE-

R8BpF was induced by the addition of 0.1 mM isopropyl β-D-1-thiogalactopyranoside (IPTG)

and the tRNA synthase/tRNA for pBpF was induced with 0.2 mM arabinose. Cells were

harvested by centrifugation and lysed by sonication. The lysate was cleared of cellular debris by

centrifugation for 45 min at 34,000 × g. SdhE-R8pBpF was purified by nickel affinity chromatography.

Quantitation of covalent flavinylation under aerobic and anaerobic growth conditions

LB supplemented with ampicillin (100 µg/ml) (1.5 ml in a 14 ml round bottom Falcon tube) was inoculated with a single colony. The cells were grown overnight at 37 °C with 270 rpm shaking, then divided into aerobic or anaerobic cultures. For aerobic growth, 25 µl of the overnight culture was used to inoculate 1 ml of LB supplemented with ampicillin (100 µg/ml) and cells were grown for 7 h at 37 °C with shaking. For anaerobic growth, 1 ml of the overnight culture inoculated 10 ml of LB supplemented with ampicillin (100 µg/ml) in a 15 mL Falcon tube; the cells were grown at 37 °C in the Isoterm rotisserie incubator (Fisher Scientific) for 17 h with slow rotation. Prior to analysis by SDS-PAGE, the A_{600} was measured to normalize protein load. Cells (0.3 to 0.9 ml) were collected by centrifugation for 1 min, and the pellets resuspended in 2X SDS loading buffer (BioRad). Each lane on the gel contains an equivalent amount of the cell culture (OD_{600}=1.0).

Quantification of covalent and non-covalent flavinylation

Covalent flavinylation of wild-type and variant QFR was detected as described (81). To analyze expression levels of the enzyme, 15 µg of isolated membranes were separated by SDS-PAGE on a 4-12% Bis-Tris gel (NuPAGE Novex). FAD was quantified by UV fluorescence (Gel Doc EZ imager) using ImageJ software. The gel was then stained with SimplyBlue Safe Stain (ThermoFisher) and the protein quantified by densitometry. The ratio between the UV and Coomassie was used to assess the level of covalent flavinylation, with wild-type QFR covalent flavinylation set to 100% and QFR-FrdA^{H44S} set to 0%.

To determine the level of total FAD present in the purified FrdA variants, A_{280}/A_{450} values were measured using a Nano-Drop1000 spectrophotometer. The A_{280}/A_{450} absorbance ratio was calculated for wild-type FrdA containing covalent FAD, and this value was set to 100%. The A_{280}/A_{450} absorbance ratio for the FrdA variants was compared to the ratio from wild-type. Because FAD was tightly associated with the variants but not covalently bound, all measured FAD absorbance was assumed to reflect non-covalent FAD specifically bound at the active site in the variants.

Measurement of Enzyme Activity

Enzymatic activity was determined in bacterial membranes containing wild type and FrdA^{E245Q} QFR variants. Succinate dehydrogenase and menaquinol-1 fumarate reductase reactions were assayed as previously described (82).

Spectroscopic evaluation of ligand binding

Ligand binding was performed using a modification of a described protocol (83). Purified wild-type and variant QFR enzymes were incubated with 3 mM malonate (to remove tightly bound oxaloacetate) in 50 mM potassium phosphate pH 7.0, 0.01% Thesit for 20 min at room temperature and passed through a PD-10 gel filtration column in the same buffer minus malonate. The resultant enzymes were stored on ice. Optical spectra were recorded using an Agilent 8453 diode array spectrophotometer in 50 mM potassium phosphate pH7.0, 0.01% Thesit at 25 °C. Difference spectra were obtained by subtraction of a ligand free spectrum from the corresponding spectrum of the enzyme in the presence of either 0.2 mM oxaloacetate or 3 mM fumarate.

Crystallization and structure determination

Crystals of the QFR-FrdA[E245Q] mutant were grown using the hanging-drop vapor diffusion method in droplets containing 1 µl of protein solution (15 mg/ml QFR FrdA[E245Q] in 25 mM Tris-HCl pH 7.4, 1 mM EDTA, 0.02 % $C_{12}E_9$) and 1 µl of the reservoir solution (275 mM NaMalonate, 19% polyethylene glycol 6000, 100 mM NaCitrate pH 4.0, 1 mM EDTA and 0.001% dithiothreitol). Droplets were equilibrated over 1 ml of the reservoir solution at 20 °C. Crystals were cryo-protected with a solution that was 80% reservoir solution and 20% of a 1:1 mix of glycerol and ethylene glycol prior to flash cooling with liquid nitrogen.

X-ray diffraction data were collected at the Advanced Photon Source (APS) beamline 21-ID-G at -173 °C using a wavelength of 0.9798 Å and a MarMosaic225 CCD detector. Data were processed and scaled using HKL2000 (84). The structure was determined using molecular replacement in the program Phaser (85) through the Phenix interface (86), and wild-type QFR (PDB entry 1L0V) as the search model. For refinement, the capping domain was separated from the flavoprotein and the positions of each subunit plus the isolated capping domain was optimized using rigid body refinement in Phenix. The capping domain was then reconnected to the flavoprotein and additional refinement was performed using standard xyz refinement in Phenix after constraining the secondary structural elements. As assessed by monitoring the R-factors and geometry, real space refinement decreased the quality of the model and was not used. The refined model was analyzed in Coot (87), but significant manual model building was not performed given the resolution.

Far-UV CD spectroscopy

Spectra were collected for wild-type FrdA subunits and FrdA variants on a Jasco J-810 CD spectropolarimeter at 20 °C using a 0.1 cm path length quartz cuvette. Measurements were

taken from 190 to 260 nm in 1 nm intervals. Secondary structure was analyzed using the

DichroWeb analysis server. Data are the average of three runs and have been corrected by

subtraction of the buffer spectra.

Thermal denaturation CD spectroscopy

Variable temperature CD spectra were taken by monitoring the change in the CD signal

(mDeg) at 220 nm from 5 °C to 85 °C in 1 °C increments with a 2 min equilibration time

between data points and a 4 sec response. Data are the average of three runs and were corrected

by subtraction of buffer spectra.

Using the *lsqcurvefit* function in Matlab R2015a, the CD data were fitted as a function of

temperature to a modified version of the Hill equation:

$$CD = \frac{AT^n}{B^n + T^n} + C$$

Where A is the maximum CD signal minus the minimum CD signal in mDeg, T is temperature in

°C, B is the midpoint of the plot of CD signal vs. temperature, n is the Hill exponent, and C is the

minimum CD signal. To determine the melting point, the derivative of this function,

$$\frac{d}{dx}\left[\frac{AT^n}{B^n + T^n} + C\right] = \frac{AB^n n T^{n-1}}{(T^n + B^n)^2}$$

was evaluated at temperature values ranging from the minimum observed temperature to the

maximum observed temperature, in steps of 0.01 °C. The temperature corresponding to the

maximum of the derivative was taken as the melting point.

Crosslinking of FrdA subunits to pBpF-incorporated SdhE

Purified His_6-SdhE-R8BpF was mixed with *E. coli* strain RP-2 lysate containing

overexpressed and untagged FrdA in a Corning 6-well plate on ice. Crosslinking was induced by

60

illumination with 365 nm light (Black-Ray 100 Watt UV lamp). The SdhE-FrdA crosslinked complex was purified by Ni^{2+} affinity chromatography and analyzed by SDS-PAGE, where a characteristic shift in molecular weight was observed. The presence of SdhE in the shifted band was verified by Western analysis with a primary antibody against the His_6-tag; the presence of FrdA in the shifted band was confirmed by monitoring UV fluorescence. For the time-course experiment, FrdA and SdhE-R8BpF samples were mixed in a 96-well plate on ice and exposed to UV light. Samples were collected at the indicated timepoints, and quenched with SDS loading buffer.

SAXS data collection and analysis

SAXS data were collected at the SIBYLS beamline at the Advanced Light Source in Berkeley, CA as described (88). Measurements of the SdhE-FrdA crosslinked complex, purified as described above and dialyzed into 50 mM MES pH 6.0 with 5% glycerol, were carried out at 283 K. Data were collected at two different concentrations (1.2 and 2.4 mg/ml) to analyze concentration dependent effects. Samples were placed 1.5 m from a MAR165 CCD detector arranged coaxial with the 11 keV monochromatic beam; 10^{12} photons/sec were impingent on the sample. A series of 0.3 sec exposures were collected for 10 sec, resulting in 32 frames per condition. Buffer subtraction and raw image data were integrated by beamline software. Guinier analysis and indirect Fourier transformation were performed in the PRIMUS (89) and GNOM (90) programs, respectively. The *ab initio* shape determination was carried out using DAMMIF (91). The resulting SAXS based model was then superimposed on models of the FrdA-SdhE-R8BpF crosslinked complex by their inertial axes alignment using the SUPCOMB program (92). The experimental scattering data were further validated with the scattering profile of the computational model of crosslinked complex using CRYSOL.

<div align="center">**Results**</div>

SdhE influence on covalent flavin attachment

Clinical studies and yeast genetics were instrumental in the discovery of the assembly factor SdhAF2 (34,93), and homologs have been identified in yeast (Sdh5, (34)) and bacteria (SdhE, (41)). We focused on the E. coli system and used Δ*sdhE* strains to evaluate the impact of SdhE on covalent flavinylation of QFR and SQR complexes. We find that anaerobic expression of QFR (FrdABCD) in Δ*sdhE* strains results in retention of covalent flavinylation, albeit at a reduced level compared to when SdhE is present (**Figure 4.1A,B**). In contrast, QFR shows significant reduction of covalent FAD when expressed aerobically (**Figure 4.1A, B**). We then tested to see whether the SQR homolog (SdhABCD), which is kinetically optimized to function under aerobic conditions, would retain covalent FAD when expressed anaerobically (**Figure 4.1 C**). Anaerobically, we observe levels of SdhA flavinylation similar to those found for FrdA when the full enzyme complexes are expressed. This suggests that the enhancement of flavinylation imparted by SdhE under aerobic conditions may be partially compensated for by anaerobiosis, when fumarate is likely to bind to the flavoprotein.
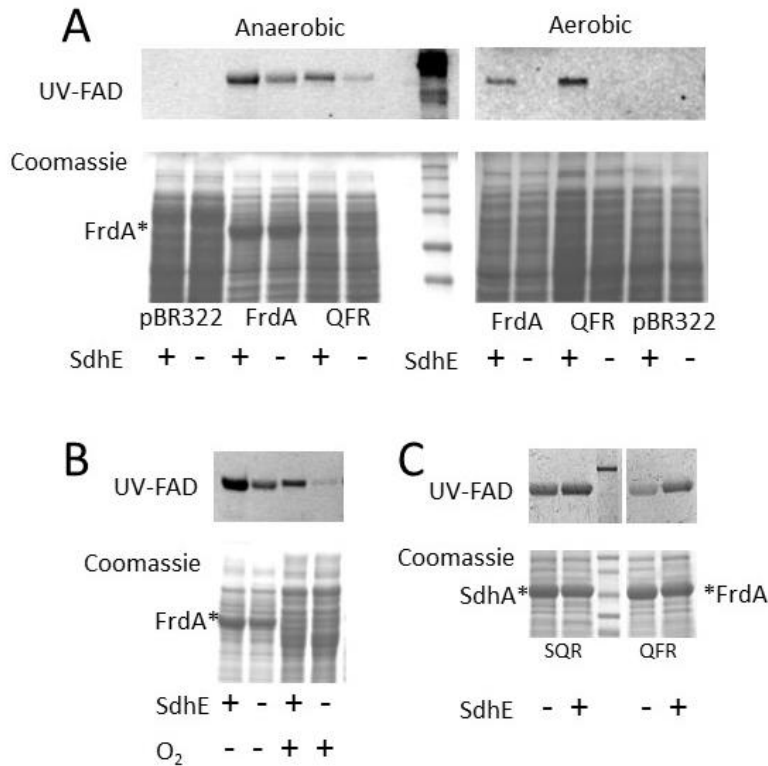
Figure 4.1: Effect of aerobic and anaerobic cell growth on flavinylation. Expression of FrdA from pFrdA and pH3 plasmids was performed in *E. coli* RP-2 (Δ*frdABCD*, Δ*sdhCDAB*) and RP-3 (Δ*frdABCD*, Δ*sdhCDAB*, Δ*sdhE*) under aerobic and anaerobic conditions. A. SDS-PAGE analysis of whole cell samples (20 µg protein per lane) shows attenuated, but not abrogated covalent flavinylation under anaerobic conditions, but substantial loss of covalent flavinylation under aerobic growth conditions. The top panels indicate UV fluorescence from the covalently-bound FAD cofactor and the bottom panels are Coomassie Blue G staining of the cell extracts. MW markers are shown on the right side of the gel for the anaerobically grown cells. Note, some of the pre-stained MW markers (BioRad, #1610374) show inherent fluorescence when exposed to a UV light. The * indicates the position of FrdA in the Coomassie stained samples. B. Analysis of isolated membrane fractions from anaerobically and aerobically grown cells. Note, there is reduced expression of FrdA in the aerobically grown cells since expression is driven by the natural FRD *(i.e.,* anaerobic) promoter. Nevertheless, there is reduced covalent flavinylation in the absence of SdhE for cells grown aerobically as compared to anaerobically. C. Effect of SdhE on flavinylation in anaerobically expressed SQR and QFR. Comparison of membrane fractions isolated from RP-3 (Δ*sdhE*) and RP-2 (+*sdhE*) cells indicates that SdhE is not essential for covalent flavinylation of either SdhA or FrdA. The top panel shows UV fluorescence of the covalent FAD. The middle lane of both panels shows prestained MW markers. The bottom panel shows Coomassie Blue G staining of proteins in the membrane fraction. The * indicates the location of SdhA or FrdA, respectively. Note, both SQR and FRD are expressed anaerobically from the FRD promoter.

QFR Mutants deficient in covalent flavinylation

We generated a library of site-directed variants within the FrdA subunit of the *E. coli* QFR complex (**Figure 4.2A**). We selected residues for mutagenesis because they exhibited one or more of the following properties: (i) they directly interact with bound substrate (FrdA^{R287}, FrdA^{H355}, FrdA^{R390};(44)); (ii) they are either previously proposed to contribute to the shuttling of protons during catalysis (FrdA^{E245}, FrdA^{R287}; (79)) or could contribute to the stability of the substrate binding site and effect the properties of other catalytic residues (FrdA^{D288}); (iii) they may stabilize the interdomain orientations or motions important for catalysis (FrdA^{E245}, FrdA^{E250} (79)); (iv) they are in regions that may be allosterically connected to the active site (FrdA^{E250}); or (v) they are near the proposed binding surface for the assembly factor SdhE (FrdA^{D129} (43)). QFR containing wild-type FrdA or FrdA^{R114}, which is a charged residue near the FAD but without any proposed mechanistic role were used as positive controls; the previously-described FrdA^{H44S} variant of QFR, which alters the normal histidyl linkage to the FAD and retains stoichiometrically-bound non-covalent FAD, was used as a negative control (23).

We evaluated the effect of these substitutions on the levels of covalent flavinylation in the intact FrdABCD enzyme produced under anaerobic conditions. To do this, we separated QFR-enriched membranes on SDS-PAGE and monitored the level of FAD fluorescence associated with the FrdA subunit (**Figure 4.2B**). Wild-type QFR, the QFR-FrdA^{R114} variant, and the QFR-FrdA^{H44S} variant were used as comparators. Five of our designed variants (FrdA^{E245Q}, FrdA^{R287K}, FrdA^{H355S}, FrdAR^{390K}, FrdAR^{390Q}) had almost a complete absence of covalent flavinylation, consistent with studies of the SQR protein (94). The FrdA^{D288N} variant showed minimal residual fluorescence, suggesting covalent flavinylation was severely compromised. Each of these variants had levels of covalent flavin attachment below that observed for QFR

64

expressed in the ΔsdhE strain that was similarly grown anaerobically (**Figure 4.1A,B**). This suggests that these side chains have a role in flavinylation that is independent of assembly factor function. It should be noted that with the exception of FrdA^{D288}, each of the amino acids associated with loss of flavinylation is known to be involved in substrate binding and/or the catalytic mechanism of fumarate-succinate interconversion (8,47,95). Accordingly, one possibility is that these side chains also directly participate in the mechanism of flavinylation.

Of these residues, we selected QFR containing the FrdA^{E245Q} variant for more detailed study. FrdAE245 exhibits loss of detectable flavinylation but has not previously been implicated in the covalent flavinylation process. It has been proposed as a proton shuttle during fumarate reduction within the context of both the *E. coli* QFR (32) and the *Shewanella* soluble fumarate reductase homolog (79), but is not directly involved in substrate binding. This residue is adjacent to FrdA^{T244}, a residue implicated in the catalytic efficiency of the enzyme (32) and associated with stoichiometric covalent FAD. FrdA^{T244} is part of an 11-amino acid loop (FrdA^{T234} to FrdA^{T244} in *E. coli* QFR) that connects the flavin-binding domain and the capping domain of the flavoprotein (**Figure 4.2A**). The location of the FrdA^{E245} side chain at the domain interface of the flavoprotein suggests that this side chain could have an additional role in stabilizing the orientations of the flavin-binding and capping domains of FrdA.

Catalytic activity of QFR complexes lacking covalent FAD

We began by investigating how the FrdA^{E245} mutation affected function within the context of the assembled QFR complex. Previous findings have shown that the QFR-FrdA^{H44S} variant lacks covalent FAD, however, it can bind stoichiometric amounts of non-covalent FAD (23). Catalytically, the QFR-FrdA^{H44S} variant retained ~50% of its ability to reduce fumarate whereas it only retains 1% of its ability to oxidize succinate (23). In the current study we found

that the QFR-FrdA^{E245Q} variant lacked detectable catalytic activity for both fumarate reduction and succinate oxidation.
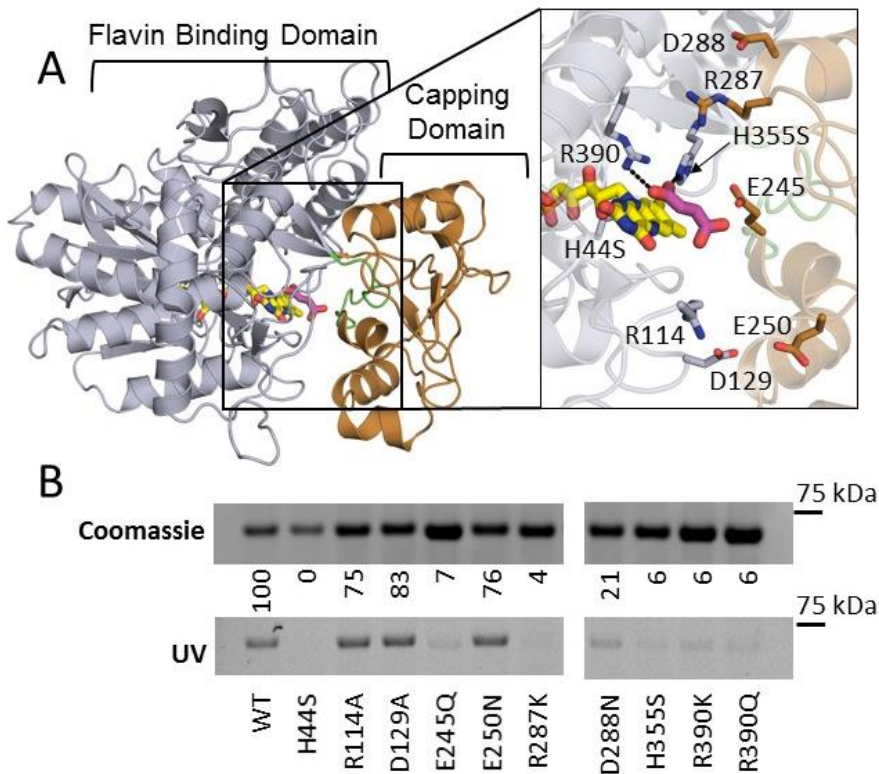
Figure 4.2: A. Location of substitutions in the FrdA subunit of QFR on the flavin binding (grey) and capping domains (copper) (PDB entry 3P4P). Flavin (yellow) and fumarate (pink) ligands are modeled and the active site loop flanking Frd^{AE245}is colored green (residues 234-244 in QFR) Zoomed window shows a close up of the location of the residues that were altered to evaluate their effect on covalent flavinyation. They are colored according to their location on either the flavin binding or capping domain.B. Quantitation of covalent FAD levels in wild-type and variant QFR complexes. Coomassie stained SDS-PAGE gels are normalized to the total amount of protein in order to assess differences in expression levels of variant QFR complexes. The same gel was illuminated with UV light to measure covalent flavinylation by flavin fluorescence. The ratio between the Coomassie signal and the flavin fluorescence was quantified. Wild-type covalent flavinylation was set to 100%, while QFR-FrdA^{H44} was set to 0%, and these were used as standards to quantify the percentage of covalent FAD in the remaining variants.

This finding is consistent with the previously-reported reduction of detectable fumarate reduction activity to <1% of wild-type levels upon mutation of the analogous residue in the soluble FrdA homolog from *S. frigidmarina*, which naturally contains non-covalent FAD as its redox cofactor (59). We anticipate that the FAD cofactor remains non-covalently bound in the analogous QFR-FrdAE^{245Q} variant. Indeed, prior studies demonstrate that in variant forms of QFR containing non-covalent FAD, the cofactor cannot be removed without KBr treatment, which is proposed to induce reversible unfolding (23).

In order to distinguish whether the QFR-FrdA^{E245Q} variant lacks activity due to altered ligand binding at the bound, non-covalent FAD, we analyzed the QFR interaction with two dicarboxylates: fumarate and oxaloacetate. We evaluated the binding of fumarate because it is the natural substrate. We also evaluated oxaloacetate because oxaloacetate is a natural tight-binding inhibitor of Complex II enzymes, with nM affinity for most homologs. In addition, oxaloacetate forms a charge transfer band with the isoalloxazine ring of the flavin, which results in a characteristic spectrum for Complex II proteins that is easier to follow than fumarate/succinate. For these two reasons, measuring oxaloacetate binding can be particularly useful for assessing altered dicarboxylate binding capacity in variants.

For this measurement, we used difference spectra obtained by subtraction of a ligand free spectrum from that of a ligand bound wild-type QFR spectrum. This experiment monitors characteristic spectral changes in the flavin spectrum that occur upon binding of dicarboxylates. These spectral changes include an increase in absorption at 500 nm indicative upon fumarate binding near the FAD cofactor and a charge-transfer band in the 600 nm region upon oxaloacetate binding near the FAD. Both of these features are observed for the wild-type QFR (**Figure 4.3A**). The QFR-FrdA^{H44S} variant containing noncovalent FAD shows spectral changes

similar to wild-type QFR, indicating that dicarboxylate binding is similar to the wild-type enzyme (**Figure 4.3B**). The difference spectra of the QFR-FrdA^{E245Q} variant, however, show no distinct features (**Figure 4.3C**). This observed lack of spectral changes from the bound FAD upon the addition of dicarboxylates is likely due to significant changes in binding capability for these ligands.
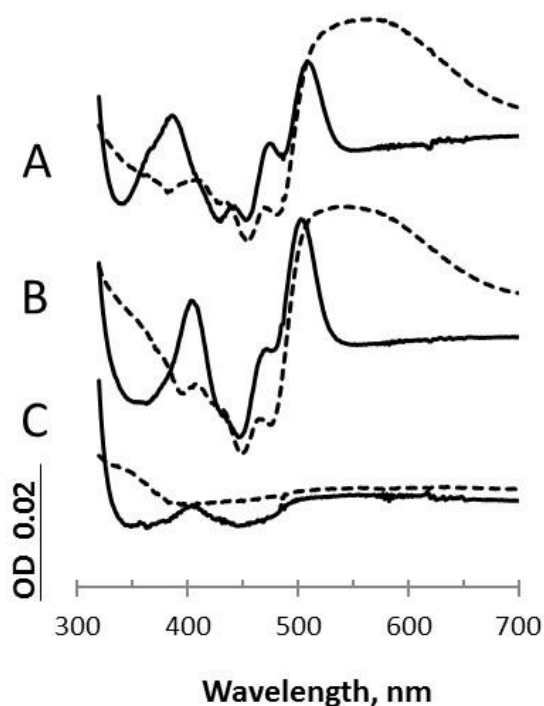
Figure 4.3: Spectra are the difference between the spectrum of the enzyme after addition of each ligand minus the spectrum of the oxidized enzyme. Difference spectra for fumarate (10 mM) is shown as solid lines, and difference spectra for oxaloacetate (0.2 mM) are shown as dashed lines. A. Wild-type QFR; B. QFR-FrdA^{H44S} C. QFR-FrdA^{E245Q}.

Crystal structure of the QFR-FrdA^{E245Q} mutant

To identify whether the lack of dicarboxylate binding is the result of an altered fold of the enzyme, or loss of the non-covalent FAD cofactor we determined the crystal structure. Crystallization trials of QFR-FrdA^{E245Q} using conditions that were previously successful for wild-type and variant enzymes did not result in the appearance of crystals in this case. As a result, we screened for distinct chemical conditions to support crystallization of this variant. These crystals diffracted to low resolution, with the best data set merging to 4.25 Å resolution (**Figure 4.4A, Table 4.1**). At this resolution, side chain conformations cannot be unambiguously assigned. Thus, we are not able to identify whether the FrdA^{E245Q} substitution has allosterically altered the positions of the dicarboxylate binding residues within the active site, which would be one explanation for why dicarboxylate binding is lost. However, the capping domain is in a similar position as it is found in the wild-type enzyme. As a result, side chains from the flavin-binding and capping domains could conceivably be presented to the active site with similar geometries as is observed in the wild-type enzyme. Indeed, the structure of the QFR-FrdA^{E245Q} complex showed close similarity to the wild-type protein, with an rms deviation of 0.33 Å for all atoms of the flavoprotein. This is consistent with previous work on the *Shewanella* soluble fumarate reductase, where mutation of the analogous residue to aspartate (E378D) resulted in little structural perturbation (79).

Notably, there was a loss of strong electron density for much of the isoalloxazine ring of the FAD, despite retention of electron density for the adenine dinucleotide (**Figure 4.4B**). This loss of electron density could arise for several reasons. One possibility is increased mobility of the isoalloxazine ring in the absence of the tethering covalent linkage. The relative structural stability of the isoalloxazine in flavoprotein homologs lacking the covalent linkage would argue

69

against, but would not preclude, this interpretation. An alternative is that the low resolution of

the data has reduced the quality of the electron density in this region. Nevertheless, it is clear

from the crystal structure that the QFR complex is folded and assembled with non-covalent FAD

in the presence of the FrdA^{E245Q} mutation.
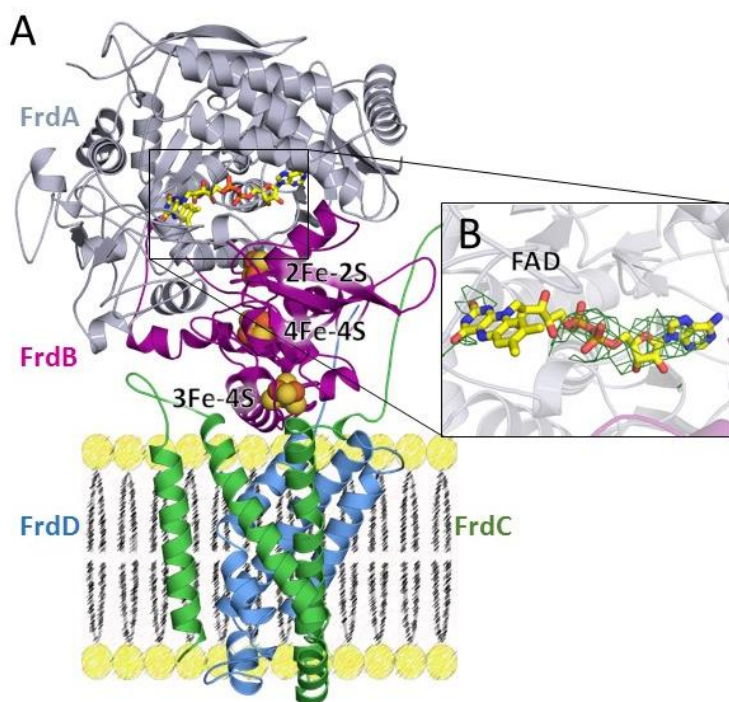
Figure 4.4: Structure of QFR containing the FrdA^{E245Q} mutation. A. Structure of QFR-FrdA^{E245Q}. The flavoprotein (FrdA) is shown in grey, the iron-sulfur protein (FrdB) is shown in magenta and the membrane subunits (FrdC and FrdD) are shown in green and blue, respectively. The locations of the cofactors (FAD as yellow sticks, and iron-sulfur clusters as spheres) are also shown. B. $|F_o| - |F_c|$ electron density maps contoured at 3σ were calculated in phenix.refine after the removal of FAD from the input PDB file. The quality of the electron density is consistent with the resolution for the adenine dinucleotide, but there is no interpretable density for the isoalloxazine ring.

Table 4.1

Crystallographic data collection and refinement statistics. Values in parentheses are for the highest resolution shell.

Data collection

PDB entry	5VPN
Beamline	APS 21-IDG
Wavelength	0.97856 Å
Resolution*	4.25 Å
Space group	$P2_12_12_1$
Unit Cell	a=133.6 Å
	b=138.1 Å
	c=220.1 Å
R_{sym}	0.166 (0.899)
R_{pim}	0.075 (0.448)
$CC_{1/2}$	0.919
I/σ*	10.6 (1.4)
Completeness	96.8% (98.2%)
Redundancy	5.5 (4.6)

Refinement

R_{cryst}	0.215
R_{free}	0.270

rms deviation

bond lengths	0.003 Å
bond angles	0.614°

Ramachandran

most favored	93.6%
allowed	6.1%
outliers	0.3%

Values in parentheses are statistics for the highest resolution shell, 4.4 Å-4.25Å resolution.
*The data have an $I/\sigma > 2$ in the outer shell at 4.4 Å resolution.

Folding and thermal stability in wild-type and variant FrdA subunits

We next assessed the function of the FrdA[E245] side chain in isolated FrdA subunits. The

rationale for additionally assessing the role of FrdA[E245] in the isolated FrdA subunits is that FrdA

containing non-covalent FAD represents the assembly intermediate, *i.e.*, covalent flavinylation is believed to occur within the isolated subunit. We first ensured that the variant FrdA subunits were properly folded. As we were unable to identify crystallization conditions that support the growth of isolated FrdA subunits, we used CD spectroscopy and thermal denaturation to measure folding and stability. Changes in stability of the isolated FrdA subunit in the presence of mutations at the FrdA[E245] could suggest whether stability affects the covalent flavinylation and maturation process, as has previously been suggested for the human complex (96). For these studies, we compared wild-type FrdA, FrdA[H44S] (lacking the histidine linkage to the FAD), FrdA[E245Q], and two additional variants of the FrdA[E245] side chain: FrdA[E245R], and FrdA[E245D]. Each of these isolated FrdA[E245] variants is associated with stoichiometric non-covalent flavin (**Figure 4.5A**), as assessed by comparing the total amount of bound FAD to the wild-type FrdA subunits and verifying that these variants lack measurable covalent FAD.

We measured the far-UV CD spectrum for wild-type FrdA, which is consistent with a predominantly helical fold (**Figure 4.5B**). The spectra for all variants tested were similar to that of wild-type FrdA, indicating that each variant FrdA subunit is properly folded and there are no major changes in the secondary structure. We next monitored changes in the ellipticity at 220 nm as a function of temperature in thermal denaturation CD spectroscopy. There were no significant differences in the melting temperature (T_m) or midpoint of the unfolding transition for the variants as compared to wild-type FrdA (**Figure 4.5C**). This indicates that neither the amino acid substitutions nor the loss of the covalent bond to the bound flavin significantly impacts FrdA subunit stability.
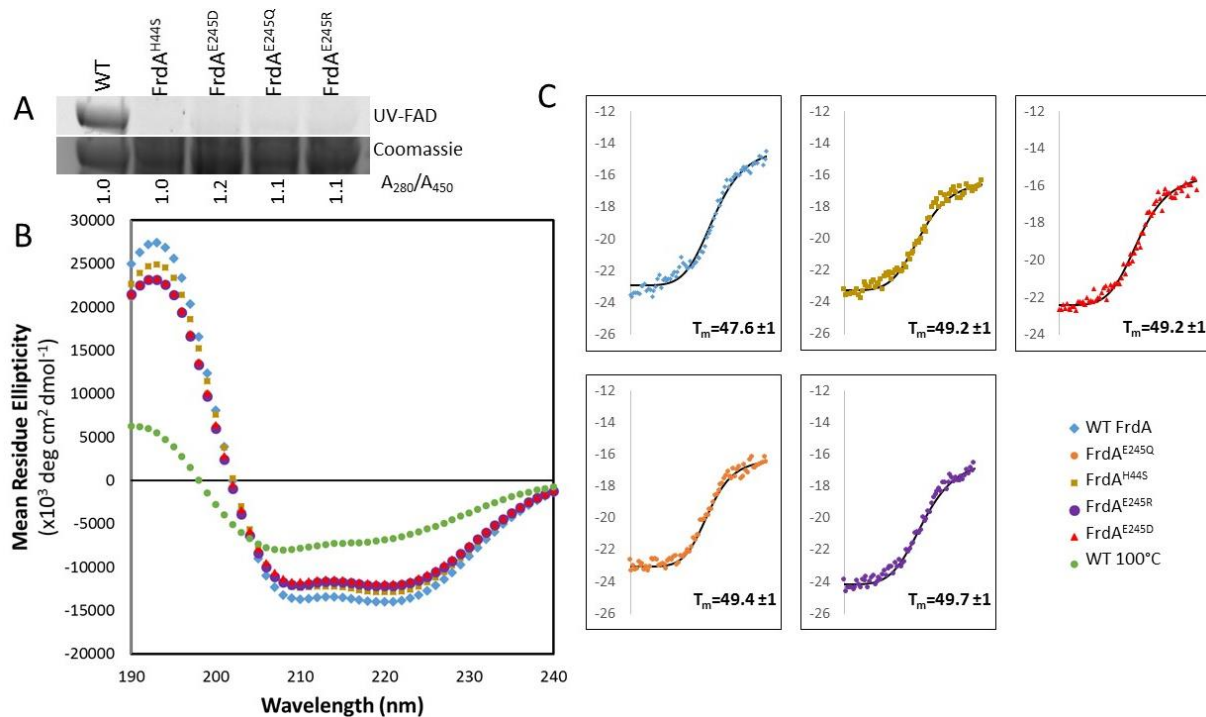
Figure 4.5: Circular Dichroism Spectroscopy of wild-type and variant FrdA subunits. A. Measurement of flavin in wild-type and variant FrdA subunits (~67 kDa). The quantity of flavin covalently associated with FrdA was measured by separating lysates on SDS-PAGE and measuring FAD fluorescence following illumination with UV light. The relative quantity of FAD associated with wild-type and variant FrdA subunits was assessed by measuring the, the A_{280}/A_{450} ratio of purified proteins. This value was normalized to 1.0 for wild-type protein. The ratio of A_{280}/A_{450} was similar in wild-type and variant subunits, indicating that these had a similar amount of flavin associated with each subunit. As *in gel* UV detection indicates that flavin is not covalently associated with the subunits, the tightly associated FAD must be non-covalently bound, likely via specific binding to the active site. B. Far-UV CD spectrum of wild-type FrdA compared to spectra for the FrdA[H44S] variant, the FrdA[E245] variants, and FrdA incubated at 100 °C for 2 h. C. Representative traces of thermal CD of wild-type FrdA, FrdA[H44S], FrdA[E245D], FrdA[E245Q] and FrdA[E245R]. The average T_m values are indicated.

Crosslinking with the assembly factor, SdhE

To identify whether the FrdA[E245] side chain influences the interaction of FrdA with the assembly factor SdhE, we monitored the ability of FrdA variants to crosslink with SdhE incorporating the artificial amino acid *para*-benzoyl phenylalanine (pBpF) at position 8. As previously described, this variant of SdhE, termed SdhE-R8BpF, readily crosslinks with wild-

type flavoprotein when illuminated with UV light (43), suggesting that this method can be used to report upon whether FrdA variants retain the ability to crosslink with SdhE.

We first measured crosslinking between wild-type FrdA and SdhE-R8BpF over the course of a 4 hour illumination with UV light (**Figure 4.6A**) and observed a time-dependent increase in FrdA-SdhE association. We selected the 3 hr time point as suitable for measuring crosslinking to variants, and measured crosslinking between SdhE-R8pBpF and the FrdA[E245D/Q/R] and FrdA[H44S] variants. Using this assay, we observed robust crosslinking between SdhE and wild-type FrdA. Indeed, the cross-linking could be observed on a Coomassie-stained SDS-PAGE gel, as previously reported (43). In contrast, crosslinking to each of the variants was substantially attenuated, and we could no longer observe the formation of a stable complex when monitoring by Coomassie-stained SDS-PAGE. To assess whether a low level of crosslinking occurred, we evaluated the formation the FrdA-SdhE crosslinked complex using Western analysis, probing with an antibody that recognizes that His6-affinity tag of SdhE. Even with Western analysis, titration of the antibody concentrations was required before signal was observed (**Figure 4.6B**).

A reduction in binding between FrdA and the SdhE assembly factor is somewhat anticipated for the FrdA[H44S] variant, as the FrdA[H44] side chain is proposed to be part of the FrdA-SdhE binding interface (43). However, the location of the FrdA[E245] side chain is on the capping domain (47). In the assembled (FrdABCD) QFR heterotetramer, this side chain is buried, but mediates contacts between the FAD-binding domain and capping domain of the FrdA subunit. One possibility for the observed loss of interaction is that the crosslinking assay appears to be exquisitely sensitive to small structural changes introduced by mutations, as was shown in prior studies (43). Thus even minor structural changes accompanying these mutations could result in a loss of crosslinking. Alternatively, it is possible that the FrdA subunit undergoes conformational

changes during SdhE binding that are altered in the context of FrdA[E245] variants. Because

FrdA[E245] is positioned on the capping domain of FrdA adjacent to a loop that links the two

domains, and because the capping domain of FrdA likely rotates upon the interaction with SdhE,

this rotation could be altered or prohibited in the context of FrdA[E245Q].
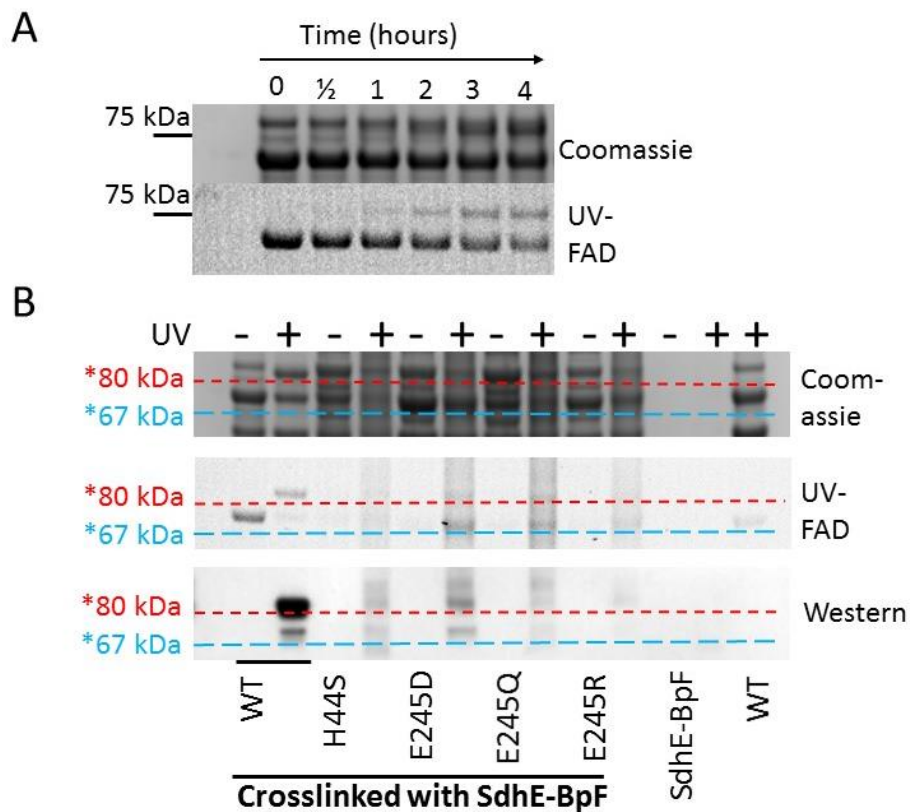
Figure 4.6: Crosslinking between wild-type and variant FrdA subunits and SdhE-R8BpF. Purified SdhE-R8BpF was mixed with lysate containing FrdA. Following UV exposure, samples were immobilized on Ni^{2+} resin, washed, and eluted with SDS-PAGE loading buffer prior to separation on an SDS-PAGE gel. A. Time course of crosslinking of SdhE-R8BpF with wild-type flavoprotein over 4 h after exposure to UV light. The position of the 75 kDa molecular weight marker is highlighted. B. Comparison of flavin fluorescence for detection of covalent FAD, Coomassie stained SDS-PAGE and anti-His$_6$ Western analysis of crosslinked samples. Horizontal lines were drawn after aligning the Coomassie, UV, and Western analyses to assist with identifying the molecular weights of the bands. The blue dashed lines are drawn just under the location of the FrdA subunit (~67 kDa) and red dashed lines are drawn just under the approximate location of the FrdA-SdhE complex (~80 kD).

SAXS of the FrdA-SdhE-R8BpF crosslinked complex

While there is currently not an experimental structure of the flavoprotein-SdhE complex, a computational model has been developed using restraints from site-specific crosslinking studies combined with mass spectrometry (43). This model proposed that the FrdA-SdhE interaction requires a rotation of the FrdA capping domain, but did not suggest how the capping domain might reorient. To investigate a potential role of FrdA[E245] in conformational changes in the FrdA subunit during SdhE binding, we performed SAXS analysis of the wild-type *E. coli* FrdA-SdhE-R8BpF crosslinked complex at protein concentrations of 1.2 mg/ml and 2.4 mg/ml. Scattering intensity profiles and linear Guinier plots indicated that the protein lacks aggregation and is monodisperse (**Figure 4.7A**). Further, a Guinier approximation exhibited good linearity at both protein concentrations and yielded R_g values of 28.11 ± 1.68 and 27.79 ± 0.92 Å with an average of R_g ~28 Å. Fourier transformation of SAXS data in the same range gave D_{max} of $82 - 86$ Å and R_g of $27 - 28$ Å (**Figure 4.7B**). We then developed several sets of coordinates for docking into the SAXS envelope. These coordinates began with the Rosetta-minimized computational model of the FrdA-SdhE complex that lacked the FrdA capping domain (43). We manually assessed several plausible alternatives for capping domain positions, with the capping domain being moved as a rigid body. Each alternative that was tested reduced, but did not completely eliminate, steric clash with either SdhE or other parts of the FrdA. This procedure identified one model exhibiting a reasonable correlation between the theoretical scattering curve and the experimental scattering curves at both protein concentrations, computing χ^2 values of 2.13 and 2.75, respectively (**Figure 4.7C**). The selected computational model of the FrdA-SdhE crosslinked complex was then superimposed on the SAXS envelope by automated alignment of inertial axes (**Figure 4.7D**). In the best model, the capping domain containing FrdA[E245] is rotated

so that the FrdA^{E245} side chain approaches the proposed SdhE binding site, but this side chain

does not appear to interact directly with SdhE. While the resolution of SAXS data is not

sufficient to place secondary structural elements or side chains, this large rotation is in contrast to

small but significant structural changes observed in the flavoprotein *p*-cresol methyl hydroxylase

upon interaction with a cytochrome subunit that promotes covalent flavinylation in that case

(97). If the FrdA-SdhE model is correct, the most likely interpretation for the loss of crosslinking

between FrdA^{E245Q} and SdhE-R8pBpF is that the mutation either prevents FrdA from adopting a

conformation that can bind SdhE or the mutation causes small surface changes that reduce SdhE

binding without being a direct part of the binding site.
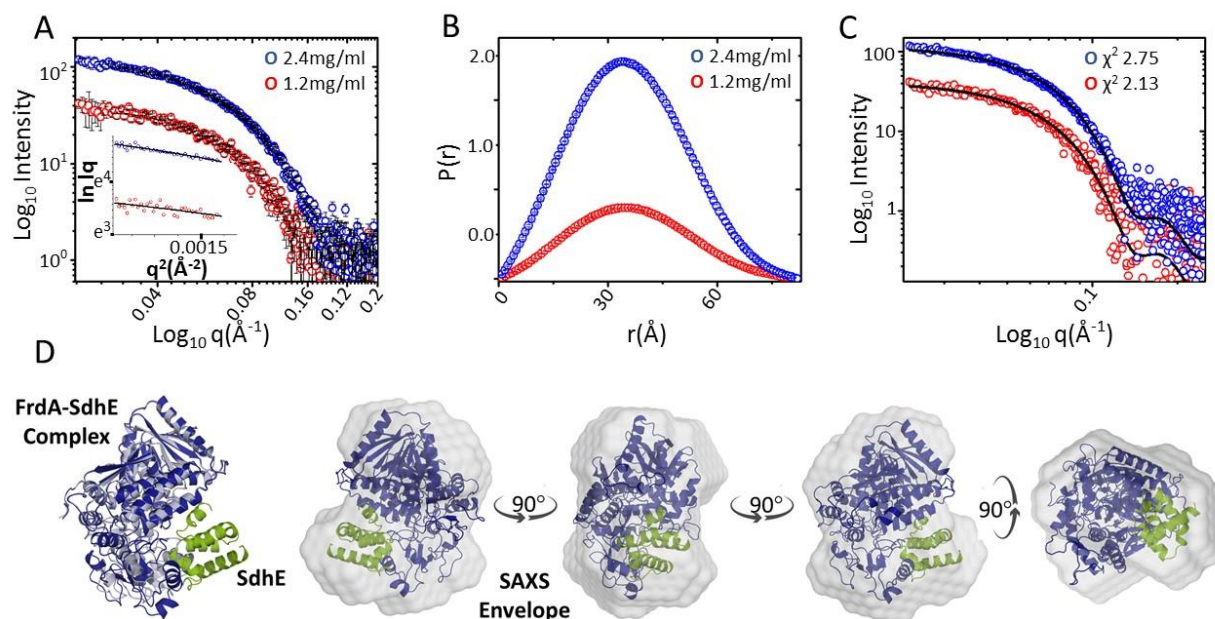
Figure 4.7: SAXS of the crosslinked FrdA-SdhE-R9pBpF complex. A. Intensity profiles in log scale of the crosslinked FrdA-SdhE complex acquired at protein concentrations of 1.2 mg/ml (red) and 2.4 mg/ml (blue). The insets show the linear fit to the Guinier region of the respective protein concentrations. B P(r) plot depicting the frequency distribution of interatomic vectors in the predominant scattering species after indirect Fourier transformation of the SAXS data provided an R_g and D_{max} of 27.25±0.32, 28.02±0.13 Å and 82.83 and 86.81 Å, respectively at lower and higher protein concentration. C. Comparison of theoretical scattering curve (black line) of the computational model of the crosslinked protein with experimental scattering curves at different protein concentrations give χ^2 values of 2.13 and 2.75, respectively. D. Conceptual model of FrdA (blue) and SdhE (green) complex superimposed on wild-type FrdA (grey, PDB entry 3P4P) and the SAXS envelope by automated alignment of inertial axes. Rotating views of the FrdA-SdhE-R8BpF model docked into the SAXS envelope.

Discussion

While we know a great deal about the mechanism of succinate and quinone oxidoreduction by Complex II superfamily members, comparatively little is known about Complex II assembly. Indeed, our understanding of protein assembly in general is underdeveloped as compared to our understanding of how individual proteins function. In the case of Complex II, one critical aspect of assembly is the insertion and attachment of its

cofactors. For well over 30 years, this process was considered fully autocatalytic, potentially

proceeding via a quinone-methide intermediate. Only within the last 10 years were any specific

assembly factors discovered, initiating a debate of the mechanisms of cofactor attachment.

SdhAF2 was identified in patients who presented clinical Complex II deficiency, but who did not

have mutations in Complex II genes (34). Phylogenetic analysis of SdhAF2 (~11 kDa) indicates

that this protein evolved prior to the development of mitochondria, a proposal consistent with its

strong conservation in all kingdoms of life (41). After its discovery, SdhAF2 was initially

believed to be essential for covalent flavinylation of human Complex II. Indeed, its mutation

recapitulates diseases associated with Complex II deficiency (34). However, recent studies of

Crisper-CAS9 Δ*sdhAF2* breast cancer cells suggest that covalent flavinylation can proceed in the

absence of SdhAF2 (78). In addition, there are examples of thermophilic bacteria and archaea

that lack SdhE genes, but still produce functional, covalently flavinylated SQR (44). Our finding

that the requirement for SdhE is more important during aerobic respiration adds complexity to

this debate, but further supports SdhE as a stimulating, non-essential factor for covalent

flavinylation.

Intriguingly, SdhE is not the only factor that can enhance the efficiency of covalent

flavinylation. It has also been shown that dicarboxylates, including citric acid cycle

intermediates, stimulate covalent flavinylation of Complex II isoforms (77). Moreover, the

deletion of the iron-sulfur protein (FrdB or SdhB) reduces, but does not eliminate covalent

flavinylation, identifying this subunit as modestly supporting the formation of the covalent

linkage (98,99). Given that neither SdhE (78), nor the iron-sulfur protein (98), nor dicarboxylates

(77) are absolutely required for covalent flavinylation of FrdA/SdhA, but that SdhE can enhance

flavinylation of human SdhA in a purified system (96), the most logical conclusion is that the

79

chemistry of covalent attachment is supported by the flavoprotein itself. But if covalent

flavinylation does proceed autocatalytically, what are the chemical requirements, and how do

SdhE, dicarboxylates, or the iron-sulfur protein enhance this?

Taken in aggregate, our findings and those from the literature support a model where

autocatalytic covalent attachment via the quinone-methide intermediate requires a pre-organized

active site with the capping domain closed tightly. A tightly closed structure would also be

anticipated to be more stable and less sensitive to proteolysis, as has been proposed (96). This

finding is consistent with observations where Sdh5 binding to yeast SdhA stabilizes Sdh5 against

LON-mediated proteolysis (100). Indeed, binding of the flavoprotein to the assembly factor

probably protects both from proteolysis. The tightly closed conformation may align active site

residues into orientations that optimally support the chemistry of covalent flavinylation.

Certainly the FrdA[H44] residue must be positioned closely enough to the isoalloxazine C(8)α to

allow formation of the covalent bond. In addition, other active site side chains may impact the

covalent flavinylation chemistry directly, for example FrdA[R390] is positioned close to the N1-C2

of the isoalloxazine ring in the assembled complex.

Overall, the data suggest that there may be more than one way to promote active site pre-

organization. The previously-reported findings that bound dicarboxylates (77), the iron-sulfur

protein (61,98,99), and SdhE (34) can each enhance covalent flavinylation are consistent with

this proposal, as each of these could function to pre-organize the active site. Bound

dicarboxylates could directly interact with and orient active site residues, which would help to

organize the active site and promote tight closure of the capping domain. The role of

dicarboxylates in covalent flavinylation is consistent with our finding that mutation of residues

that impact dicarboxylate binding directly or indirectly reduces covalent flavinylation to levels

just above detection (**Figure 4.2**), and substantially below those observed in Δ*sdhE* strains grown under the same conditions (**Figure 4.1**). However, substrate turnover might not be necessary. Indeed, prior studies of other catalytically-compromised QFR and SQR variants indicate that covalent flavinylation is usually retained (32,101).

The binding of FrdA to SdhE or the iron-sulfur protein may similarly promote the organization of active site residues. A computational model developed in the context of experimental distance restraints strongly suggests that this FrdA-SdhE interaction promotes a conformational change in FrdA that closes the capping domain of the flavoprotein tightly over bound dicarboxylate (43). Similarly, the position of the iron-sulfur protein in the assembled complex may restrict the motions of the capping domain. SdhE may be particularly important during aerobic respiration with succinate. It is plausible that succinate may have lower affinity for an active site containing non-covalent FAD, the capping domain may not close as tightly prior to the formation of the covalent linkage. As a result, an auxiliary factor such as SdhE may increase the efficiency of covalent flavinylation under aerobic conditions (**Figure 4.1**). An additional intriguing interpretation of a difference in flavinylation under aerobic versus anaerobic conditions is that SdhE may have evolved during the transition and adaption of cells to an aerobic environment. It may also be consistent with the idea that SQR formed from a QFR at the transition from anaerobic to aerobic life, with the covalent bond fulfilling the need for higher redox potential to oxidize succinate versus reduce fumarate.

Covalent flavinylation via a mechanism that uses a quinone-methide intermediate would also require a proton shuttle. While the FrdA[E245] side chain is proposed as part of a proton delivery pathway during fumarate reduction, it is not clear whether it plays the same role during covalent flavinylation. Pre-organization of the active site would have the impact of aligning the

proton shuttling pathway consisting of FrdA^{R287}, FrdA^{E245}, and FrdAR^{248} (**Figure 4.8A**).

However, FrdA^{R248} variants retain covalent flavin (102). One interpretation of this finding is that

this proton delivery pathway is used during fumarate reduction but not during covalent

flavinylation. An alternative possibility could be considered in light of the rotation of the capping

domain when FrdA is in complex with SdhE. The FrdA-SdhE model would suggest that this

rotated capping domain could allow the FrdA^{E245} side chain to be directly exposed solvent, such

that the FrdA^{R248} side chain that normally participates in proton delivery could be bypassed

during covalent flavin attachment (**Figure 4.8B**). The amino acid residue equivalent to FrdA^{D288}

is conserved in the complex II family of enzymes (*E. coli* SdhA^{D287}, and in the mature (*i.e.,* 42

amino acid transit peptide processed) human SdhA^{D299}. In the available x-ray structures of

bacterial, yeast, and mammalian complex II the aspartate residue is hydrogen bonded to a

conserved Asn residue (FrdA^{N389}, *E. coli* SdhA^{N398}, human SdhA^{N408}), which is adjacent to

FrdA^{R390} (*E. coli* SdhA^{R399}, human SdhA^{R409}). FrdA^{R390} is known to be essential for covalent

flavinylation in bacteria (**Figure 4.2B**) and mutation of the equivalent residue in humans is

associated with disease (103). FrdA^{R390} is thought to stabilize the negative charge at the N(1)-

C(2) position of the isoalloxazine that develops in the quinone-methide tautomer and thus is

essential for development of the tautomer. It is reasonable to suggest that mutation of FrdA^{D288} to

a neutral amino acid such as Asn impacts the architecture of the active site. This would be

expected to affect dicarboxylate binding and the environment around FrdA^{R390} such that it is

unable to sufficiently stabilize the negative charge that is required near the isoalloxazine N(1)-

C(2) position during the autocatalytic formation of the covalent flavin linkage. It's also possible,

given the potential reorganization of the active site upon SdhE binding, that FrdA^{D288} has a role

in proton shuttling in covalent flavinylation (**Figure 4.8B**). It is likely that SdhE helps impact the

active site architecture by stabilizing the environment near the flavin to help align the active site

residues during the time necessary for formation of the covalent flavin bond. Further insight into

the role of SdhE in covalent flavinylation requires the determination of a high-resolution

structure of the FrdA-SdhE complex.
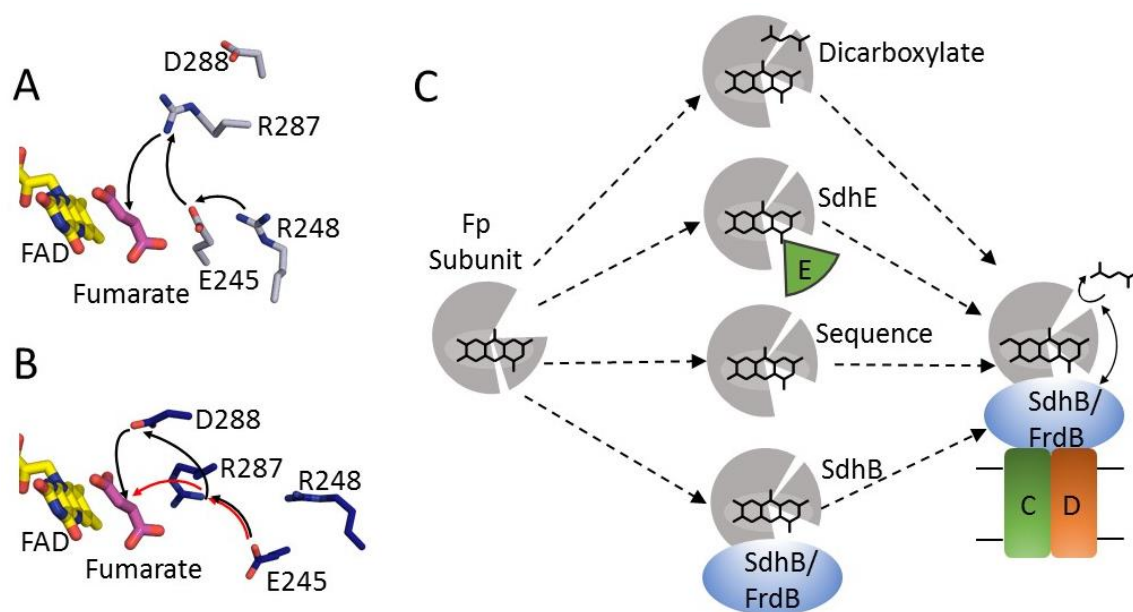
Figure 4.8: Model for side chains in covalent flavinylation. A. Active site organization in wild-type QFR with fumarate bound (grey, PDB entry 3P4P). FAD (yellow) and fumarate (pink), and side chains or FrdA[245], FrdA[248], FrdA[287] and FrdA[288] are shown as sticks. The black arrows indicate the direction of proton transfer during fumarate reduction. B. The same view for the FrdA-SdhE-R8BpF model (blue). The black and red arrows indicate two potential alternate proton transfer pathways after reorganization of the active site as a result of domain rotation in the model. C. Scheme for organization of the flavoprotein (grey) active site to promote auto-catalysis of the covalent flavin bond. In this model, closure of the capping domain after binding of flavin (represented as stick model of the isoalloxazine ring) and proper orientation of the attachment site can be facilitated in several ways: (i) binding of dicarboxylate; (ii) binding of the assembly factor; (iii) enhanced stability and preorganization by sequence in thermophilic bacteria; (iv) binding of the iron-sulfur subunit. After this organization, covalent flavinylation can occur (indicated by additional bond) followed by complex assembly.

Summary

The discovery of a new assembly factor, SdhE/Sdh5/SdhAF2, essential for covalent flavinylation in humans and some bacteria, challenged the long-held belief that covalent flavinylation in complex II homologs was an autocatalytic process. Following its identification as a gene associated with Complex II related disease, several theories were proposed to explain its role assembly of covalent flavin into the mature complex. It was proposed that SdhAF2 may act as an FAD transporter, sequestering FAD from the mitochondrial matrix for assembly into Complex II. Alternatively, it was suggested that SdhAF2 acts as an assembly factor, facilitating covalent flavin attachment either by orienting flavoprotein residues for catalysis or by providing some of the side chains needed for the chemistry. These hypotheses for the role of SdhAF2 in flavin linkage were further complicated by uncertainty regarding assembly of mature Complex II. Although flavinylation was expected to occur in the mitochondria, it was unknown if folding of the soluble domains or the entire complex preceded trafficking to the mitochondria. As such, it was unclear if SdhAF2 interacted with isolated flavoprotein, or with flavoprotein that was partially or fully assembled into mature Complex II.

The work presented here has complemented findings by other groups within this field to answer many of these questions regarding the role of SdhAF2 and assembly of Complex II. Our discovery that the bacterial homolog, SdhE, interacts with flavoprotein at the iron-sulfur binding site provided clear evidence that covalent flavinylation occurs in isolated flavoprotein prior to complex assembly. Our findings also confirmed that SdhE acts as an assembly factor, rather than as a simple FAD transporter. Specifically, based on a computational model informed by crosslinking studies, we proposed that SdhE positions the two flavoprotein domains in an

orientation that allows for retention of the dicaroboxylate cofactor and alignment of residues for catalysis of the covalent flavin bond.

Together, the data argues in favor of multiple complementary mechanisms that promote the pre-organization of the Complex II active site during covalent flavinylation. One or more molecular players (bound dicarboxylate, SdhE, iron-sulfur protein, or potentially others) could facilitate the correct orientation of active site residues and promote tight domain closure over the isoalloxazine. The findings support the original proposal of Walsh (45) that covalent attachment is self-catalytic and argue against a direct role for SdhE in the chemistry of covalent flavinylation. Rather the role of SdhE or its homologous molecular chaperones (SdhAF2/Sdh5) is to stabilize the flavoprotein in a tightly closed conformation to organize the active site residues and to allow time for the covalent flavinylation to occur.

CHAPTER 5

LIPIDIC CUBIC PHASE CRYSTALLIZATION OF A COMPLEX BETWEEN THE

ESCHERICHIA COLI MEMBRANE PROTEIN QUINOL:FUMARATE REDUCTASE AND

A FLAGELLAR MOTOR PROTEIN

Introduction

Motility in bacteria is a key component to both survival and infection. Chemotaxis, or the

ability of bacteria to move towards nutrients and away from damaging agents, is usually

mitigated by a two-component signaling pathway that promotes a change in rotational direction

of a flagellar motor. This rotational change is controlled by movement of the 'switch', a ring-like

complex between multiple copies of FliG, FliN and FliM proteins at the base of the flagellar

motor, but the exact mechanism of switching has not been fully elucidated. Several studies have

indicated that the mechanism of switching involves a direct interaction between the activated

response regulator CheY and the motor proteins FliM (104) or FliN (105).

A recent paper demonstrated that switching can also be controlled by an interaction

between FliG and the bacterial respiratory complex, QFR (106). QFR is an integral membrane

protein produced primarily during anaerobic growth when fumarate is the terminal electron

acceptor. While fumarate had been demonstrated to be capable of inducing a change in flagellar

rotation (107) the QFR:FliG interaction had not been previously shown and was perhaps

unexpected, as it demonstrated a function for QFR under aerobic conditions and was independent

of the presence of CheY. The authors also demonstrated that QFR and FliG form a specific 1:1

complex with low μM affinity and that the effect of fumarate on switching was due to its interaction with QFR and not with flagellar motor proteins.

In the present study, we investigate the specific mode of interaction between these two proteins using structural studies. Initial crystals of this ~160 kD membrane complex grown in lipidic cubic phase resulted in extremely low diffraction (~20-30 Å) and were optimized with the use of a novel additive screen. This resulted in greatly improved crystal quality and a significant improvement in resolution (to 4.7 Å).

Materials and Methods

Expression and Purification of QFR

Wild-type QFR was expressed as described (43) from plasmid pH3, which encodes the $frdA^+B^+C^+D^+$ operon under the control of the fumarate reductase promoter. QFR was expressed in *E. coli* strain DW35, where insertion of a kanamycin cassette disrupts the *frd* and *sdh* operons. Expression is induced in anerobic conditions, which is achieved by increasing the culture volume in the flasks (1.6 L of LB in a 2 L growth flask), and reducing the shaking to 150 rpm. Cells were harvested by centrifugation and disrupted by sonication. Membranes were isolated by ultracentrifugation.

For crystallization, QFR was purified as described (80). Membranes were resuspended in 25 mM Tris pH 7.4, 0.1 mM EDTA containing complete protease inhibitor tablets (Roche) and solubilized in 2% thesit detergent ($C_{12}E_9$, Anatrace). The insoluble fraction was removed by centrifugation and the supernatant containing membranes was filtered and applied to a Q-Sepharose column from which protein was eluted with a linear NaCl gradient from 50 mM to 1

M. The NaCl concentration was reduced by dilution and reconcentration using a 30 kD

molecular weight cut-off filter (Amicon). QFR was then further purified using a Poros 50HQ

column, eluting with a linear NaCl gradient from 50 mM to 1 M. The protein was then

concentrated as above and injected onto a Superdex 200 Increase 10/300 column. Protein

concentration was determined using the Bradford assay.

Expression and Purification of FliG

FliG was expressed in *E.coli* strain BL21(DE3) pLysS from a pGMM5000, a plasmid

derived from pET22b the encodes for a clockwise biased mutant, *fliG*(ΔPEV) (108,109)

construct has a C-terminal His$_6$-tag and expression controlled by a T7 promoter is IPTG

inducible. FliG(ΔPEV) was purified using nickel affinity chromatogrphy followed by gel

filtration in a buffer minimally containing 25 mM Tris pH 7.4. FliG was screened for stability in

various detergents and it was determined that both FliG and QFR were stable in Anapoe-C$_{12}$E$_8$

(Anatrace). As such, the proteins were mixed with a 10-fold excess of FliG to allow for binding

before a final gel filtration purification step in 20 mM Tris pH 7.4, 0.1 mM EDTA and 1 mM

C$_{12}$E$_8$. Isolated fractions were concentrated to ~25mg/ml for crystallization trials.

Microscale Thermophoresis

Binding of QFR to FliG(ΔPEV) was measured using intrinsic flavin fluorescence. QFR

membranes isolated by centrifugation were resuspended in buffer containing 25 mM Tris-Hcl pH

7.4 and 0.1 mM EDTA for 2 hours by stirring. Solutions containing native membranes at a

constant concentration 25 μM and purified FliG at concentrations ranging from 1.7 nm-

54,000nm were loaded into MST Premium-coated glass capillaries. MST analysis was performed

using the Monolith NT.115.

Crystallization of the QFR:FliG complex

Co-crystals of QFR and FliG were grown using lipidic cubic phase (LCP) crystallization. For crystal screening, the complex solution was mixed with monopalmitolein (1-(9Z-hexadecenoyl)-rac-glycerol), monoolein (1-(9Z-octadecenoyl)-rac-glycerol, 9.9 MAG), or monovaccenin (1-(11Z-octadecenoyl)-rac-glycerol, 11.7 MAG) using a gas-tight syringe for pipetting by a Xantus cubic lipid phase robot. Broad crystallization screens for LCP were set up using the Hampton StockOptions Salt screen varied buffers from pH 6.5 to 8.5, and 15%-30% PEG 400 (110) and optimized with additive screen reagents (described in Table 5.1). Crystals were extracted from the LCP plates and frozen by plunging into liquid nitrogen. X-ray diffraction experiments were performed under cryogenic conditions at the Advanced Photon Source (APS) beamlines 23-IDB and 23-IDD at -173 °C using a wavelength of 1.0332 Å and a Pilatus3 6M detector.

Results and Discussion

Purification of FliG

For co-crystallization with QFR, a clockwise biased mutant of FliG, FliG(ΔPEV), was used. This mutant was expected to mimic the relevant conformation for binding of FliG to QFR and gel filtration experiments performed in our lab indicated that FliG(ΔPEV) formed a more stable complex with QFR. FliG(ΔPEV) was purified using two chromatography steps: Ni-affinity (**Figure 5.1**) and gel filtration. FliG(ΔPEV) has only one tryptophan resulting in a very low signal at 280 nm. As a result, elution of FliG(ΔPEV) during size exclusion was monitored at 220 nm and 230 nm, in addition to 280 nm. Aggregation was also believed to be an issue, as a large aggregate peak was observed in the eluent from gel filtration (**Figure 5.2A**). This aggregate

peak could be removed by an additional gel filtrations step (**Figure 5.2B**), resulting in protein of

high purity for crystallization trials. Interestingly, preliminary negative stain electron microscopy

images of the suspected aggregate peak suggested that it was a multimeric complex of FliG (data

not shown). Regardless, cell disruption and purification of FliG, as well as co-crystallization

experiments with QFR, were done in the same day.
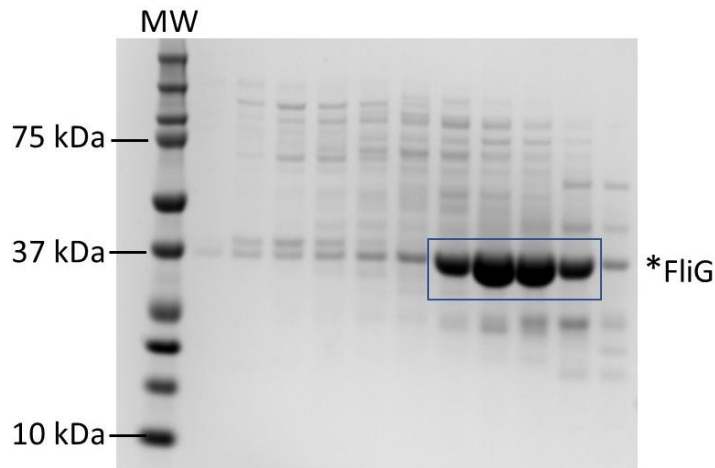
Figure 5.1: Fractions collected from initial step gradient elution of FliG(ΔPEV) from a Ni-affinity column. Fractions were loaded onto a NuPAGE 4-12% Bis-Tris gel. The fractions isolated and combined for further purification are highlighted in a blue box. The asterisk indicates the position of full length FliG(ΔPEV) (~37 kDa).
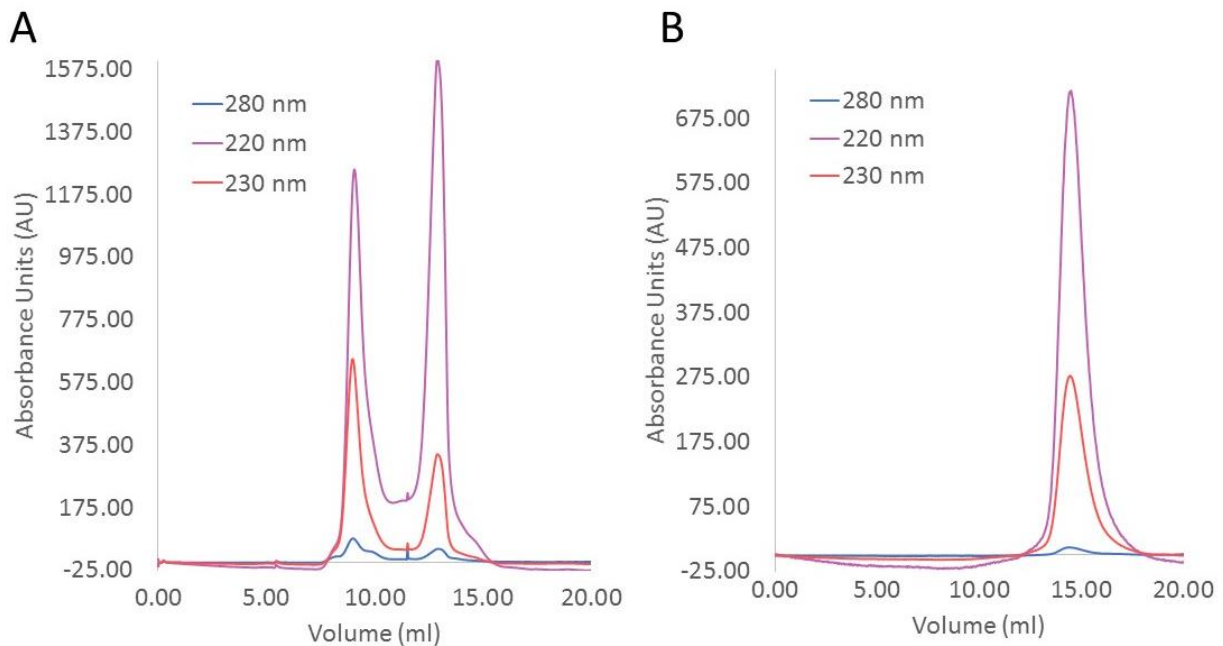
Figure 5.2: A. Elution profile of FliG(ΔPEV) from a gel filtration column immediately following Ni-affinity. FliG(ΔPEV) exhibits low signal at 280 nm, and elution is monitored at 220 and 230 nm. Two peaks are observed. The first peak (~9 ml) corresponds to either aggregate or a higher order oligomer of FliG(ΔPEV) and the second peak corresponds to monomeric FliG(ΔPEV). B. Elution profile of monomeric FliG peak collected and run through a second gel filtration step. As a note, these specific runs were done on two different gel filtration columns.

Microscale Thermophoresis

Real-time surface plasmon resonance analysis using wild-type FliG and QFR showed a dissociation constant in the low micromolar range (K_d=1.1 µM) (106). Using microscale thermophoresis (MST), we tested whether the binding affinity of QFR to the (ΔPEV) variant would be similar (**Figure 5.3**). The use of MST allowed for the binding affinity to be measured using impure QFR in the native membranes and without labeling using intrinsic FAD fluorescence. Pure FliG was added at varying concentrations to capillaries pre-loaded with QFR membranes and fluorescence was monitored in response gradient temperature changes. Saturation could not be achieved, but the results were consistent with a K_d in the low micromolar

range. Results obtained using QFR in detergent micelles, as opposed to membrane fractions, were also consistent with a low micromolar binding affinity.
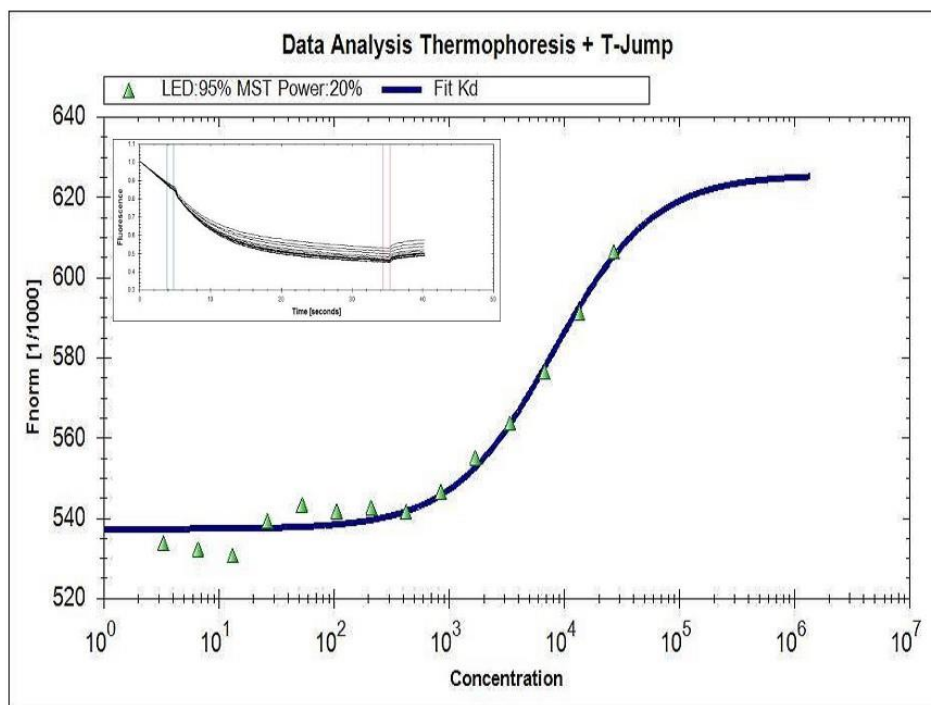
Figure 5.3: Microscale Thermophoresis of QFR and FliG(ΔPEV). Unlabeled FliG(ΔPEV) (1.7 nm to 54,000 nm) was incubated with QFR containing membranes at a constant concentration of 25 µM before measurement using the Monolith NT.115. All concentrations are in nM on the graph. No saturation was reached, but that data are consistent with binding in the low µM range.

Lipidic cubic phase crystallization of QFR and FliG(ΔPEV).

QFR is a membrane protein and requires a hydrophobic environment for stability in solution. As such, FliG and QFR were screened for stability in various detergents for co-crystallization. It was determined that both FliG and QFR were stable in $C_{12}E_8$, using aggregation visible on gel filtration as an indicator. For crystal screening, the proteins were

mixed with a 10-fold excess of FliG to allow for binding before a final gel filtration purification step in 20 mM Tris pH 7.4, 0.1 mM EDTA and 1 mM $C_{12}E_8$. Isolated fractions were concentrated to ~25mg/ml for crystallization trials.

Structures of membrane protein complexes are extremely rare due to the challenge in obtaining high quality crystals that diffract to reasonable resolution, but lipidic cubic phase crystallization has proven a powerful technique for obtaining higher resolution structures of membrane proteins. Considering this, crystallization of the QFR:FliG(ΔPEV) complex was attempted using LCP. For initial LCP attempts, a solution containing QFR and FliG(ΔPEV was mixed with monoolein (1-(9Z-octadecenoyl)-rac-glycerol, 9.9 MAG) in a gas-tight syringe for pipetting by a Xantus cubic lipid phase robot. Broad crystallization screens for LCP were set up using the Hampton StockOptions Salt screen with varied buffers from pH 6.5 to 8.5, and 15%-30% PEG 400 (110). Initial microcrystals grew in various wells with ammonium fluoride as the salt, but with poor diffraction (**Figure 5.4A,B**). We expanded these conditions into several 96-well screens to allow for fine screening of the best conditions under which crystals formed in the broad screen (100-600 mM ammonium fluoride, 5-30% PEG 400, and Bis-TRIS and TRIS buffers with a pH range of 6.0 to 9.0). This resulted in the formation of higher quality crystals, but they still exhibited poor diffraction (**Figure 5.4C,D**).

To further improve crystal quality, we tested the use of different lipids on the crystals grown in the optimized screens. Crystal size was altered in the presence of various lipids (**Figure 5.5**), but only resulted in a small improvement in diffraction quality. The best diffracting crystals at this point in optimization were dispersed with the lipid monovaccenin (1-(11Z-octadecenoyl)-rac-glycerol, 11.7 MAG), and as such, monovaccenin and monoolein were used in subsequent screens.
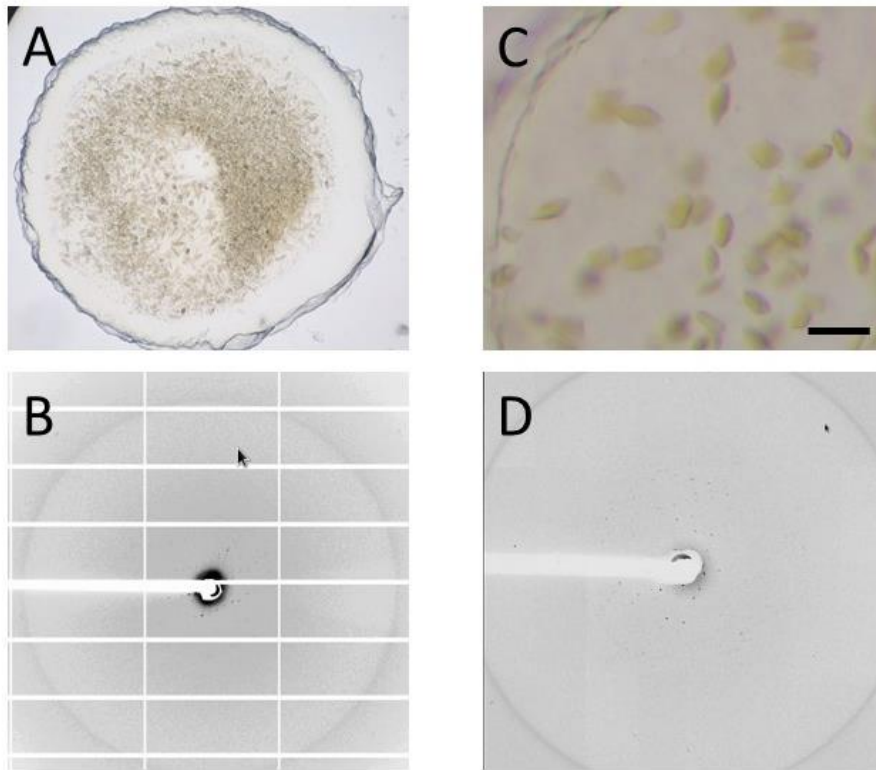
Figure 5.4: A, Example of initial microcrystals of the QFR:FliG complex in lipidic mesophase. QFR contains both iron-sulfur clusters and flavin adenine dinucleotide, resulting in a unique brown color (~408 nm absorbance). B. Representative diffraction pattern of these initial crystals (resolution limit is ~18 Å). C. Example of improved crystals from microscreening of initial conditions and (D.) corresponding diffraction pattern (resolution limit is ~7.4 Å). The bar represents 40 µm.

Figure 5.5: Representative examples of crystals obtained using varied lipids: (A.) monopalmitolein (B.) monoolein and (C.) monovaccenin. A change in relative crystal size can be observed as a result of dispersion with different lipids.

Finally, using the conditions for previously published structures determined using LCP, we created a unique additive screen to use with our best crystal conditions (Table 5.1). Additives were prepared in 10x solutions and then added to the precipitant solution as 10% of the final volume in 96-well screens with 200-600 mM ammonium fluoride, 100 mM Bis-TRIS pH 7.5 and 22-24% PEG 400. This screen resulted in crystals of up to 240 microns in size grown in mesophase (**Figure 5.6**), which made location of the crystals easier than is typical for the microcrystals commonly obtained in LCP and identified by rasterting. Several datasets were collected with crystals under the conditions of this screen with the following additives: pentaerythritol propoxylate, isopropanol, 1 butanol and methyl tert-butyl ether.
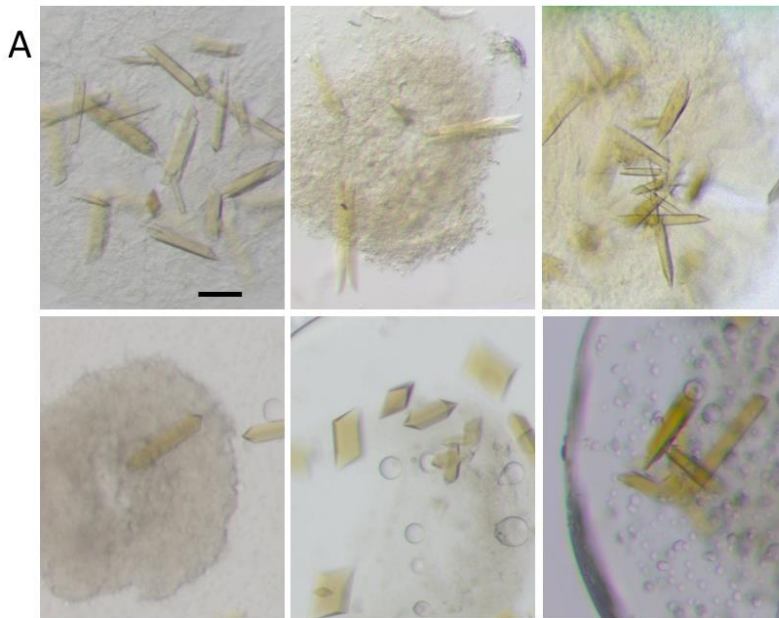
Figure 5.6: Examples of LCP crystals of the QFR:FliG complex optimized with the use of additives. The bar represents 100 µm.

Table 5.1

Additive Screen for Lipidic Cubic Phase Crystallization.

Reagent	Concentration
2-Methyl-2,4-pentanediol	30%
DMSO	30%
1,3-butanediol	40%
1,4-butanediol	60%
pentaerythritol propoxylate	50%
Jeffamine M-600	50%
t-butanol	40%
isopropanol	20%
1,4-dioxane	30%
2-propanol	40%
glycerol	30%
ethylene glycerol	30%
2,5-hexanediol	30%
1,2-hexanediol	30%
1-butanol	7%
1,2,3-heptanetriol	10%
(R,S)-dobutamine	10 mM
TCEP	100mM
benzamidine hydrochloride	20%(w/v)
ethanol	30%
PPG P400	30%
eticlopride	10 mM
taurine	100 mM
Nickel choride	0.1M
strontium choride	100 mM
Hexamine cobalt choride	50 mM
methyl tert-butyl ether	30%
1-propanol	40%
phosphonoformate	100mM

Data Collection and Discussion

Using this additive screen, in combination with changes to lipid composition and fine screening of crystal conditions, were able to collect several datasets with diffraction up to 4.7 Å (**Figure 5.7**). Crystals belonged to the orthorhombic space group $P2_12_12_1$ with unit cell parameters $a = 136.31$, $b = 131.73$, $c = 261.24$ and $\alpha\beta\gamma = 90°$ or the monoclinic space group $P2_1$ with unit cell parameters $a = 73.97$, $b = 132.50$, $c = 305.77$ and $\beta = 90.01°$. Although we were able to collect several datasets, efforts to merge the datasets and determine the structure by molecular replacement were unsuccessful. We tried molecular replacement using structures of wild type QFR currently available in the PDB as well as FliG structures, although there are currently no structures of full length FliG from *E. coli* and the available structures had low sequence identity (27-34%). Changing the input model and phasing strategy using multiple iterations did not result in a correct solution for any of the datasets.
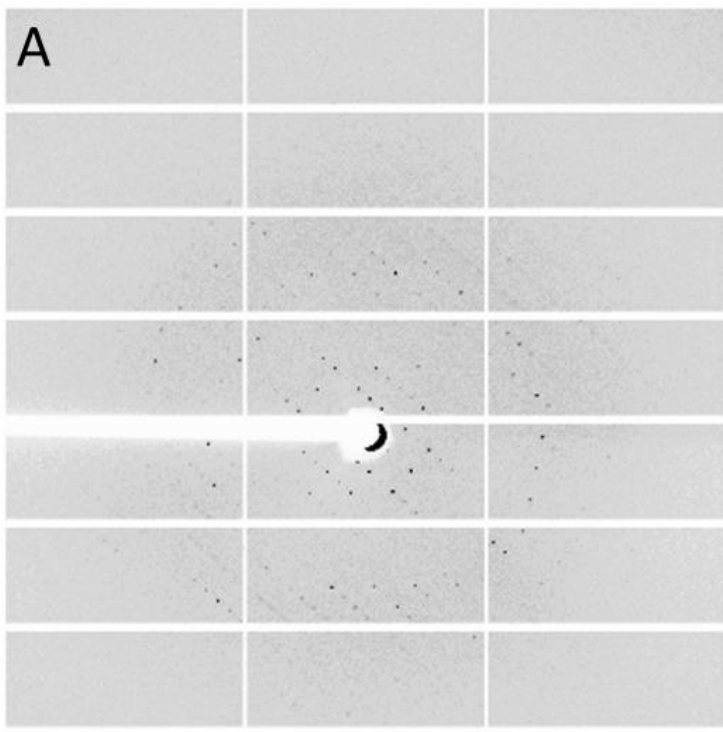
Figure 5.7: Representative diffraction pattern of optimized LCP crystals (resolution limit is ~4.7 Å).

Without a refined structure, we were not able to definitively confirm that the crystals contained both FliG and QFR. In part due to the difficulty of isolating crystals grown in lipidic mesophases, we were also unable to use more traditional methods for identifying the crystal contents. However, we do have some evidence to suggest that these crystals are composed of the complex. First, we set up the optimized LCP screens using wild type QFR alone under the same conditions. While crystals grew in approximately 80% of the wells using the complex mixture, we only observed growth for crystals of wild type in a few wells and the crystals were comparatively smaller in size. In addition, we were able to grow crystals of a mutant of QFR alone, with an E245Q substitution in the flavoprotein subunit, under one of the LCP conditions

for which complex crystals grew. Crystals from this dataset diffracted to only 7.4 Å, but we were easily able to determine the phases using molecular replacement and to obtain low resolution electron density maps. The ease of molecular replacement for this isolated mutant of QFR in comparison with the failure of molecular replacement for all of the QFR:FliG datasets suggests that something is different about the data for these structures. Finally, the unit cell parameters for datasets of the complex we collected differ significantly from those of the currently available structures for wild type QFR.

Summary

While these observations cannot confirm the presence of complex in the crystals, it seems a reasonable possibility to consider that they contain both QFR and FliG until we are able to fully resolve a structure. In the future, we plan to attempt alternative methods of phasing, although the use of heavy atoms for experimental phasing, for example, has proven more challenging *in meso*. Furthermore, we were able to successfully optimize the quality and resolution of LCP crystals and our approach in developing screens may provide guidelines for this this process in other systems. Future efforts will likely focus on alternative methods of phasing, although the use of heavy atoms for experimental phasing, for example, has proven more challenging in meso. While we have not yet fully elucidated the co-structure, our efforts at optimization have led to a significant improvement in both in crystal quality and resolution. Furthermore, our approach in developing additive screens may provide guidelines for lipidic cubic phase crystallization in other systems.

CHAPTER 6

SUMMARY AND CONCLUSIONS

Complex II has been studied for over 100 years and in that time significant advances have been made in our understanding of the structure of this heterotetrameric complex and its function in energy metabolism. However, key questions about complex assembly and the mechanism of covalent flavinylation remained. The work reported in this document further advances our knowledge of assembly of the mature complex, including how an assembly factor might facilitate covalent linking of flavin. We find that while attachment of the covalently bound flavin may proceed through autocatalytic processes for Complex II superfamily members, multiple pathways may have evolved to support this chemistry, either through the addition of electron donor/acceptors or adaptation of the active site through interactions with assembly factors or additional subunits of a complex.

Studies described in Chapter 2, including expression and purification of the isolated E. coli flavoprotein subunit, or FrdA, provided us with the tools to study assembly and covalent flavinylation in Complex II. Working with the bacterial homologs, we expressed the E. coli FrdA subunit in the absence of the rest of the complex (FrdB, FrdC, FrdD) and used this to study its interaction with the assembly factor, termed SdhE in E. coli. Using size exclusion chromatography and FAD-UV fluorescence, we determined that, in contrast to published studies (41), SdhE did not bind FAD and was unlikely to act as an FAD transporter. We also established that purified SdhE did not appear to interact with purified E. coli FrdA flavoprotein under the conditions tested; one interpretation of this finding is that additional factors could be required for

the interaction that had been demonstrated in vivo. These additional factors could be proteins, small molecules electron acceptors or a required experimental condition. In fact, a recent study demonstrated that in vitro reconstitution of the covalent bond in the human enzyme was pH dependent (96). As we did not identify the necessary conditions for the SdhE:FrdA interaction in our studies and studies in the human enzyme were published after our work, we considered alternative ways to 'trap' the interaction between SdhE and FrdA as described in Chapter 3.

After various methods to demonstrate an in-vitro interaction between SdhE and FrdA failed, we used a series of SdhE mutants designed by Gary Cecchini's lab at UCSF (43). These mutants were designed to incorporate an artificial amino acid at 16 amino acid sites, capable of crosslinking to nearby residues of an interacting partner. As described in Chapter 3, we used crosslinked complexes produced by the Cecchini laboratory to identify two distinct points of interaction in the binding interface between SdhE and FrdA. These experimentally determined sites were then used as input for developing a computational model of the SdhE:FrdA complex. The Rosetta generated models effectively formed a single cluster and the conserved surface patch of SdhE (58) was directed towards the flavoprotein in all of the docked orientations. The high level of agreement between docked positions, generated using only two constraints, strengthens the proposition that we have correctly identified the orientation of these two proteins in the complex and that this interacting surface includes the conserved RGxxE motif of SdhE (59).

This computational model served as the first structural view of how SdhE and FrdA might interact and allowed us to generate an informed model of not only the interaction, but also of assembly of the mature complex. Based on this modeling, we determined that SdhE interacts with the flavoprotein at the same interface as the iron-sulfur subunit, indicating that covalent

flavinylation occurs before the flavoprotein is assembled into the mature QFR or SQR heterotetramer. This discovery provided new information about the order of complex assembly as well as trafficking in the human complex, where the isolated flavoprotein must be transported to the mitochondria prior to assembly.

Our findings here are consistent with SdhE acting as an assembly factor, rather than as a simple FAD transporter. We further determined that SdhE interacts with FrdA that already contained FAD. Similar to non-covalent mutants of QFR (23), we also determined that isolated flavoprotein contained non-covalent flavin that was tightly bound at stoichiometric levels, as described in Chapter 4. Using the computational model as a guide, we propose a model for SdhE:FrdA interaction, whereby SdhE orients the two flavoprotein domains to promote closure over the dicarboxylate cofactor and orientation of key residues for involved in catalysis of the covalent flavin bond. This model for SdhE action is similar to that of cytochrome subunit of p-cresol methylhydroxylase (Figure 2.1, (61)), where binding of the cytochrome subunit orients residues to facilitate covalent 8α-O-tyrosyl FAD attachment in the flavoprotein subunit of that enzyme.

This model for SdhE:FrdA interaction is consistent with our SAXS modeling of the complex (Chapter 4), in which SdhE binding promotes closure of the capping domain over the dicarboxylate binding site. The SAXS modeling provided us with an experimentally informed model whereby we could not only identify the SdhE binding site, but also evaluate the location of important residues. Using an averaged Rosetta model of the crosslinked FrdA:SdhER8BpF complex as a starting point, we determined the best fit of an intact model of the crosslinked complex into the SAXS envelope. In this model, SdhE is again oriented such that the RGxxE motif faces the flavoprotein subunit and overlaps with the iron-sulfur subunit binding site. As

predicted in our earlier model (Chapter 3), the SAXs data are consistent with the interpretation SdhE acted as a 'wedge' between the two flavoprotein domains, resulting in a tightly closed capping domain.

Additional work in this chapter provided us with insight into how specific residues may influence covalent flavin linkage and guided our evaluation of this new crosslinked model. We identified several residues that are important for covalent flavinylation and completed a more in-depth analysis of one of those residues, an FrdAE245Q mutant. We found this residue interesting because it was not close to the site of flavin attachment, as with some of the residues we identified, and did not have a known role in covalent flavinylation. However, substitution at this site reduced covalent flavinylation to levels below those observed in a ΔsdhE strain. Its central location between the two flavoprotein domains and its known role in proton shuttling during fumarate reduction suggested a few hypotheses for its role in covalent flavinylation that we investigated in our work, namely that FrdAE245Q: (i) could be important for modulating interdomain motions, (ii) substitutions with glutamine affect dicarboxylate turnover, (iii) substitutions with glutamine reduce stability, and (iv) is important for the SdhE/flavoprotein interaction.

Our work confirmed that substitutions of this amino acid did not induce changes in stability or folding as measured by Far-UV circular dichroism and thermal denaturation studies, and did not result in conformational changes that could be observed in a low-resolution crystal structure. We also demonstrated that FrdAE245Q was catalytically inactive and deficient in binding of dicarboxylates. In addition, we found that FrdAE245Q had a reduced capacity for interaction with the assembly factor, but analysis of the SAXS model indicated that this was not likely due to disruption of a direct interaction between FrdAE245Q and the surface of SdhE.

Rather, it seems possible that FrdAE245Q may have a role in prohibiting the optimal alignment of key residues for covalent flavin linkage when bound to SdhE or may participate in an alternative proton shuttling pathway specific to substrate turnover during covalent flavinylation, when the normal positioning of catalytic residues is altered in the context of a tightly closed capping domain.

Although we investigated several aspects of covalent flavinylation, including the role of an assembly factor and specific residues involved in the mechanism, perhaps one of our most interesting findings, with respect to research in flavoenzymes, was that there seemed to be overlap between multiple factors capable of supporting auto-catalytic covalent flavin attachment. Our work demonstrated that no factor is absolutely required for covalent flavinylation, but that many factors can enhance this process. Additionally, it seems that a pre-organized active site is an important underlying principle for covalent flavin attachment, and that in the context of Complex II, this can be stimulated by binding of the dicarboxylic substrate, assembly factor or the iron-sulfur subunit. Overall, our findings support the idea that covalent flavinylation in Complex II is auto-catalytic and that the assembly factor, SdhE in E. coli, enhances this process.

Independent of our work to investigate assembly and covalent flavinylation in Complex II, we also investigated a potential alternative role for the bacterial homolog, QFR, in signaling. We attempted to determine a structure of the complex between QFR and the bacterial flagellar motor protein, FliG, which is involved in switching of bacterial flagella in response to changes in environmental stimuli. We were unable to determine a crystal structure of the complex, but we developed valuable techniques for the optimization of LCP crystals. In our protocol, initial broad screening for crystallization conditions was followed by lipid screening using a unique 96-well matrix protocol and a novel additive screen developed in our lab. As a result, we significantly

improved crystal quality and obtained crystals large enough to exclude the rastering often

required in LCP screening. We also significantly improved the resolution of the original crystals

(20-30 Å), with final crystals diffracting to 4.5 Å resolution. These methods may prove useful to

other groups in their efforts to crystallize large membrane proteins or membrane complexes

using LCP crystallization.

CHAPTER 7

FUTURE DIRECTIONS

The work described in this document has explored mechanisms of assembly and covalent flavination in Complex II, as well as structural studies of a unique interaction between a bacterial homolog of Complex II, QFR, and a flagellar motor protein, FliG, which expands our current knowledge of the function of this important enzyme. Our work resolves long standing questions about the order of assembly of the mature heterotetrameric complex and provides insight into how an assembly factor helps to promote autocatalysis of covalent linkage to the flavin cofactor. Nevertheless, many questions remain about complex assembly, the specific mechanism of covalent flavinylation and the roles of additional, newly identified factors involved in assembly and cofactor insertion. These questions may be addressed in future work that utilizes both the bacterial homologs and human Complex II, as well as their associated assembly factors.

Our work to identify the relevant binding surfaces for an SdhE:FrdA complex revealed that the SdhE binding site overlaps with that of the iron-sulfur subunit. This provided clear evidence that SdhE enhanced flavinylation occurs in the isolated flavoprotein prior to its assembly into the complex. However, it is unclear how the next stages of assembly may proceed and key questions remain, such as how SdhE is removed from the flavoprotein and what constitutes the next step in assembly? In addition, there are perhaps questions concerning how SdhE initially competes with the iron-sulfur subunit for binding to the flavoprotein, as it is anticipated that the iron-sulfur subunit is likely to form a more stable complex with the flavoprotein. Indeed, our collaborators in the Cecchini lab have determined that a small fraction

of FrdA is flavinylated in the absence of SdhE, possibly by the iron-sulfur subunit, FrdB in E. coli ((111) and unpublished observation). As such, it appears that both SdhE and SdhB are capable of stimulating autocatalytic flavinylation, but with SdhE being more efficient. Understanding how one promotes flavinylation over the other may help to answer important questions about the evolution of the assembly factor and possibly why the assembly factor is not required in some organisms. It is possible that the iron-sulfur subunit (FrdB in E. coli) has a higher affinity for the flavoprotein with covalently bound flavin. However, our circular dichroism studies suggest that the folding of the flavoprotein with non-covalent FAD is nearly identical to that of flavoprotein with covalently incorporated FAD. These aspects of assembly were not investigated directly in the current studies, but as we have developed conditions for the isolation of the flavoprotein and assembly factor, it is possible that future studies could investigate the binding of flavoprotein with and without covalently bound flavin to SdhE and FrdB. If findings that the flavinylation is pH dependent in the human enzyme (96) do not hold for the bacterial complex, these studies may need to be done in lysate, in a background that excludes endogenous SdhE and FrdB. There are a few techniques for binding studies that can be performed with non-purified protein, but we have demonstrated in our studies that microscale thermophoresis is a viable technique for such studies of Complex II, as fluorescence of the flavin cofactor can be used for a signal and reduces the need to use artificial labeling. Additionally, studies using the iron-sulfur subunit, FrdB, would need to be conducted in an anaerobic chamber to protect the 3Fe:4S cluster, which is oxygen sensitive in the isolated subunit but not in the context of the fully assembled complex (112).

The identification of an additional assembly factor for flavinylation in the human complex, termed SDH-AF4, that is believed to facilitate assembly of the flavoprotein/iron-sulfur

subunits provides another possible explanation for how the next stage of complex assembly proceeds (113). This assembly factor has a homolog in yeast but no clear sequence counterpart in bacteria. Preliminary work has suggested that it may interact with the flavoprotein subunit after covalent flavin attachment and appears to be important for facilitating its association with the iron-sulfur subunit (113). SDH-AF4 could interact with the SDH-AF2-flavoprotein complex and facilitate the removal of the SDH-AF2 and interaction with the iron-sulfur subunit, or it could interact with the flavoprotein after SDH-AF2 removal. Although not discussed in this document, our collaborators in the Cecchini lab have developed conditions for the recombinant expression of SDH-AF2 and SDH-AF4, and determined conditions for the expression of the SdhA flavoprotein from the human complex. As such, it is conceivable that one could use binding studies to directly investigate whether SDH-AF4 interacts with the SDH-AF2/flavoprotein complex, with the flavoprotein after SDH-AF2 is removed. It would also be important to investigate whether SDH-AF4 binds directly to the iron-sulfur subunit. A crystal structure of SDH-AF4 alone or in the relevant complex would also provide additional insights into the role of this assembly factor in Complex II assembly and potentially inform hypotheses as to why it appears bacteria do not require this assembly factor.

In addition to questions concerning assembly of the mature complex, there are still unresolved questions about the specific mechanism of covalent flavinlylation and how the assembly factor, termed SdhE in E. coli, promotes this process. For example, although our studies resulted in a structural model of the FrdA:SdhE complex strengthened by input from binding studies and SAXS analysis, it is still a model that has inherent limitations over an actual structure of the complex. In order to gain specific information about the interaction between SdhE and FrdA, a co-structure would be ideal. In the current work, we described efforts to use

this system to obtain a co-crystal structure and report several crystal 'hits' in the initial broad screening. As described in Chapter 4, purification of the crosslinked complex separate from flavoprotein alone proved difficult, and were not completed as part of the work described in this document. However, our lab recently determined the structure of the crosslinked complex using the system described and preliminary analysis of this structure offers exciting insights into the role of SdhE in flavinylation (unpublished work). As a result, the lab is currently focused on biochemical and biophysical studies that test the theories developed after analysis of this structure.

Using this structure as a guide, mutagenesis studies could be employed to investigate the importance of residues involved in binding the assembly factor and flavinylation. Mutants could be designed at sites predicted to disrupt binding between the two proteins and analysis of the effect of these mutations, on binding and flavinylation, may result in a strengthened model for how SdhE stimulates covalent flavinylation. In addition, a close analysis of the FAD binding site in the SdhE bound structure may inform mutagenesis experiments that investigate the organization of the FrdA active site that promotes autocatalysis of the covalent flavin bond. For example, based on our final FrdA:SdhER8BpF model, FrdAE245Q is proposed to have a role in aligning key residues and possibly an alternative proton pathway associated with covalent flavinylation. An evaluation of the crosslinked structure provides a high resolution view into active site organization in the context of SdhE binding and could be used to predict amino acid sites where changes may impact the role of FrdAE245Q or other residues involved in covalent flavinylation.

Although there are many studies that could be done to further elucidate the mechanism of covalent flavinylation and the role of SdhE in this process, it will also be important to identify all

required elements for the FrdA:SdhE interaction. In our crosslinking studies, we determined that lysate was required to observe an interaction between SdhE and FrdA, suggesting that additional factors may be required. In our early studies, bands associated with purified SdhE and FrdA were identified using mass spectrometry (Chapter 3), and one ~22 kDa band of interest was identified as 'catabolite gene activator', a predicted transcription factor about which very little is known. This ~22kDa band was found in isolated samples of both SdhE and FrdA and Western analysis suggested that it may bind SdhE (Chapter 4). A simple experiment to identify this and other potential protein factors may be to determine if the levels of covalent flavinylation are attenuated in a strain lacking the catabolite gene activator, which has already been obtained from the E. coli Genetic Stock Center (64).

However, it is also possible that the additional factor may not be a protein. In a recent study using the human enzyme the authors determined that flavoprotein in the human complex, SDHA, appeared unstable after complete purification and that an interaction with SdhE appeared to be pH dependent (96). In this work, the authors developed an in-vitro system for covalent flavinylation of the human flavoprotein, which minimally required the human assembly factor, SDH5, and a pH of ~6.5. They also determined that dicarboxylates stimulated the flavinylation reaction, but were not required. It is worth noting, however, that their initial observation was also that lysate was required, as in vitro flavinylation did not proceed using fully purified flavoprotein. The authors ultimately determined that his6-tagged SDHA immobilized on Ni-NTA resin could be isolated and used for in vitro flavinylation using only SDH5 in phosphate buffer at pH 6.5. While the authors present a careful examination of the conditions for flavinylation, they do not present evidence that they investigated the possibility that washes did not remove all outside components of the lysate. It would be important to establish that the

immobilized SDHA did not contain other components. One experiment may be to remove the immobilized SDHA by denaturation in loading buffer and to analyze the contents by SDS-PAGE electrophoresis. It may also be interesting to repeat this experiment in the bacterial flavoprotein, where we find increased stability over the isolated flavoprotein in the human enzyme. In bacteria, it may be possible to investigate the pH dependence of this reaction using pure protein.

While future work may complement directly our contributions to an increased understanding of assembly and covalent flavinylation in Complex II, there are also other important aspects of assembly to pursue. In recent years, several assembly factors have been identified as having a role in Complex II assembly, as well as new interaction partners, making it clear that there is still much to learn about this vital complex. For example, two LYR motif proteins were recently identified in the yeast and human complexes and are believed to be important for insertion of the iron-sulfur clusters (114). An interaction between QFR and FliG, a flagellar motor protein, was also discovered and suggests a role of the bacterial homolog in chemotactic signaling (Chapter 5, (106)). Additionally, the precise role of the heme cofactor in Complex II is unknown, although studies have determined that it is important for assembly of the mammalian complex and possibly for removing reactive oxygen species (115). These, and other recent findings, point to the increasing complexity of Complex II and the great potential of future work to delineate not only the mechanisms of assembly and cofactor insertion but the intriguing process of evolution of this complex from bacteria to human.

REFERENCES

1. Starbird, C. A., Maklashina, E., Cecchini, G., and Iverson, T. M. (2001) Flavoenzymes: Covalent versus Noncovalent. in *eLS*, John Wiley & Sons, Ltd. pp

2. Karplus, P. A., Fox, K. M., and Massey, V. (1995) Flavoprotein structure and mechanism. 8. Structure-function relations for old yellow enzyme. *FASEB journal : official publication of the Federation of American Societies for Experimental Biology* **9**, 1518-1526

3. Miller, J. R., Guan, N., Hubalek, F., and Edmondson, D. E. (2000) The FAD binding sites of human liver monoamine oxidases A and B: investigation of the role of flavin ribityl side chain hydroxyl groups in the covalent flavinylation reaction and catalytic activities. *Biochimica et biophysica acta* **1476**, 27-32

4. Grein, F., Ramos, A. R., Venceslau, S. S., and Pereira, I. A. (2013) Unifying concepts in anaerobic respiration: insights from dissimilatory sulfur metabolism. *Biochimica et biophysica acta* **1827**, 145-160

5. Welte, C., and Deppenmeier, U. (2014) Bioenergetics and anaerobic respiratory chains of aceticlastic methanogens. *Biochimica et biophysica acta* **1837**, 1130-1147

6. Cecchini, G., Schroder, I., Gunsalus, R. P., and Maklashina, E. (2002) Succinate dehydrogenase and fumarate reductase from Escherichia coli. *Biochimica et biophysica acta* **1553**, 140-157

7. Medina, M. (2009) Structural and mechanistic aspects of flavoproteins: photosynthetic electron transfer from photosystem I to NADP+. *The FEBS journal* **276**, 3942-3958

8. Cecchini, G. (2003) Function and structure of complex II of the respiratory chain. *Annual review of biochemistry* **72**, 77-109

9. Akman, S. A., Doroshow, J. H., Burke, T. G., and Dizdaroglu, M. (1992) DNA base modifications induced in isolated human chromatin by NADH dehydrogenase-catalyzed reduction of doxorubicin. *Biochemistry* **31**, 3500-3506

10. DeRosa, M. C., Sancar, A., and Barton, J. K. (2005) Electrically monitoring DNA repair by photolyase. *Proceedings of the National Academy of Sciences of the United States of America* **102**, 10788-10792

11. van Pee, K. H., and Patallo, E. P. (2006) Flavin-dependent halogenases involved in secondary metabolism in bacteria. *Applied microbiology and biotechnology* **70**, 631-641

112

12.   Mowafy, A. M., Kurihara, T., Kurata, A., Uemura, T., and Esaki, N. (2010) 2-haloacrylate hydratase, a new class of flavoenzyme that catalyzes the addition of water to the substrate for dehalogenation. *Applied and environmental microbiology* **76**, 6032-6037

13.   Kearney, E. B., and Singer, T. P. (1955) On the prosthetic group of succinic dehydrogenase. *Biochimica et biophysica acta* **17**, 596-597

14.   Walker, W. H., Salach, J., Gutman, M., Singer, T. P., Hyde, J. S., and Ehrenberg, A. (1969) Endor studies on the covalently bound flavin at the active center of succinate dehydrogenase. *FEBS letters* **5**, 237-240

15.   Walker, W. H., Kearney, E. B., Seng, R., and Singer, T. P. (1971) Sequence and structure of a cysteinyl flavin peptide from monoamine oxidase. *Biochemical and biophysical research communications* **44**, 287-292

16.   Kearney, E. B., Salach, J. I., Walker, W. H., Seng, R., and Singer, T. P. (1971) Structure of the covalently bound flavin of monoamine oxidase. *Biochemical and biophysical research communications* **42**, 490-496

17.   Binda, C., Li, M., Hubalek, F., Restelli, N., Edmondson, D. E., and Mattevi, A. (2003) Insights into the mode of inhibition of human mitochondrial monoamine oxidase B from high-resolution crystal structures. *Proceedings of the National Academy of Sciences of the United States of America* **100**, 9750-9755

18.   Mirza, I. A., Burk, D. L., Xiong, B., Iwaki, H., Hasegawa, Y., Grosse, S., Lau, P. C., and Berghuis, A. M. (2013) Structural analysis of a novel cyclohexylamine oxidase from Brevibacterium oxydans IH-35A. *PloS one* **8**, e60072

19.   Kopacz, M. M., Rovida, S., van Duijn, E., Fraaije, M. W., and Mattevi, A. (2011) Structure-based redesign of cofactor binding in putrescine oxidase. *Biochemistry* **50**, 4209-4217

20.   Stavropoulos, P., Blobel, G., and Hoelz, A. (2006) Crystal structure and mechanism of human lysine-specific demethylase-1. *Nature structural & molecular biology* **13**, 626-632

21.   Yang, M., Gocke, C. B., Luo, X., Borek, D., Tomchick, D. R., Machius, M., Otwinowski, Z., and Yu, H. (2006) Structural basis for CoREST-dependent demethylation of nucleosomes by the human LSD1 histone demethylase. *Molecular cell* **23**, 377-387

22.   Chen, Y., Yang, Y., Wang, F., Wan, K., Yamane, K., Zhang, Y., and Lei, M. (2006) Crystal structure of human histone lysine-specific demethylase 1 (LSD1). *Proceedings of the National Academy of Sciences of the United States of America* **103**, 13956-13961

23.   Blaut, M., Whittaker, K., Valdovinos, A., Ackrell, B. A., Gunsalus, R. P., and Cecchini, G. (1989) Fumarate reductase mutants of Escherichia coli that lack covalently bound flavin. *The Journal of biological chemistry* **264**, 13599-13604

24.   Turner, K. L., Doherty, M. K., Heering, H. A., Armstrong, F. A., Reid, G. A., and Chapman, S. K. (1999) Redox properties of flavocytochrome c3 from Shewanella frigidimarina NCIMB400. *Biochemistry* **38**, 3302-3309

25.   Fraaije, M. W., van den Heuvel, R. H., van Berkel, W. J., and Mattevi, A. (1999) Covalent flavinylation is essential for efficient redox catalysis in vanillyl-alcohol oxidase. *The Journal of biological chemistry* **274**, 35514-35520

26.   Huang, C. H., Lai, W. L., Lee, M. H., Chen, C. J., Vasella, A., Tsai, Y. C., and Liaw, S. H. (2005) Crystal structure of glucooligosaccharide oxidase from Acremonium strictum: a novel flavinylation of 6-S-cysteinyl, 8alpha-N1-histidyl FAD. *The Journal of biological chemistry* **280**, 38831-38838

27.   Huang, C. H., Winkler, A., Chen, C. L., Lai, W. L., Tsai, Y. C., Macheroux, P., and Liaw, S. H. (2008) Functional roles of the 6-S-cysteinyl, 8alpha-N1-histidyl FAD in glucooligosaccharide oxidase from Acremonium strictum. *The Journal of biological chemistry* **283**, 30990-30996

28.   Kopacz, M. M., and Fraaije, M. W. (2014) Turning a monocovalent flavoprotein into a bicovalent flavoprotein by structure-inspired mutagenesis. *Bioorganic & medicinal chemistry* **22**, 5621-5627

29.   Vey, J. L., Al-Mestarihi, A., Hu, Y., Funk, M. A., Bachmann, B. O., and Iverson, T. M. (2010) Structure and mechanism of ORF36, an amino sugar oxidizing enzyme in everninomicin biosynthesis. *Biochemistry* **49**, 9306-9317

30.   Bruender, N. A., Thoden, J. B., and Holden, H. M. (2010) X-ray structure of kijd3, a key enzyme involved in the biosynthesis of D-kijanose. *Biochemistry* **49**, 3517-3524

31.   van Hellemond, E. W., Mazon, H., Heck, A. J., van den Heuvel, R. H., Heuts, D. P., Janssen, D. B., and Fraaije, M. W. (2008) ADP competes with FAD binding in putrescine oxidase. *The Journal of biological chemistry* **283**, 28259-28264

32.   Tomasiak, T. M., Maklashina, E., Cecchini, G., and Iverson, T. M. (2008) A threonine on the active site loop controls transition state formation in Escherichia coli respiratory complex II. *The Journal of biological chemistry* **283**, 15460-15468

33.   Mattevi, A., Tedeschi, G., Bacchella, L., Coda, A., Negri, A., and Ronchi, S. (1999) Structure of L-aspartate oxidase: implications for the succinate dehydrogenase/fumarate reductase oxidoreductase family. *Structure (London, England : 1993)* **7**, 745-756

34.   Hao, H. X., Khalimonchuk, O., Schraders, M., Dephoure, N., Bayley, J. P., Kunst, H., Devilee, P., Cremers, C. W., Schiffman, J. D., Bentz, B. G., Gygi, S. P., Winge, D. R., Kremer, H., and Rutter, J. (2009) SDH5, a gene required for flavination of succinate dehydrogenase, is mutated in paraganglioma. *Science* **325**, 1139-1142

35.   Brandsch, R., and Bichler, V. (1986) Studies in vitro on the flavinylation of 6-hydroxy-D-nicotine oxidase. *European journal of biochemistry / FEBS* **160**, 285-289

36.   Brandsch, R., and Bichler, V. (1991) Autoflavinylation of apo6-hydroxy-D-nicotine oxidase. *The Journal of biological chemistry* **266**, 19056-19062

37.   Brizio, C., Brandsch, R., Douka, M., Wait, R., and Barile, M. (2008) The purified recombinant precursor of rat mitochondrial dimethylglycine dehydrogenase binds FAD via an autocatalytic reaction. *International journal of biological macromolecules* **42**, 455-462

38.   Bandrin, S. V., Rabinovich, P. M., and Stepanov, A. I. (1983) [3 linkage groups of the genes of riboflavin biosynthesis in Escherichia coli]. *Genetika* **19**, 1419-1425

39.   Hassan-Abdallah, A., Bruckner, R. C., Zhao, G., and Jorns, M. S. (2005) Biosynthesis of covalently bound flavin: isolation and in vitro flavinylation of the monomeric sarcosine oxidase apoprotein. *Biochemistry* **44**, 6452-6462

40.   Jin, J., Mazon, H., van den Heuvel, R. H., Heck, A. J., Janssen, D. B., and Fraaije, M. W. (2008) Covalent flavinylation of vanillyl-alcohol oxidase is an autocatalytic process. *The FEBS journal* **275**, 5191-5200

41.   McNeil, M. B., Clulow, J. S., Wilf, N. M., Salmond, G. P., and Fineran, P. C. (2012) SdhE is a conserved protein required for flavinylation of succinate dehydrogenase in bacteria. *The Journal of biological chemistry* **287**, 18418-18428

42.   McNeil, M. B., Hampton, H. G., Hards, K. J., Watson, B. N., Cook, G. M., and Fineran, P. C. (2014) The succinate dehydrogenase assembly factor, SdhE, is required for the flavinylation and activation of fumarate reductase in bacteria. *FEBS letters* **588**, 414-421

43.   Maklashina, E., Rajagukguk, S., Starbird, C. A., McDonald, W. H., Koganitsky, A., Eisenbach, M., Iverson, T. M., and Cecchini, G. (2016) Binding of the Covalent Flavin Assembly Factor to the Flavoprotein Subunit of Complex II. *The Journal of biological chemistry* **291**, 2904-2916

44.   Kounosu, A. (2014) Analysis of covalent flavinylation using thermostable succinate dehydrogenase from Thermus thermophilus and Sulfolobus tokodaii lacking SdhE homologs. *FEBS letters* **588**, 1058-1063

45.   Walsh, C. (1980) Flavin Coenzymes: At the crossroads of Biological Redox Chemistry. *Acc Chem Res* **13**, 148-155

46. Iverson, T. M. (2013) Catalytic mechanisms of complex II enzymes: a structural perspective. *Biochimica et biophysica acta* **1827**, 648-657

47. Iverson, T. M., Luna-Chavez, C., Cecchini, G., and Rees, D. C. (1999) Structure of the Escherichia coli fumarate reductase respiratory complex. *Science (New York, N.Y.)* **284**, 1961-1966

48. Lancaster, C. R., Kroger, A., Auer, M., and Michel, H. (1999) Structure of fumarate reductase from Wolinella succinogenes at 2.2 A resolution. *Nature* **402**, 377-385

49. Rose, P. W., Beran, B., Bi, C., Bluhm, W. F., Dimitropoulos, D., Goodsell, D. S., Prlic, A., Quesada, M., Quinn, G. B., Westbrook, J. D., Young, J., Yukich, B., Zardecki, C., Berman, H. M., and Bourne, P. E. (2011) The RCSB Protein Data Bank: redesigned web site and web services. *Nucleic acids research* **39**, D392-401

50. Overington, J. P., Al-Lazikani, B., and Hopkins, A. L. (2006) How many drug targets are there? *Nature reviews. Drug discovery* **5**, 993-996

51. Eshaghi, S., Hedren, M., Nasser, M. I., Hammarberg, T., Thornell, A., and Nordlund, P. (2005) An efficient strategy for high-throughput expression screening of recombinant integral membrane proteins. *Protein science : a publication of the Protein Society* **14**, 676-683

52. Long, S. B., Tao, X., Campbell, E. B., and MacKinnon, R. (2007) Atomic structure of a voltage-dependent K+ channel in a lipid membrane-like environment. *Nature* **450**, 376-382

53. Rasmussen, S. G., DeVree, B. T., Zou, Y., Kruse, A. C., Chung, K. Y., Kobilka, T. S., Thian, F. S., Chae, P. S., Pardon, E., Calinski, D., Mathiesen, J. M., Shah, S. T., Lyons, J. A., Caffrey, M., Gellman, S. H., Steyaert, J., Skiniotis, G., Weis, W. I., Sunahara, R. K., and Kobilka, B. K. (2011) Crystal structure of the beta2 adrenergic receptor-Gs protein complex. *Nature* **477**, 549-555

54. Landau, E. M., and Rosenbusch, J. P. (1996) Lipidic cubic phases: a novel concept for the crystallization of membrane proteins. *Proceedings of the National Academy of Sciences of the United States of America* **93**, 14532-14535

55. Rasmussen, S. G., Choi, H. J., Fung, J. J., Pardon, E., Casarosa, P., Chae, P. S., Devree, B. T., Rosenbaum, D. M., Thian, F. S., Kobilka, T. S., Schnapp, A., Konetzki, I., Sunahara, R. K., Gellman, S. H., Pautsch, A., Steyaert, J., Weis, W. I., and Kobilka, B. K. (2011) Structure of a nanobody-stabilized active state of the beta(2) adrenoceptor. *Nature* **469**, 175-180

56. Deng, D., Sun, P., Yan, C., Ke, M., Jiang, X., Xiong, L., Ren, W., Hirata, K., Yamamoto, M., Fan, S., and Yan, N. (2015) Molecular basis of ligand recognition and transport by glucose transporters. *Nature* **526**, 391-396

57.   Lim, K., Doseeva, V., Demirkan, E. S., Pullalarevu, S., Krajewski, W., Galkin, A., Howard, A., and Herzberg, O. (2005) Crystal structure of the YgfY from Escherichia coli, a protein that may be involved in transcriptional regulation. *Proteins* **58**, 759-763

58.   Eletsky, A., Jeong, M. Y., Kim, H., Lee, H. W., Xiao, R., Pagliarini, D. J., Prestegard, J. H., Winge, D. R., Montelione, G. T., and Szyperski, T. (2012) Solution NMR structure of yeast succinate dehydrogenase flavinylation factor Sdh5 reveals a putative Sdh1 binding site. *Biochemistry* **51**, 8475-8477

59.   McNeil, M. B., and Fineran, P. C. (2013) The conserved RGxxE motif of the bacterial FAD assembly factor SdhE is required for succinate dehydrogenase flavinylation and activity. *Biochemistry* **52**, 7628-7640

60.   Cunane, L. M., Chen, Z. W., McIntire, W. S., and Mathews, F. S. (2005) p-Cresol methylhydroxylase: alteration of the structure of the flavoprotein subunit upon its binding to the cytochrome subunit. *Biochemistry* **44**, 2963-2973

61.   Kim, J., Fuller, J. H., Kuusk, V., Cunane, L., Chen, Z. W., Mathews, F. S., and McIntire, W. S. (1995) The cytochrome subunit is necessary for covalent FAD attachment to the flavoprotein subunit of p-cresol methylhydroxylase. *The Journal of biological chemistry* **270**, 31202-31209

62.   Westenberg, D. J., Gunsalus, R. P., Ackrell, B. A., Sices, H., and Cecchini, G. (1993) Escherichia coli fumarate reductase frdC and frdD mutants. Identification of amino acid residues involved in catalytic activity with quinones. *The Journal of biological chemistry* **268**, 815-822

63.   Kitagawa, M., Ara, T., Arifuzzaman, M., Ioka-Nakamichi, T., Inamoto, E., Toyonaga, H., and Mori, H. (2005) Complete set of ORF clones of Escherichia coli ASKA library (a complete set of E. coli K-12 ORF archive): unique resources for biological research. *DNA research : an international journal for rapid publication of reports on genes and genomes* **12**, 291-299

64.   Baba, T., Ara, T., Hasegawa, M., Takai, Y., Okumura, Y., Baba, M., Datsenko, K. A., Tomita, M., Wanner, B. L., and Mori, H. (2006) Construction of Escherichia coli K-12 in-frame, single-gene knockout mutants: the Keio collection. *Molecular systems biology* **2**, 2006 0008

65.   Iverson, T. M., Maklashina, E., and Cecchini, G. (2012) Structural basis for malfunction in complex II. *The Journal of biological chemistry* **287**, 35430-35438

66.   Lobley, A., Whitmore, L., and Wallace, B. A. (2002) DICHROWEB: an interactive website for the analysis of protein secondary structure from circular dichroism spectra. *Bioinformatics (Oxford, England)* **18**, 211-212

67.   Iverson, T. M., Luna-Chavez, C., Croal, L. R., Cecchini, G., and Rees, D. C. (2002) Crystallographic studies of the Escherichia coli quinol-fumarate reductase with inhibitors bound to the quinol-binding site. *The Journal of biological chemistry* **277**, 16124-16130

68.   Pierce, B. G., Wiehe, K., Hwang, H., Kim, B. H., Vreven, T., and Weng, Z. (2014) ZDOCK server: interactive docking prediction of protein-protein complexes and symmetric multimers. *Bioinformatics (Oxford, England)* **30**, 1771-1773

69.   Gray, J. J., Moughon, S., Wang, C., Schueler-Furman, O., Kuhlman, B., Rohl, C. A., and Baker, D. (2003) Protein-protein docking with simultaneous optimization of rigid-body displacement and side-chain conformations. *Journal of molecular biology* **331**, 281-299

70.   Young, T. S., Ahmad, I., Yin, J. A., and Schultz, P. G. (2010) An enhanced system for unnatural amino acid mutagenesis in E. coli. *Journal of molecular biology* **395**, 361-374

71.   Sato, S., Mimasu, S., Sato, A., Hino, N., Sakamoto, K., Umehara, T., and Yokoyama, S. (2011) Crystallographic study of a site-specifically cross-linked protein complex with a genetically incorporated photoreactive amino acid. *Biochemistry* **50**, 250-257

72.   Bamford, V., Dobbin, P. S., Richardson, D. J., and Hemmings, A. M. (1999) Open conformation of a flavocytochrome c3 fumarate reductase. *Nature structural biology* **6**, 1104-1107

73.   Sun, F., Huo, X., Zhai, Y., Wang, A., Xu, J., Su, D., Bartlam, M., and Rao, Z. (2005) Crystal structure of mitochondrial respiratory membrane protein complex II. *Cell* **121**, 1043-1057

74.   Taylor, P., Pealing, S. L., Reid, G. A., Chapman, S. K., and Walkinshaw, M. D. (1999) Structural and mechanistic mapping of a unique fumarate reductase. *Nature structural biology* **6**, 1108-1112

75.   Leys, D., Tsapin, A. S., Nealson, K. H., Meyer, T. E., Cusanovich, M. A., and Van Beeumen, J. J. (1999) Structure and mechanism of the flavocytochrome c fumarate reductase of Shewanella putrefaciens MR-1. *Nature structural biology* **6**, 1113-1117

76.   Bossi, R. T., Negri, A., Tedeschi, G., and Mattevi, A. (2002) Structure of FAD-bound L-aspartate oxidase: insight into substrate specificity and catalysis. *Biochemistry* **41**, 3018-3024

77.   Brandsch, R., and Bichler, V. (1989) Covalent cofactor binding to flavoenzymes requires specific effectors. *European journal of biochemistry* **182**, 125-128

78.   Bezawork-Geleta, A., Dong, L., Rohlena, J., and Neuzil, J. (2016) The Assembly Factor SDHAF2 Is Dispensable for Flavination of the Catalytic Subunit of Mitochondrial

Complex II in Breast Cancer Cells. *The Journal of biological chemistry* **291**, 21414-21420

79. Pankhurst, K. L., Mowat, C. G., Rothery, E. L., Hudson, J. M., Jones, A. K., Miles, C. S., Walkinshaw, M. D., Armstrong, F. A., Reid, G. A., and Chapman, S. K. (2006) A proton delivery pathway in the soluble fumarate reductase from Shewanella frigidimarina. *The Journal of biological chemistry* **281**, 20589-20597

80. Luna-Chavez, C., Iverson, T. M., Rees, D. C., and Cecchini, G. (2000) Overexpression, purification, and crystallization of the membrane-bound fumarate reductase from Escherichia coli. *Protein expression and purification* **19**, 188-196

81. Bafunno, V., Giancaspero, T. A., Brizio, C., Bufano, D., Passarella, S., Boles, E., and Barile, M. (2004) Riboflavin uptake and FAD synthesis in Saccharomyces cerevisiae mitochondria: involvement of the Flx1p carrier in FAD export. *The Journal of biological chemistry* **279**, 95-102

82. Maklashina, E., and Cecchini, G. (1999) Comparison of catalytic activity and inhibitors of quinone reactions of succinate dehydrogenase (Succinate-ubiquinone oxidoreductase) and fumarate reductase (Menaquinol-fumarate oxidoreductase) from Escherichia coli. *Archives of biochemistry and biophysics* **369**, 223-232

83. Tomasiak, T. M., Archuleta, T. L., Andrell, J., Luna-Chavez, C., Davis, T. A., Sarwar, M., Ham, A. J., McDonald, W. H., Yankovskaya, V., Stern, H. A., Johnston, J. N., Maklashina, E., Cecchini, G., and Iverson, T. M. (2011) Geometric restraint drives on- and off-pathway catalysis by the Escherichia coli menaquinol:fumarate reductase. *The Journal of biological chemistry* **286**, 3047-3056

84. Otwinowski, Z., and Minor, W. (1997) [20] Processing of X-ray diffraction data collected in oscillation mode. *Methods in enzymology* **276**, 307-326

85. McCoy, A. J., Grosse-Kunstleve, R. W., Adams, P. D., Winn, M. D., Storoni, L. C., and Read, R. J. (2007) Phaser crystallographic software. *Journal of applied crystallography* **40**, 658-674

86. Adams, P. D., Afonine, P. V., Bunkoczi, G., Chen, V. B., Davis, I. W., Echols, N., Headd, J. J., Hung, L. W., Kapral, G. J., Grosse-Kunstleve, R. W., McCoy, A. J., Moriarty, N. W., Oeffner, R., Read, R. J., Richardson, D. C., Richardson, J. S., Terwilliger, T. C., and Zwart, P. H. (2010) PHENIX: a comprehensive Python-based system for macromolecular structure solution. *Acta crystallographica. Section D, Biological crystallography* **66**, 213-221

87. Emsley, P., and Cowtan, K. (2004) Coot: model-building tools for molecular graphics. *Acta crystallographica. Section D, Biological crystallography* **60**, 2126-2132

88. Hura, G. L., Menon, A. L., Hammel, M., Rambo, R. P., Poole, F. L., 2nd, Tsutakawa, S. E., Jenney, F. E., Jr., Classen, S., Frankel, K. A., Hopkins, R. C., Yang, S. J., Scott, J. W.,

Dillard, B. D., Adams, M. W., and Tainer, J. A. (2009) Robust, high-throughput solution structural analyses by small angle X-ray scattering (SAXS). *Nature methods* **6**, 606-612

89.   Konarev, P. V., Volkov, V. V., Sokolova, A. V., Koch, M. H. J., and Svergun, D. I. (2003) PRIMUS: a Windows PC-based system for small-angle scattering data analysis. *Journal of applied crystallography* **36**, 1277-1282

90.   Svergun, D. (1992) Determination of the regularization parameter in indirect-transform methods using perceptual criteria. *Journal of applied crystallography* **25**, 495-503

91.   Franke, D., and Svergun, D. I. (2009) DAMMIF, a program for rapid ab-initio shape determination in small-angle scattering. *Journal of applied crystallography* **42**, 342-346

92.   Kozin, M. B., and Svergun, D. I. (2001) Automated matching of high- and low-resolution structural models. *Journal of applied crystallography* **34**, 33-41

93.   Bayley, J. P., Devilee, P., and Taschner, P. E. (2005) The SDH mutation database: an online resource for succinate dehydrogenase sequence variants involved in pheochromocytoma, paraganglioma and mitochondrial complex II deficiency. *BMC medical genetics* **6**, 39

94.   Cheng, V. W., Piragasam, R. S., Rothery, R. A., Maklashina, E., Cecchini, G., and Weiner, J. H. (2015) Redox state of flavin adenine dinucleotide drives substrate binding and product release in Escherichia coli succinate dehydrogenase. *Biochemistry* **54**, 1043-1052

95.   Reid, G. A., Miles, C. S., Moysey, R. K., Pankhurst, K. L., and Chapman, S. K. (2000) Catalysis in fumarate reductase. *Biochimica et Biophysica Acta (BBA) - Bioenergetics* **1459**, 310-315

96.   Zafreen, L., Walker-Kopp, N., Huang, L. S., and Berry, E. (2016) In-vitro, SDH5-dependent flavinylation of immobilized human respiratory complex II flavoprotein. *Archives of biochemistry and biophysics* **604**, 47-56

97.   Efimov, I., Cronin, C. N., and McIntire, W. S. (2001) Effects of noncovalent and covalent FAD binding on the redox and catalytic properties of p-cresol methylhydroxylase. *Biochemistry* **40**, 2155-2166

98.   Robinson, K. M., and Lemire, B. D. (1996) Covalent attachment of FAD to the yeast succinate dehydrogenase flavoprotein requires import into mitochondria, presequence removal, and folding. *The Journal of biological chemistry* **271**, 4055-4060

99. Kim, H. J., Jeong, M. Y., Na, U., and Winge, D. R. (2012) Flavinylation and assembly of succinate dehydrogenase are dependent on the C-terminal tail of the flavoprotein subunit. *The Journal of biological chemistry* **287**, 40670-40679

100. Bezawork-Geleta, A., Saiyed, T., Dougan, D. A., and Truscott, K. N. (2014) Mitochondrial matrix proteostasis is linked to hereditary paraganglioma: LON-mediated turnover of the human flavinylation factor SDH5 is regulated by its interaction with SDHA. *FASEB journal : official publication of the Federation of American Societies for Experimental Biology* **28**, 1794-1804

101. Maklashina, E., Iverson, T. M., Sher, Y., Kotlyar, V., Andrell, J., Mirza, O., Hudson, J. M., Armstrong, F. A., Rothery, R. A., Weiner, J. H., and Cecchini, G. (2006) Fumarate reductase and succinate oxidase activity of Escherichia coli complex II homologs are perturbed differently by mutation of the flavin binding domain. *The Journal of biological chemistry* **281**, 11357-11365

102. Schroder, I., Gunsalus, R. P., Ackrell, B. A., Cochran, B., and Cecchini, G. (1991) Identification of active site residues of Escherichia coli fumarate reductase by site-directed mutagenesis. *The Journal of biological chemistry* **266**, 13572-13579

103. Birch-Machin, M. A., Taylor, R. W., Cochran, B., Ackrell, B. A., and Turnbull, D. M. (2000) Late-onset optic atrophy, ataxia, and myopathy associated with a mutation of a complex II gene. *Annals of neurology* **48**, 330-335

104. Lee, S. Y., Cho, H. S., Pelton, J. G., Yan, D., Henderson, R. K., King, D. S., Huang, L., Kustu, S., Berry, E. A., and Wemmer, D. E. (2001) Crystal structure of an activated response regulator bound to its target. *Nature structural biology* **8**, 52-56

105. Sarkar, M. K., Paul, K., and Blair, D. (2010) Chemotaxis signaling protein CheY binds to the rotor protein FliN to control the direction of flagellar rotation in Escherichia coli. *Proceedings of the National Academy of Sciences of the United States of America* **107**, 9370-9375

106. Cohen-Ben-Lulu, G. N., Francis, N. R., Shimoni, E., Noy, D., Davidov, Y., Prasad, K., Sagi, Y., Cecchini, G., Johnstone, R. M., and Eisenbach, M. (2008) The bacterial flagellar switch complex is getting more complex. *The EMBO journal* **27**, 1134-1144

107. Barak, R., and Eisenbach, M. (1992) Fumarate or a fumarate metabolite restores switching ability to rotating flagella of bacterial envelopes. *Journal of bacteriology* **174**, 643-645

108. Garza, A. G., Biran, R., Wohlschlegel, J. A., and Manson, M. D. (1996) Mutations in motB suppressible by changes in stator or rotor components of the bacterial flagellar motor. *Journal of molecular biology* **258**, 270-285

109. Minamino, T., Imada, K., Kinoshita, M., Nakamura, S., Morimoto, Y. V., and Namba, K. (2011) Structural insight into the rotational switching mechanism of the bacterial flagellar motor. *PLoS biology* **9**, e1000616

110. Xu, F., Liu, W., Hanson, M. A., Stevens, R. C., and Cherezov, V. (2011) Development of an Automated High Throughput LCP-FRAP Assay to Guide Membrane Protein Crystallization in Lipid Mesophases. *Crystal growth & design* **11**, 1193-1201

111. Starbird, C. A., Maklashina, E., Sharma, P., Qualls-Histed, S., Cecchini, G., and Iverson, T. M. (2017) Structural and biochemical analyses reveal insights into covalent flavinylation of the Escherichia coli Complex II homolog quinol:fumarate reductase. *The Journal of biological chemistry*

112. Cecchini, G., Sices, H., Schroder, I., and Gunsalus, R. P. (1995) Aerobic inactivation of fumarate reductase from Escherichia coli by mutation of the [3Fe-4S]-quinone binding domain. *Journal of bacteriology* **177**, 4587-4592

113. Van Vranken, J. G., Bricker, D. K., Dephoure, N., Gygi, S. P., Cox, J. E., Thummel, C. S., and Rutter, J. (2014) SDHAF4 promotes mitochondrial succinate dehydrogenase activity and prevents neurodegeneration. *Cell metabolism* **20**, 241-252

114. Na, U., Yu, W., Cox, J., Bricker, D. K., Brockmann, K., Rutter, J., Thummel, C. S., and Winge, D. R. (2014) The LYR factors SDHAF1 and SDHAF3 mediate maturation of the iron-sulfur subunit of succinate dehydrogenase. *Cell metabolism* **20**, 253-266

115. Kim, H. J., Khalimonchuk, O., Smith, P. M., and Winge, D. R. (2012) Structure, function, and assembly of heme centers in mitochondrial respiratory complexes. *Biochimica et biophysica acta* **1823**, 1604-1616